PULSED ELECTROMAGNETIC GAS ACCELERATION

1 July 1970 to 31 December 1970

Semi-annual Report 634p

DEI SUB NUMINE VIGET

PRINCETON UNIVERSITY
DEPARTMENT OF
AEROSPACE AND MECHANICAL SCIENCES

National Aeronautics and Space Administration
NGL 31-001-005

PULSED ELECTROMAGNETIC GAS ACCELERATION

1 July 1970 to 31 December 1970

Semi-annual Report 634p

Prepared by: R. G. Jahn
ROBERT G. JAHN
Professor and
Principal Investigator

and

W von Jaskowsky
Woldemar F. Von Jaskowsky
Sr. Research Engineer and
Lecturer

Kenn E. Clark
Kenn E. Clark
Research Staff Member

January 1971

School of Engineering and Applied Science
Department of Aerospace and Mechanical Sciences
Guggenheim Aerospace Propulsion Laboratories
PRINCETON UNIVERSITY
Princeton, NJ 08540

ABSTRACT

Detailed experimental mapping of the potential and current distributions throughout the discharge chamber of a quasi-steady MPD arc indicates that the anode fall voltage varies inversely with local anode current density, over a large range of arc currents and mass flow rates. The corresponding anode power loss is found to drop from about 50% to 10% as the power is increased from 1 to 10 megawatts.

In an associated study in a parallel-plate accelerator, where expansion of the flow beyond the discharge region is precluded by the one-dimensional geometry, low exhaust speeds and high downstream temperatures are observed, which yield information on the energy deposition ratio within the arc.

Other experimental investigations of the structure of MPD discharges and attendant accelerator performance continue: spectroscopic-interferometric techniques yield further temperature and velocity details; pressure profiles in the discharge chamber are determined with a piezoelectric detector in a Plexiglas rod; terminal voltage and axial exhaust velocities are catalogued as functions of anode orifice diameter; a new mass-injection system facilitates study of a variety of propellant gases; and the characteristics of a quasi-steady MPD arc with a hollow cathode are found to compare favorably with the performance of a solid cathode arc over a range of currents and mass flows.

CONTENTS

ILLUSTRATIONS

ILLUSTRATIONS

TABLES

CURRENT STUDENT PARTICIPATION

Student	Period	Degree	Thesis Topic
BRUCKNER, Adam P.	1966-	Ph.D. Cand.	Radiation Studies of Gas Accelerating Discharges
CORY, John S.	1969-	Ph.D. Cand.	Jump Conditions for MPD Accelerators
DI CAPUA, Marco S.	1966-	Ph.D. Cand.	Energy Deposition in Parallel-Plate Plasma Accelerators
FOURNIER, Georges	1969-	B.S.E. Cand.	Optical Spectroscopy of Accelerator Exhaust Flow
FRADKIN, David B.	1969-	Ph.D. Cand.	Spectroscopic Velocity Measurements in Quasi-Steady Accelerators
HOUGH, Michael E.	1969-	B.S.E. Cand.	Mass Spectrometry of Accelerator Exhaust Flow
OBERTH, Ronald C.	1966-1970	Ph.D.	Anode Phenomena in High-Current Discharges
PARMENTIER, Noël	1970-	M.S.E. Cand.	Quasi-Steady MPD Arc with Hollow Cathode
SABER, Aaron J.	1969-	Ph.D. Cand.	Thrust Measurements on Quasi-Steady Accelerators
TURCHI, Peter J.	1963-1970	Ph.D.	The Cathode Region of a Quasi-Steady MPD Arcjet
VILLANI, Daniel D.	1969-	Ph.D. Cand.	Power Sources for Quasi-Steady Accelerators
WHITE, Fred W.	1969-	M.S.E. Cand.	Propellant Injection Techniques for Quasi-Steady Accelerators

INTRODUCTION

This semi-annual report consists of two reviews of Ph.D. research programs recently completed in our laboratory, along with more concise descriptions of other selected projects presently in progress. The first section describes the work of R. C. Oberth on anode processes in our quasi-steady MPD arcs, which constituted one portion of his thesis, "Anode Phenomena in High-Current Discharges," the full text of which is available on request. The second section describes a series of experiments concerning the energy deposition ratio in our parallel-plate accelerator, which is a major portion of the Ph.D. thesis of M. S. DiCapua, also available on request. Both of these programs were presented as papers at the AIAA Aerospace Sciences Meeting in New York, on January 27, 1971.

In the third section, we present a variety of studies in progress, including recent spectroscopic results, development of techniques for measurement of arc chamber pressure profiles, anode-size effects on MPD accelerator performance, design and calibration of a gas injection system for the forthcoming propellant survey, and the beginning of a very promising program on hollow-cathode, quasi-steady arcs. Discussion of other studies in progress, such as the Fabry-Perot interferometer velocity and temperature measurements, strain gauge thrust profile measurements, mass spectrometer exhaust-species samplings, and the turbo-pulse gas injector is deferred until the following report.

I. ANODE PROCESSES IN QUASI-STEADY MPD ARCS (Oberth)

A. Background

Investigation of anode phenomena in high-current plasma accelerators is motivated by the well-known, yet poorly understood, severe anode power losses which can plague these devices. Experimental studies on steady, low-power MPD arcs indicate that from 30% to 60% of the total input power may be lost at the anode, but also suggest a tendency towards lower fractional anode power loss with increasing arc power.[A-1,A-2] Effective exploitation of the latter effect has been hindered by the magnitude of the heat transfer and by the intolerable power demands which accompany steady MPD arc operation beyond the kilowatt power range. Transpiration cooling of the anode can help somewhat to reduce anode heat loss by blowing some of it back into the arc stream,[A-3] but the associated design complexity and thruster weight limit the applicability of this technique. A more promising means of reducing the relative anode power loss and thereby increasing the thermal efficiency of MPD arc thrusters is through high-power, quasi-steady arc operation.[101]

The quasi-steady device employed in the present study of anode power loss and anode current conduction embodies the conventional MPD arc geometry, but on a scale large enough to permit detailed interior diagnostics. A schematic diagram and photograph of this apparatus are shown in Figs. 1 and 2. Briefly,[101] it consists of a cylindrical discharge chamber with a 3/4-in.-diam conical tungsten cathode and a 7 1/2-in.-diam aluminum anode with a 4-in.-diam orifice. It is powered

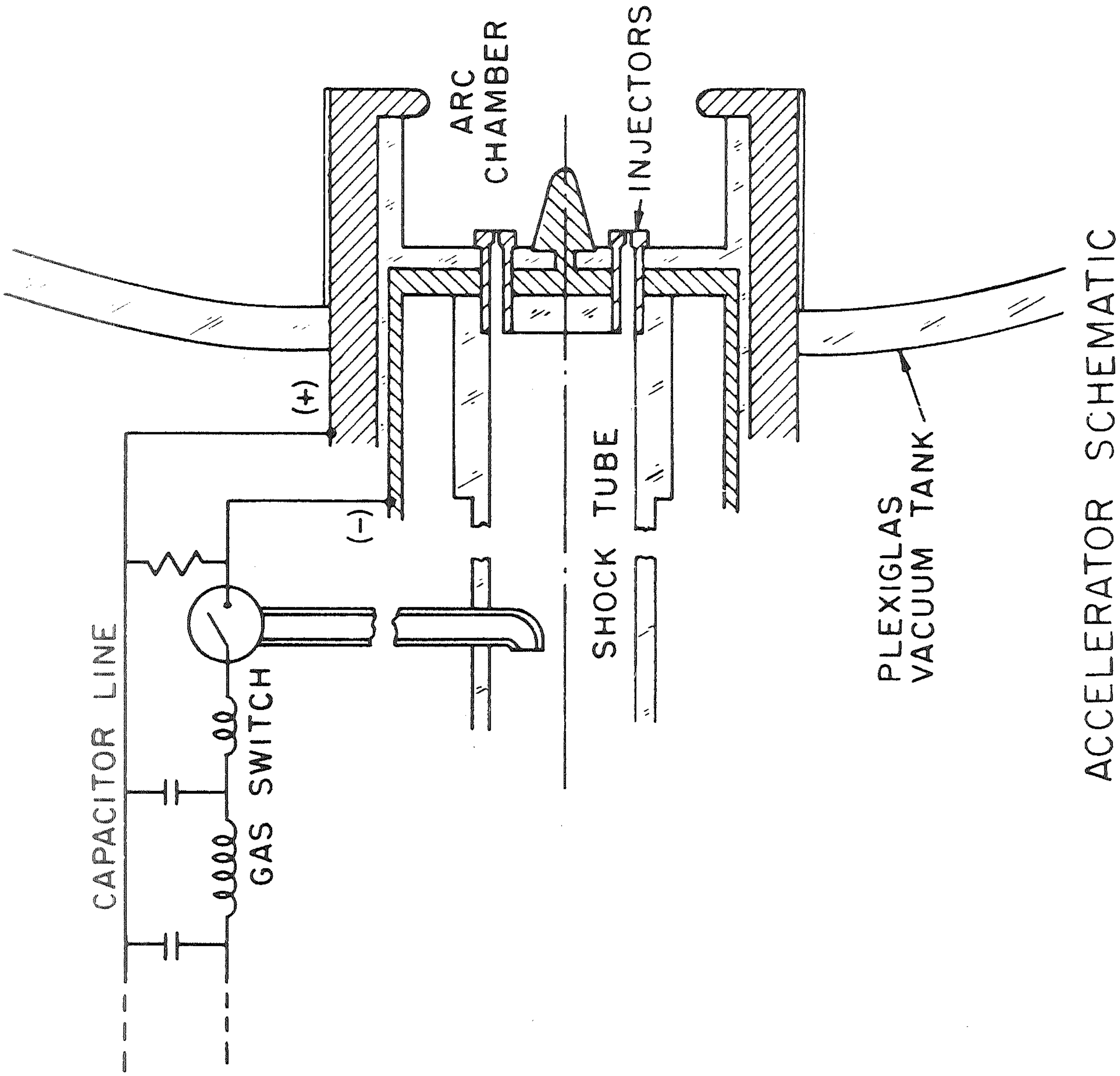

FIGURE 1

AP 25 R 4558 69 C

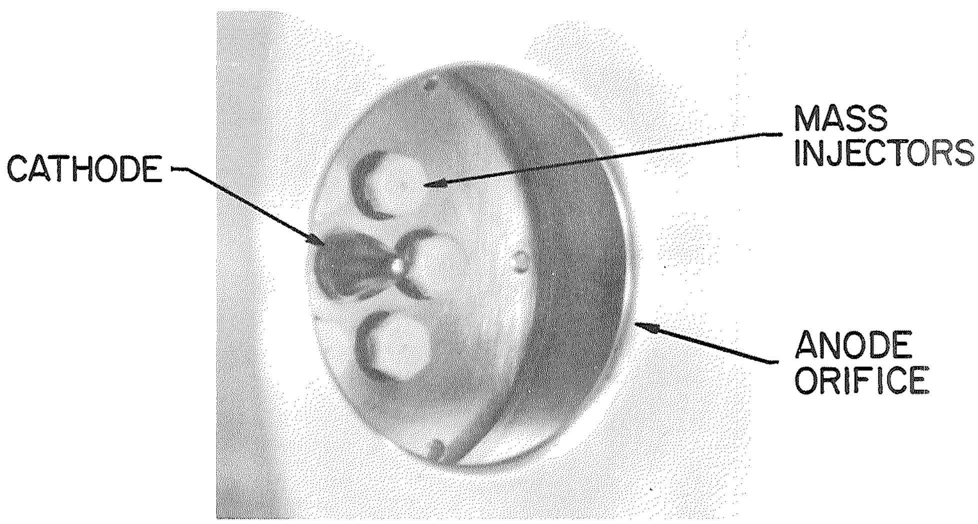

PERSPECTIVE VIEW OF ACCELERATOR CHAMBER

FIGURE 2
AP 25 P-368 71

by a 130 μfd x 10 kV capacitor line which can provide rectangular current pulses ranging from 4 kA x 600 μsec to 140 kA x 20 μsec. Propellant gas is injected at selected rates through six calibrated orifices in the arc chamber end plate from a high pressure reservoir abruptly established by the end wall stagnation of the flow in a simple shock tube. An adjustable bleed line from the same shock tube triggers the discharge current switch, thereby controlling the correlation of the mass flow pattern with the arc current profile.[87]

Earlier studies on this device[87,98] established the main features of the current density distribution and plasma potential patterns at various combinations of arc current and argon mass flow rate. For example, Fig. 3 shows the distribution of current density in the arc chamber and along the anode surface at an arc current of 17.5 kA and mass flow rate of 5.9 g/sec, which is a "matched" operating condition.[87] These current contours indicate that most of the arc current concentrates on the upstream lip of the anode in preference to other portions of the anode surface. Figure 4 displays floating potential contours for the same matched conditions, as well as for operation at an "underfed" mass flow of 1.2 g/sec, and an "overfed" flow of 36.0 g/sec. The most obvious aspect of these patterns is that the major portion of the arc power is deposited in the cathode region of the arc, implying that this region of high current density and high electric field is primarily responsible for the high plasma velocities observed downstream.[98] With regard to the anode regions, these patterns display the magnitude of the normal anode fall, and stress the importance of matching the mass flow rate to the total arc current. Figure 4b, for the matched mass flow of 5.9 g/sec, displays an anode fall of less than 15 V over the upstream lip of the anode where current density is a maximum, and somewhat higher values on the downstream face where current density is lower. The dependence of anode fall voltage on local anode current density and its implication for anode power losses are discussed below.

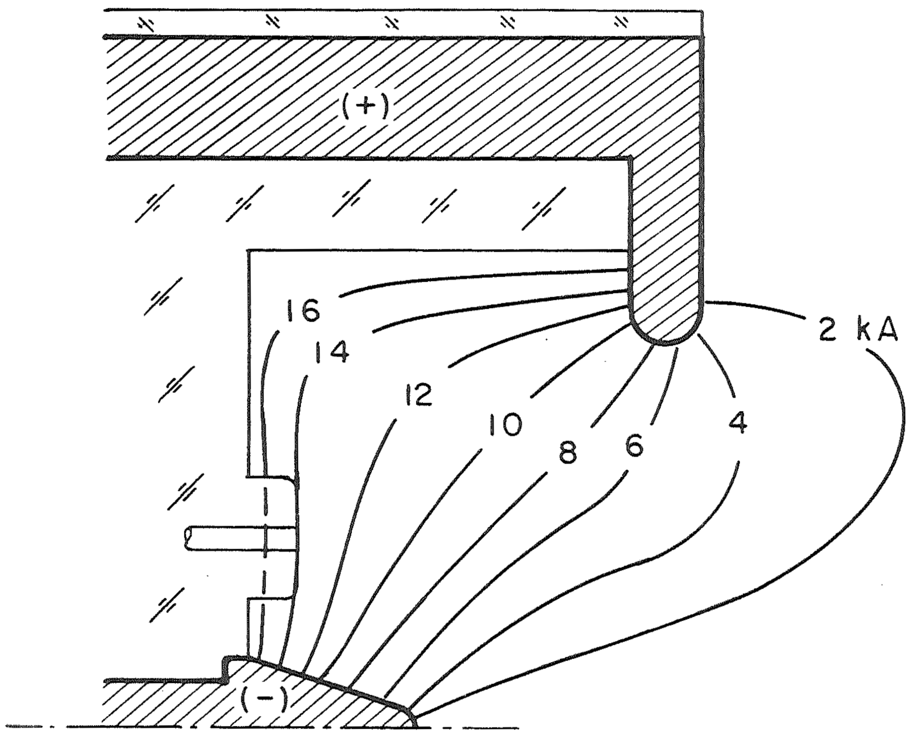

QUASI-STEADY CURRENT DISTRIBUTION;
$J = 17.5$ kA, $\dot{m} = 5.9$ g/sec

FIGURE 3
AP 25 R 4602 70

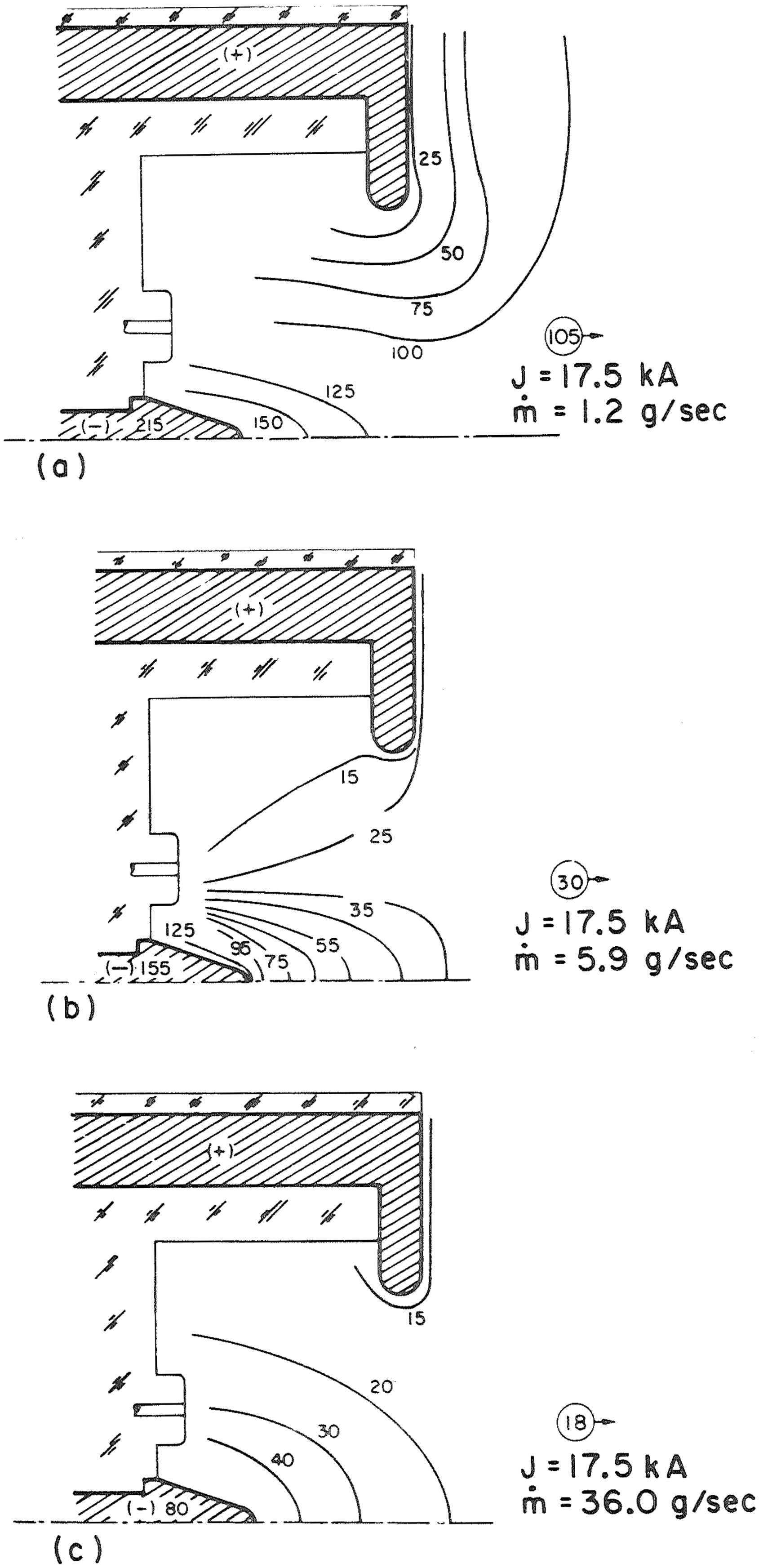

EQUIPOTENTIAL PROFILES FOR THREE DIFFERENT MASS FLOW RATES

FIGURE 4

AP 25 R 4560 70

In the underfed case (Fig. 4a), a substantially larger and broader electric field appears adjacent to the anode surface, suggesting the onset of anode conduction difficulties at this underfed operating condition. The relation of the mass flow rate to the field development and conduction processes in the anode region is also discussed below.

B. Anode Fall Measurements

In order to explore further the dependence of anode fall voltage on local anode current density, a series of detailed electrostatic and magnetic probe measurements have been taken over the anode surface during quasi-steady arc operation at three different matched conditions, 8.7 kA x 1.2 g/sec, 17.5 kA x 5.9 g/sec, 42.0 kA x 36.0 g/sec, where the arc behavior is well-defined and reproducible. The anode falls are determined from floating potential measurements taken adjacent to the surface with electrostatic probes whose exposed elements are 1/16-in.-diam hemispheres. Some of these are inserted axially upstream into the discharge and bent to allow access to the regions behind the anode lip; the front face of the anode is monitored by radially-inserted probes. All leads to the probe sensing surfaces are coaxially shielded, and the signals are presented to the oscilloscope via a Tektronix Model 6013A voltage probe of 10^8 ohm impedance. Simultaneously with the collection of floating potential data, the magnetic field values over the anode surface are measured by magnetic induction coils, 100 turns of #40 Formvar wire on 3/32-in.-diam nylon spools, which are mounted on bent shafts to permit access to the back anode region. From the measured values of magnetic field at these locations, the anode current density distribution is readily deduced.[A-4]

In the present context, anode fall voltage refers to the voltage difference between the anode surface and a point in the plasma about 0.1 cm off of the surface. The measured values of floating potential must be corrected to plasma potentials before the true anode fall voltages can be assigned. For an argon plasma in which ion streaming velocities are negligible--a good assumption for most of the region adjacent to the anode surface--the difference between floating and plasma potential is given by:[A-5]

$$V_p - V_f = \frac{kT_e}{e}\left[\ln\left(\frac{m_i}{m_e}\right)^{\frac{1}{2}} - \ln\left(\frac{T_i}{T_e}\right)^{\frac{1}{2}}\right] \approx 4.5\frac{kT_e}{e} \qquad \text{(I-1)}$$

T_e and T_i are taken to be 1.5 eV and 15 eV, respectively, based on several other studies,[103] so that floating potential measurements should be adjusted some 7 V closer to anode potential.

A composite graph of anode fall versus corresponding local anode current density for the three matched operating conditions is shown in Fig. 5. The indicated inverse dependence of anode fall on local anode current density can be reasonably approximated by the reciprocal fit, $V_a = 1.5 \times 10^3/j_a$, which in turn implies a constant anode power density, $p_a = j_a V_a = 1500$ W/cm^2. Regardless of its precise form, the observed inverse dependence of anode fall on local anode current density clearly has major implications for the overall efficiency of high power accelerators of this class.

The anode fall data appear to agree qualitatively with the classical anode fall theories of Bez and Höcker.[A-6,A-7] Their model is based on the assumption that the major function of the anode fall is the production of ions, and that this is accomplished by either of two mechanisms: "field ionization" and "thermal ionization." "Field ionization" involves collisional ionization by electrons that have been directly accelerated by the anode fall field; the anode fall voltage is therefore greater than the ionization potential of the operating gas and the anode current densities are generally low, say less than about 50 A/cm^2. "Thermal ionization," on the other hand, involves ionization by electrons whose motion has become thermalized in the fall zone by elastic collisions. Since only the high energy electrons in the distribution need engage in

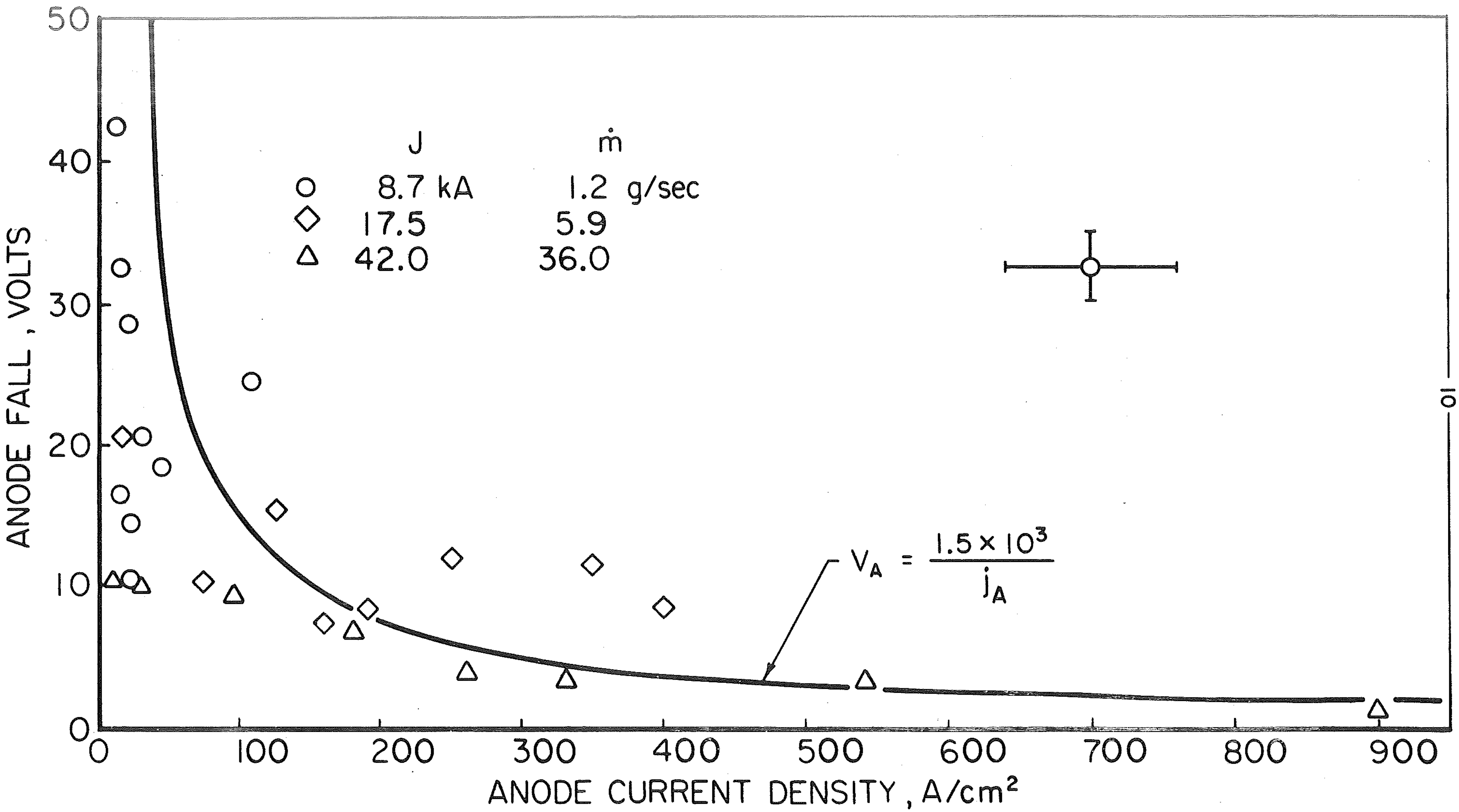

ANODE FALL VARIATION WITH LOCAL CURRENT DENSITY

FIGURE 5

AP 25 R 4591 70

ionizing collisions, the anode fall can now be lower than the ionization potential of the gas, but much higher anode current densities may be accommodated. In this spirit, the anode fall data of Fig. 5 may reflect a transition from field ionization at low anode current densities to thermal ionization at high anode current densities with a corresponding decrease in anode fall voltage.

C. Anode Power Loss

The total power loss at the anode of a high-current arc discharge may be written:

$$P_a = P_{ca} + P_{ra} + \int_{\substack{\text{anode}\\ \text{surface}}} j_a \left(\frac{5}{2} \frac{kT_e}{e} + V_a + \phi_a \right) dA \qquad \text{(I-2)}$$

where P_{ca} and P_{ra} are the convective and radiative contributions, and the integral represents the heat transfer implicit in the electron current to the anode surface. Here T_e is the electron temperature of the adjacent plasma, V_a denotes the anode fall, and ϕ_a is the work function of the anode metal. The term $5/2 j_a kT_e/e$ accounts for the transport of electron thermal energy from the plasma. Recent experiments employing a semiconductor photo diode suggest that only a few percent of the total input arc power is radiated from the highly luminous arc plasma formed in the cathode region. Since only a small percentage of this radiation is intercepted by the anode surface, the radiative term, P_{ra}, may be neglected for the present.

Convective heat transfer from the streaming plasma to the anode surface is assumed to be significant only at the lip region of the anode, where it may be expressed in terms of an enthalpy difference[A-8]

$$P_{ca} = C_h A(h_s - h_a) \qquad \text{(I-3)}$$

where C_h is a heat transfer coefficient based on enthalpies, A is the area of flow interaction with the anode, h_s is the plasma enthalpy at the outer edge of the boundary layer and h_a is the enthalpy of the plasma in thermal equilibrium with the wall. Assuming a laminar boundary layer at the anode surface, based on a low Reynolds number estimate ($\sim$ 100), and employing reasonable estimates of plasma viscosity, thermal conductivity, and specific heat, based on measurements of electron temperature and number density at the lip region of the anode, the convective heat transfer coefficient is estimated to be about 5×10^{-3} gm/cm^2 – sec.[111] Likewise, the plasma enthalpy at the outer edge of the boundary layer for a flow velocity of 10^4 m/sec is about 1.5×10^5 J/gm.[98] Neglecting the plasma enthalpy at the wall places an upper limit on the convective heat transfer to the anode which, for a reasonable area of flow interaction, takes a value of $P_{ca} \approx$ 20 kW. This is only about 1% of the total input arc power for matched quasi-steady arc operation at 17.5 kA, hence is also neglected.

There remains only the integral term representing energy carried to the anode by conduction electrons. Since T_e and ϕ_a are essentially constant over most of the anode surface, this may be rewritten

$$P_a = J\left(\frac{5}{2}\,kT_e/e + \phi_a\right) + \int_{\substack{\text{anode}\\ \text{surface}}} j_a V_a \, dA \qquad \text{(I-4)}$$

where J is the total arc current. For operation at the three matched conditions cited earlier, the empirical relation, $V_a = 1.5 \times 10^3/j_a$ (watt/amp/cm^2), can be used to evaluate the integral. Taking approximate values of T_e and ϕ_a of 1.5 eV and 3.5 V respectively, and an anode surface area of 300 cm^2, the result takes the form

$$P_a \approx 7.25\,J + 450 \qquad \text{(kW)} \qquad \text{(I-5)}$$

for J in kA.

Since the arc current increases less than linearly with total arc power, it is clear that fractional anode power loss decreases substantially with arc power. This result is displayed in Fig. 6 which plots the fractional anode power loss for the three matched conditions against the total input arc power P_t. Observe that P_a/P_t decreases from over 50% to less than 10% for an increase in arc power from 1.5 to 10 megawatts. It follows that correspondingly higher thermal efficiencies should prevail for the higher power operation.

D. Anode Current Conduction

Models of the mechanisms of current conduction to the anode surface ultimately rest on the values of electron density and temperature prevailing in the adjacent plasma. To accumulate this information, a series of double Langmuir probe measurements have been carried out at various locations in the quasi-steady MPD discharge. Briefly,[103,109] these probes consist of two separately shielded and biased 1/8-in.-long exposed tips of 3-mil tungsten wire oriented parallel to the flow axis to minimize streaming effects, and mounted on the same support tube to sample essentially the same plasma. A schematic of the probe and circuitry is shown in Fig. 7. The probe radius is considerably less than the anticipated electron-ion mean free paths and electron gyro radii in the anode region of the arc, thus reducing the influence of collisional and magnetic field effects on probe behavior, but it is substantially larger than the local Debye length, thereby removing the influence of sheath size on the electron saturation current drawn by the probe. One of the probes is mounted on a bent support shaft to allow access to the back portion of the anode. The probe voltages developed across different resistor pairs are monitored with Tektronix P6006 voltage probes and displayed on an oscilloscope. The electron temperature is obtained from the ratio of the two probe tip currents and the difference in probe voltages, provided both tips operate on the electron-retarding branch of the probe char-

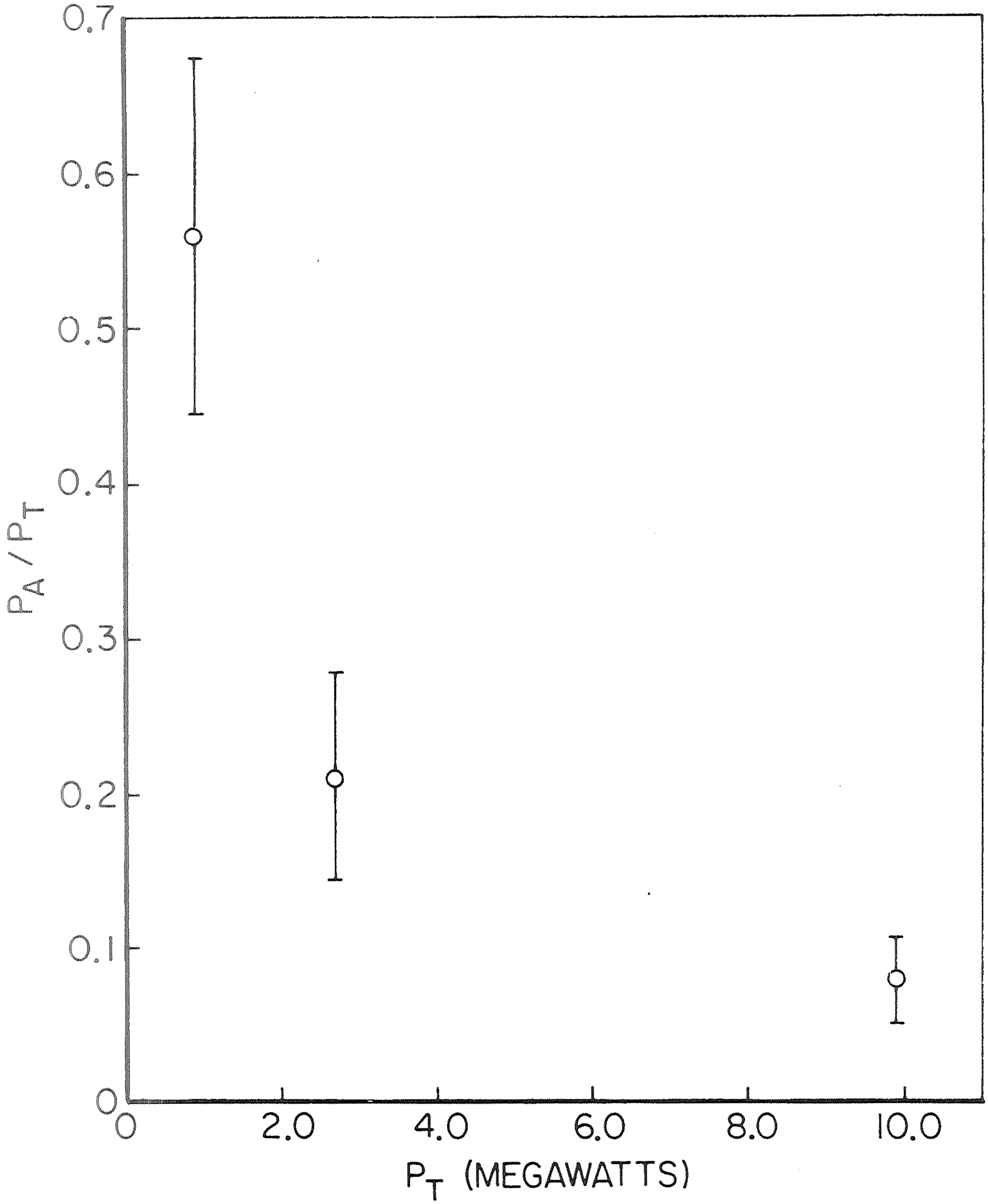

FRACTIONAL ANODE POWER VARIATION WITH TOTAL ARC POWER AT MATCHED CONDITIONS

FIGURE 6

AP 25 R 4672 70

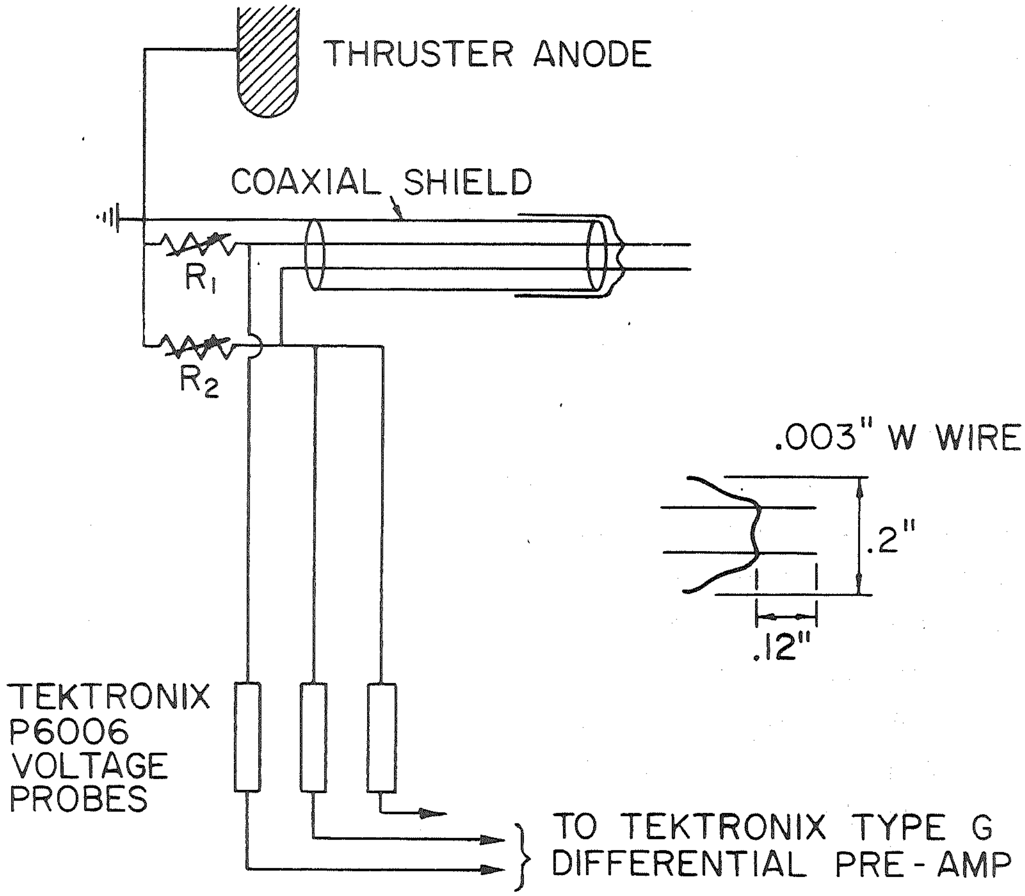

SCHEMATIC OF TWIN LANGMUIR PROBE AND CIRCUITRY

FIGURE 7

AP 25 R 4606 70

acteristic where the ion current to the probe can be neglected, in which case,

$$kT_e = e\Delta V_{12}/\ln(I_1/I_2) \tag{I-6}$$

Electron number density is determined somewhat less precisely by ascertaining when one of the probe tips begins to draw electron saturation current and thus is at the local plasma potential, as evidenced by a sudden increase in the values of kT_e computed via relation (I-6). From the measured current to the probe tip at this condition, and from the previously determined electron temperature, the local electron number density is extracted from the relation

$$I_p^* = n_e e A_p (kT_e/2\pi m_e)^{\frac{1}{2}} \tag{I-7}$$

The observed plasma potential and current density patterns in the vicinity of the anode surface also provide useful hints in the formulation of anode current conduction models. Recall the previous measurements with floating electrostatic probes which revealed that substantial electric fields develop in the anode region for operation below the matched mass flow for a given arc current (Fig. 4a), while at matched or overfed mass flows all fields were confined to the cathode region of the discharge except for a narrow sheath drop adjacent to the anode surface (Figs. 4b,c). Figure 8 superimposes on plots of plasma potential contours, determined from floating potential data by the method outlined in Sec. B, the corresponding current contours for quasi-steady operation at mass flows of 1.2 g/sec, 5.9 g/sec, and 36.0 g/sec, and a common current of 17.5 kA. In addition to the previously observed electric field growth around the anode for the 1.2 g/sec case (Fig. 8a), it is also apparent that a greater portion of the anode surface participates in the current conduction at this underfed situation.

In matched and overfed operation of the arc, where there is negligible electric field in the plasma adjacent to the anode fall region, it must be presumed that the required anode

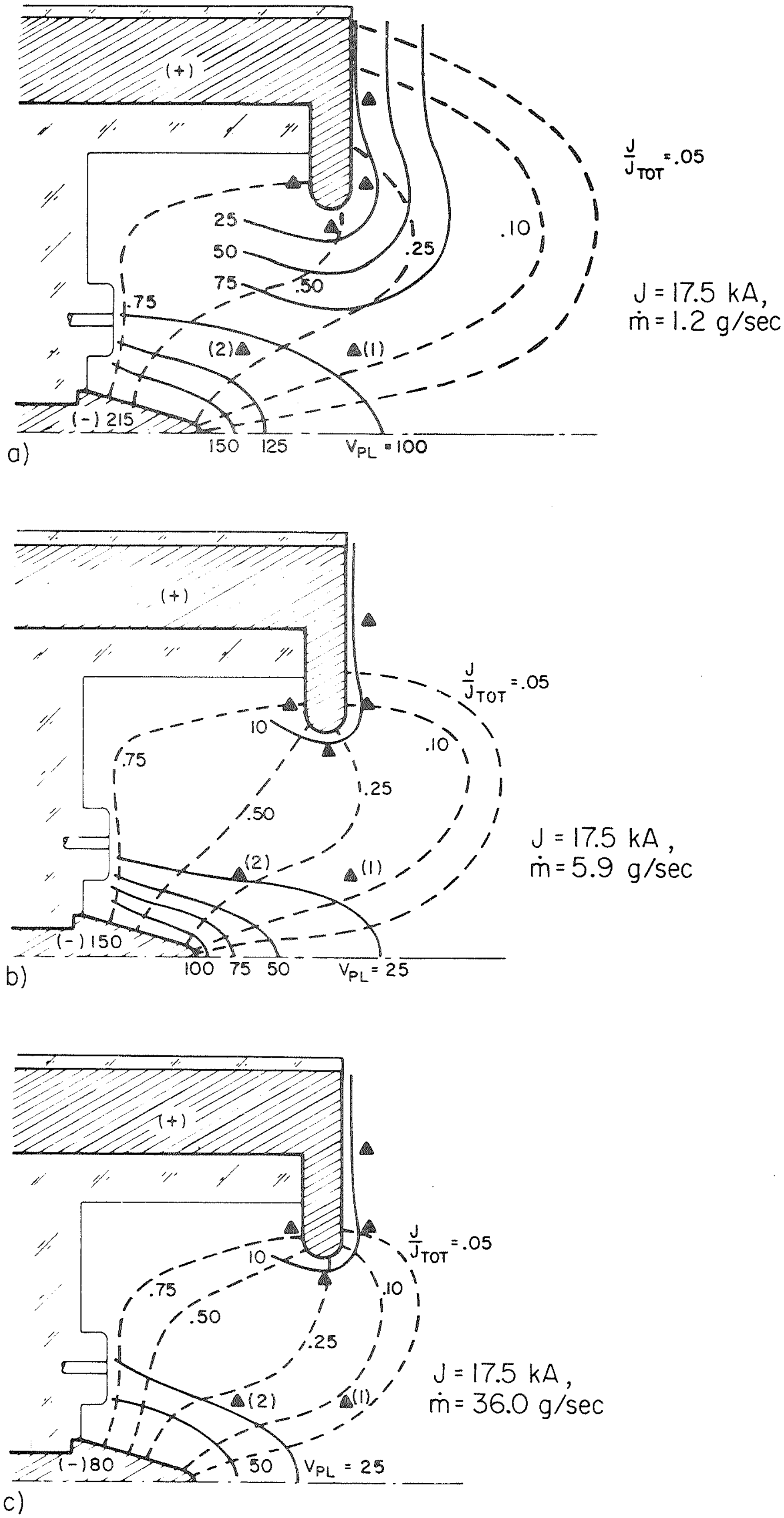

PLASMA POTENTIAL AND ENCLOSED
CURRENT CONTOURS

FIGURE 8

AP 25 R 4701 71

current enters the fall region largely via thermal electron diffusion from the equipotential plasma. This can be verified by an elementary calculation based on the observed electron temperatures and densities in that region. Assuming a Maxwell-Boltzmann distribution for the electrons near the plasma boundary, the electron current density at this location due to thermal flux is simply

$$j_e = en_e\bar{c}_e/4 = en_e(kT_e/2\pi m_e)^{\frac{1}{2}} \tag{I-8}$$

Figures 9a,b compare this thermal flux current density, computed at four anode locations (Fig. 8) and two different mass flow rates, with the actual anode current density distribution determined from magnetic probe data. The anode surface has been linearized in these diagrams, so that in going from left to right one progresses from the insulator wall at the back anode, around the lip, to the front face. The favorable comparison verifies that the plasma in the vicinity of the anode is sufficiently dense and thermally active so that the required discharge current can be passed through it to the anode without the need for large local electric fields. One may even speculate that it is this match of ambient plasma conditions to the discharge current that identifies the matched mass flow for a given arc current operation, although other criteria, such as the identification of number density flow with the required arc current, may also be relevant.[87]

Regrettably, it has not been possible to make the same comparison for the underfed condition, $\dot{m}$ = 1.2 g/sec. In this case the electrostatic and magnetic probe data in the vicinity of the anode are exceedingly noisy and irreproducible, indicative of an unhappy domain of arc operation, and it is therefore impossible to define characteristic values of the plasma properties and current densities over most of the anode surface other than to identify the sizable electric field extending far from the anode surface, and the greater extension of the current pattern over the surface region (Fig. 8a). In the absence of better data at the anode, the following hypothesis is

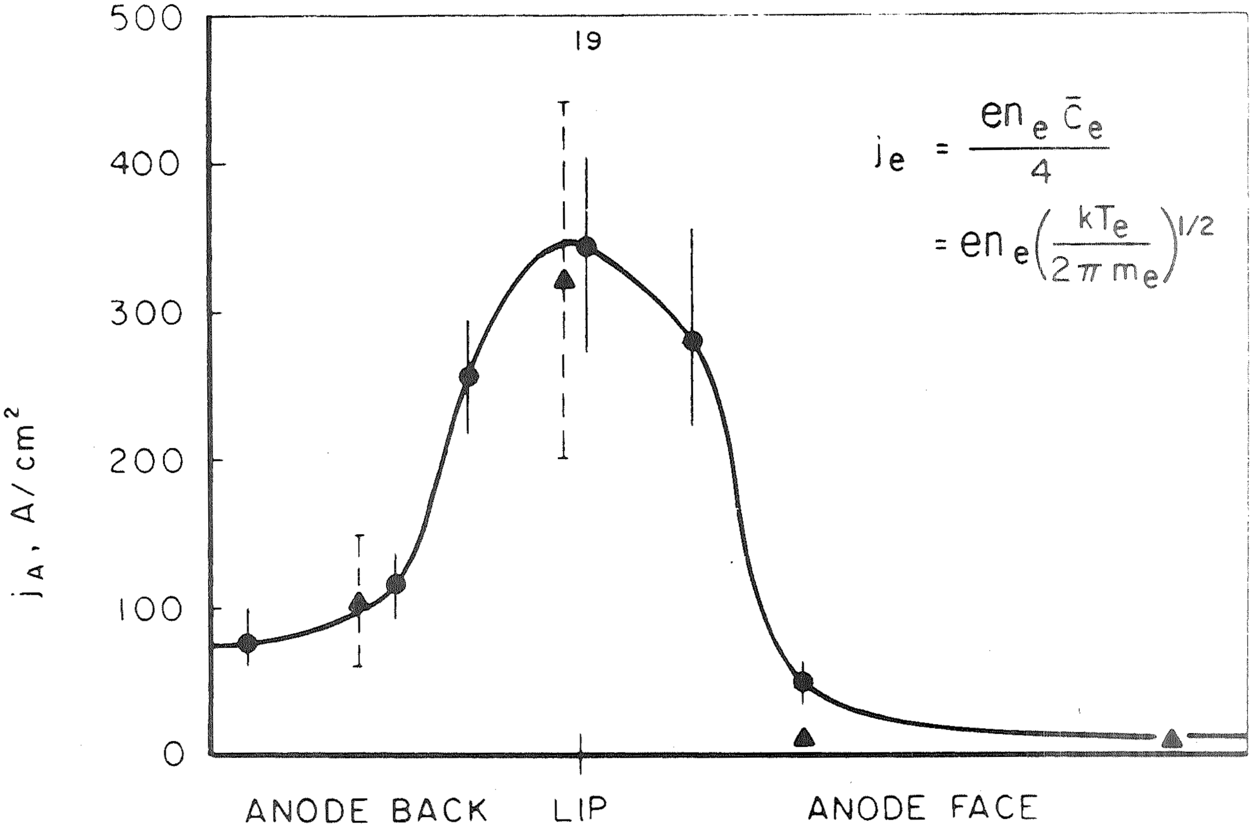

(a) $\dot{m} = 5.9$ g/sec

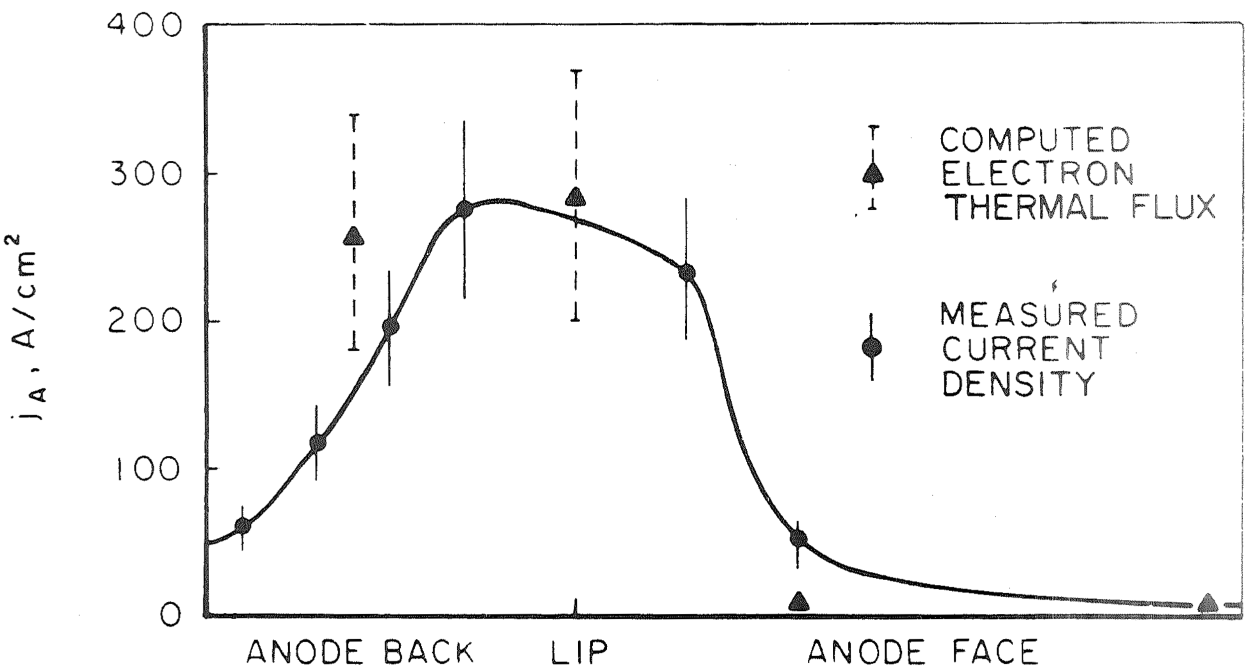

(b) $\dot{m} = 36.0$ g/sec

COMPUTED ELECTRON THERMAL FLUX COMPARED TO MEASURED CURRENT DENSITY AT ANODE SURFACE

FIGURE 9

AP 25 R 4613 70

advanced: At this low mass flow the electron number density near the anode is lower than that demanded by the thermal flux condition invoked above, presumably due to the lower overall density level in the chamber. Hence, in order to satisfy the current demands at the anode, the arc establishes an anode field whose function is to increase the electron flux at the anode to the proper level, and the arc current spreads itself over a larger portion of the anode surface to alleviate somewhat the local demand for electron flux density.

It may be instructive to distinguish two means by which this anode region electric field may function to accomplish the needed increase in electron flux to the anode surface: (a) local resistive heating of the plasma to increase the ionization level and/or the electron temperature to the point where the thermal flux of electrons again becomes adequate; (b) electron conduction in the prevailing field of the required magnitude to just compensate for the deficiency of thermal electron flux at this low density situation. Two elementary calculations estimate the relative effectiveness of these two mechanisms.

First, the complete expression for the electron flux to the anode is derived by considering a Maxwell-Boltzmann distribution that has been shifted by the drift velocity of electrons towards the anode, u_e, and integrating over one-half of the velocity space; i.e., over all those electrons moving towards the anode surface. Taking the x-direction perpendicular to the anode surface this yields

$$j_e = n_e e\left(\frac{m_e}{2\pi kT_e}\right)^{3/2} \int_0^{\infty}\int_{-\infty}^{\infty}\int_{-\infty}^{\infty} v_x \times e^{-m_e/2kT_e\,[(v_x-u_e)^2+v_y^2+v_z^2]}\,dv_x dv_y dv_z$$

$$= \frac{n_e e\bar{c}_e}{4}\, e^{-m_e u_e^2/2kT_e} + \frac{n_e e u_e}{2}\left\{1 + 2\,\mathrm{erf}\left[\left(\frac{m_e u_e^2}{kT_e}\right)^{\frac{1}{2}}\right]\right\} \quad \text{(I-9)}$$

where $\bar{c}_e = (8kT_e/\pi m_e)^{1/2}$ is the mean thermal velocity of the electrons. For the high temperature plasmas that arise in discharges of this nature, the electron thermal velocities are much greater than their drift velocities, hence $u_e^2 \ll 2kT_e/m_e$ and $u_e \ll \bar{c}_e$, and the lowest approximation to j_e is just the expression used earlier for the isotropic electron distribution,

$$j_e \approx n_e e \bar{c}_e/4 \qquad \text{(I-8)}$$

Now let $(\Delta j_e)_R$ and $(\Delta j_e)_C$ define the increases in electron flux to the anode produced by resistive heating of the plasma and by electron conduction respectively, where

$$(\Delta j_e)_R = \left(\frac{\partial j_e}{\partial n_e}\right)\Delta n_e + \left(\frac{\partial j_e}{\partial T_e}\right)\Delta T_e \qquad \text{(I-10)}$$

$$(\Delta j_e)_C = \left(\frac{\partial j_e}{\partial u_e}\right)\Delta u_e \qquad \text{(I-11)}$$

The relative importance of the two terms in the expressions for $(\Delta j_e)_R$ depends strongly on the state of the plasma under consideration. For example, if the plasma is only partially ionized, further energy input will increase the degree of ionization with the electron temperature changing only slightly until full ionization is approached. If the plasma is almost completely ionized, on the other hand, the energy addition will first be reflected by an increase in the electron temperature rather than by the onset of substantial second ionization because of the high energy threshold of the latter process. Unfortunately, few data are presently available on the ionization levels in the anode region of the quasi-steady MPD discharge. However, measurements of electron temperature near the anode indicate that T_e does not increase in response to anode field development at underfed mass flows and, hence, the second term on the right of Eq. (I-10) will be neglected.

With reference to Eq. (I-9), the required derivatives can be expressed:

$$\frac{\partial j_e}{\partial n_e} \approx \frac{e\bar{c}_e}{4} e^{-m_e u_e^2/2kT_e} \tag{I-12}$$

$$\frac{\partial j_e}{\partial u_e} \approx n_e \frac{e}{2} \left\{ 1 + 2 \text{ erf } \left[\left(\frac{m_e u_e^2}{2kT_e} \right)^{\frac{1}{2}} \right] \right\} \tag{I-13}$$

Again employing $u_e^2 << 2kT_e/m_e$ to simplify the above forms, a ratio is established which compares the relative effectiveness of plasma heating and electron conduction in terms of raising the electron flux at the anode:

$$\frac{\Delta j_e)_R}{\Delta j_e)_C} \approx \left(\frac{2kT_e}{\pi m_e} \right)^{\frac{1}{2}} \frac{\Delta n_e}{\Delta u_e n_e} \approx \frac{\Delta \bar{n}_e}{2 \Delta \bar{u}_e} \tag{I-14}$$

where $\Delta \bar{n}_e$ is the fractional increment in electron density and $\Delta \bar{u}_e$ is the increment in electron drift velocity perpendicular to the anode normalized by the electron mean thermal velocity.

The respective increases in electron number density and electron drift velocity, Δn_e and Δu_e, must now be related to the field increase at the anode, ΔE_a, by means of suitable ionization and conduction models. First, current conduction in the anode region of the discharge is probably tensor in nature, with the components of current parallel and perpendicular to the anode field given by $j_{/\!/} = \sigma E_a/(1 + \Omega_e^2)$ and $j_\perp = \sigma \Omega_e E_a/(1 + \Omega_e^2)$, where σ is the scalar conductivity and Ω_e the electron Hall parameter. The perpendicular current component lies in the r — z plane and is directed towards the downstream portions of the anode. The increase in electron drift velocity toward the anode surface, parallel to E_a, in response to the anode field increase, ΔE_a, is

$$\Delta u_e = \Delta \left(\frac{j_{/\!/}}{n_e e} \right) = \frac{\Delta E_a}{(1 + \Omega_e^2) n_e e} \tag{I-15}$$

The rate of resistive heating in the anode field region plasma is just j^2/σ,[A-9] where j is the resultant current density given by $j = \sigma E_a/(1 + \Omega_e^2)^{1/2}$. Assuming that all of this energy goes into ionization and its immediately attendant processes, such as radiation and excitation, the rate of electron production in the anode field region may be expressed:

$$\frac{dn_e}{dt} = \frac{j^2/\sigma}{eV_i^*} = \frac{\sigma E_a^2}{(1 + \Omega_e^2)eV_i^*} \tag{I-16}$$

where V_i^* is the effective ionization potential of argon in the prevailing environment, which is probably about twice the atomic ionization potential.[A-10] To compute an ionization increment, Δn_e, from Eq. (I-16), we invoke a time increment, Δt_i, equal to the transit time for electron drift across the anode field region; i.e., $\Delta t_i = d_a/u_e$ where d_a is the average thickness of the anode field region. Thus the increase in electron number density at the anode due to resistive heating of the plasma becomes

$$\Delta n_e = \frac{j^2/\sigma}{eV_i^*}\ \Delta t_i = \frac{\sigma E_a^2}{(1 + \Omega_e^2)eV_i^*}\ \frac{d_a}{u_e} \tag{I-17}$$

Using $u_e = j_{\parallel}/n_e e$ and $E_a \approx \Delta E_a$, this reduces to

$$\Delta n_e = n_e d_a \Delta E_a/V_i^* \tag{I-18}$$

Substituting the expressions for Δu_e and Δn_e, given by Eqs. (I-15) and (I-18), into Eq. (I-14) yields the following ratio comparing the effectiveness of resistive heating and electron conduction as means of satisfying anode current demands at the underfed condition,

$$\frac{(\Delta j_e)_R}{(\Delta j_e)_C} = \left(\frac{2kT_e}{\pi m_e}\right)^{1/2} \frac{n_e e d_a}{\sigma V_i^*}\ (1 + \Omega_e^2) \tag{I-19}$$

Using the Spitzer value for σ[A-11] along with the appropriate numerical values, $d_a = 2$ cm, and $V_i^* = 33$ V,[A-10] the ratio becomes

$$\frac{(\Delta j_e)_R}{(\Delta j_e)_C} = 1 \times 10^{-14} n_e (1 + \Omega_e^2)/T_e \qquad \text{(I-20)}$$

for n_e in cm^{-3} and T_e in eV.

With reference to Fig. 8a, the relative indication of current and potential contours indicate that $\Omega_e \approx 1$ at the lip region of the anode, and from twin Langmuir probe data at the matched conditions, n_e and T_e in this region are on the order of $10^{14} cm^{-3}$ and 1.5 eV respectively. Thus, at the important lip region of the anode, the above ratio becomes of order unity, implying that both processes contribute significantly to the increase in anode current. It is perhaps significant that this condition prevails when $\Omega_e = 1$; i.e., when the collisionless Hall current and collision-dominated scalar current contribute equally to the total arc current near the anode.

E. Conclusions

High-power, quasi-steady MPD arcs promise high specific impulse and high efficiency plasma acceleration. Certain results of the present study speak directly to the high thermal efficiency potential of these devices. For example, an inverse dependence of anode fall voltage on local anode current density is observed for matched, quasi-steady arc operation at current levels of 8.7, 17.5, and 42.0 kA and argon mass flow rates of 1.2, 5.9, and 36.0 g/sec. Using the resulting empirical relationship, $V_a = 1.5 \times 10^3/j_a$ (volt/amp/cm^2), fractional anode power loss is computed to decrease from over 50% to less than 10% as arc pulse power increases from 1 to 10 megawatts.

Also, the importance of mass flow rate to the satisfactory operation of the quasi-steady MPD discharge, in particular to the arc behavior in the anode region, is reaffirmed. For matched and overfed mass flows, the discharge electric fields are significant only in the major acceleration region near the cathode, and in a narrow fall region adjacent to the anode surface. Anode current conduction at these conditions is accomplished largely by the thermal electron flux from the adjacent arc plasma. In fact, the ability of the anode plasma to carry the requisite current by thermal flux appears to bear on the specification of the matched mass flow for a given arc current.

At underfed mass flows, substantial electric fields develop around the anode in order to augment anode current conduction from the lower density plasma. Calculations indicate that these fields raise the electron flux at the anode surface both by resistive heating of the plasma, and by field-driven electron conduction. Since much of the power deposited in this anode field envelope probably is ultimately transferred to the anode surface, decreased thermal efficiencies at underfed mass flows must be anticipated. This, combined with observations of noisy arc operation and enhanced erosion, indicate a regime of operation to be avoided.

II. ENERGY DEPOSITION IN PARALLEL-PLATE PLASMA ACCELERATORS (Di Capua)

A. Introduction

In any magnetoplasmadynamic accelerator, the initial apportionment of input power to the kinetic and thermal modes of the plasma bears heavily on the overall efficiency of the acceleration process. While some of the thermal energy of the plasma may subsequently be converted to streaming kinetic energy by flow expansion downstream of the discharge region, various irreversible losses, such as heat transfer to the electrodes and other surfaces, radiation, and frozen flow effects invariably take a heavy toll of this electrothermal conversion. High-performance accelerators therefore should minimize the fraction of input power initially delivered to plasma heating.

A parallel-plate accelerator[97] is a particularly convenient configuration for study of this initial energy deposition ratio. While retaining the essential features of high-power, self-field MPD accelerators, i.e., diffuse conduction of current densities of the order of $10^6 - 10^7$ A/m^2 through propellant mass flows of many grams/sec, this geometry minimizes downstream flow expansion and acceleration, thereby preserving the initial energy deposition ratio for more convenient study. For example, the downstream Mach number, which is one indicator of this ratio, changes little with distance in this type of accelerator. Similarly, the motional emf, whose ratio to terminal voltage is also a valuable indication of the energy deposition ratio, is more readily assessed in this geometry.

Thus, although the one-dimensional downstream channeling of the flow clearly must lower the thrust efficiency of parallel-plate accelerators by precluding any significant aerodynamic conversion, their study improves our understanding of certain mechanisms which are essential to effective operation of the more promising coaxial MPD arcs.

B. Equipment

The parallel-plate accelerator, shown schematically in Fig. 10, is 48-in. long and has a 6-in. x 2-in. cross section formed by two 5-in.-long aluminum electrodes followed by 43-in.-long nylon plates, all with Plexiglas side walls.[97] Argon propellant is delivered through an interchangeable set of four calibrated orifices at the rear of the channel from a high pressure reservoir which is established by the stagnation of the flow in a shock tube of appropriate geometry.[103] This feed system can deliver a maximum of 100 g/sec into the breech of the accelerator. The power source is a pulse-forming network of 0.040 Ω impedance matched to the discharge load by an electrolytic series resistor[107] and is capable of delivering 100 kA for 250 μsec, or 27 kA for 1 msec when charged to 7.2 kV. The switch is itself a confined gas-triggered discharge of a size and configuration capable of handling the large power developed during the pulse, and is initiated by flow from an auxiliary adjustable orifice from the mass-supply shock tube. The switch is normally timed to initiate the discharge some 1.5 msec after the start of gas injection into the accelerator, by which time a steady flow has been established in the channel upstream of the electrode-insulator junction, at a pressure of about 10 Torr. It then requires about 60 μsec after discharge initiation for the current pattern to stabilize at the electrode-insulator junction in the characteristic quasi-steady configuration (Fig. 11).[97] During the initiation phase, some fraction of the ambient gas is expelled downstream by a "snow-plow" process reminiscent of short-pulse

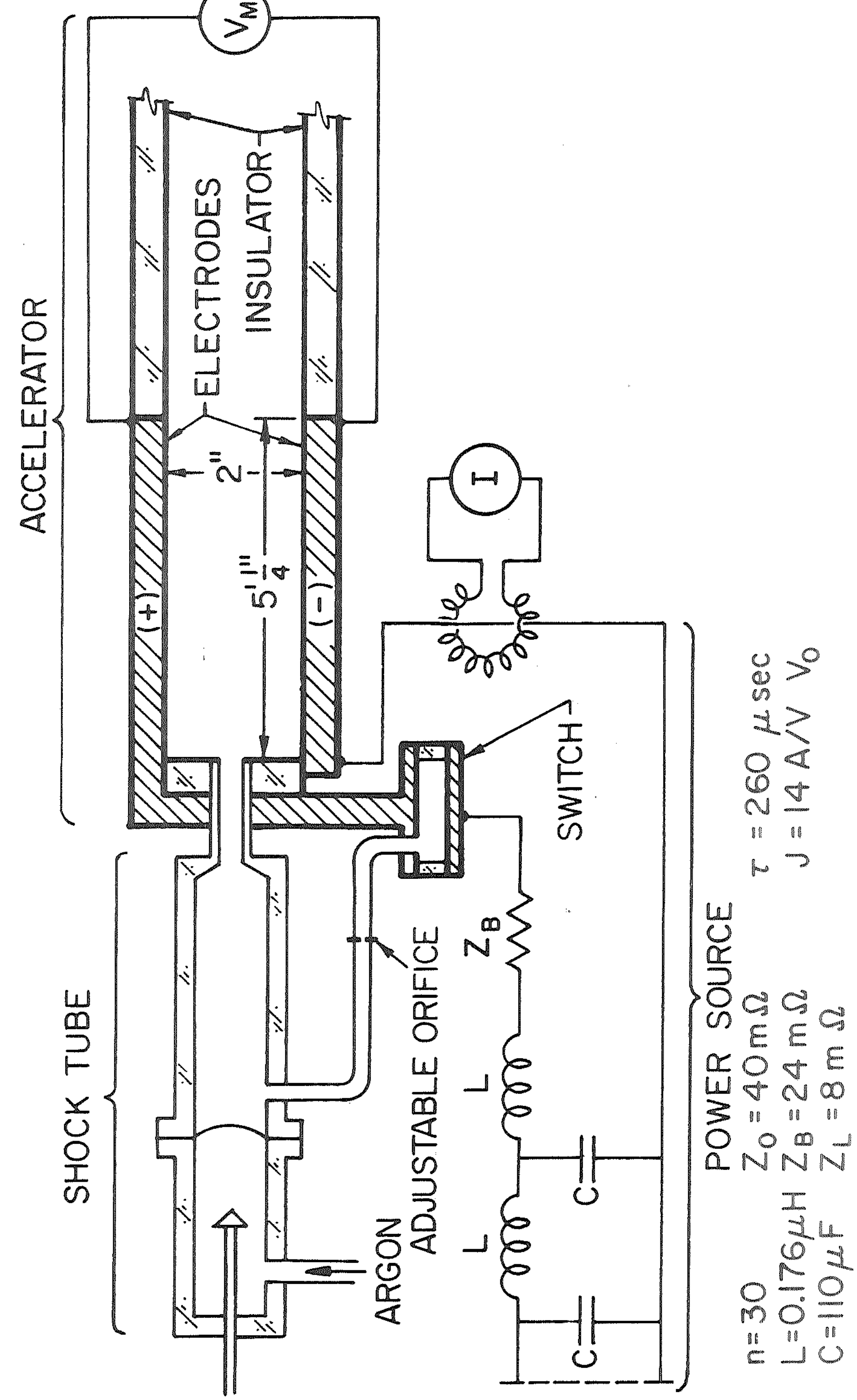

SCHEMATIC OF PARALLEL-PLATE ACCELERATOR

FIGURE 10
AP 25 R 4674 70

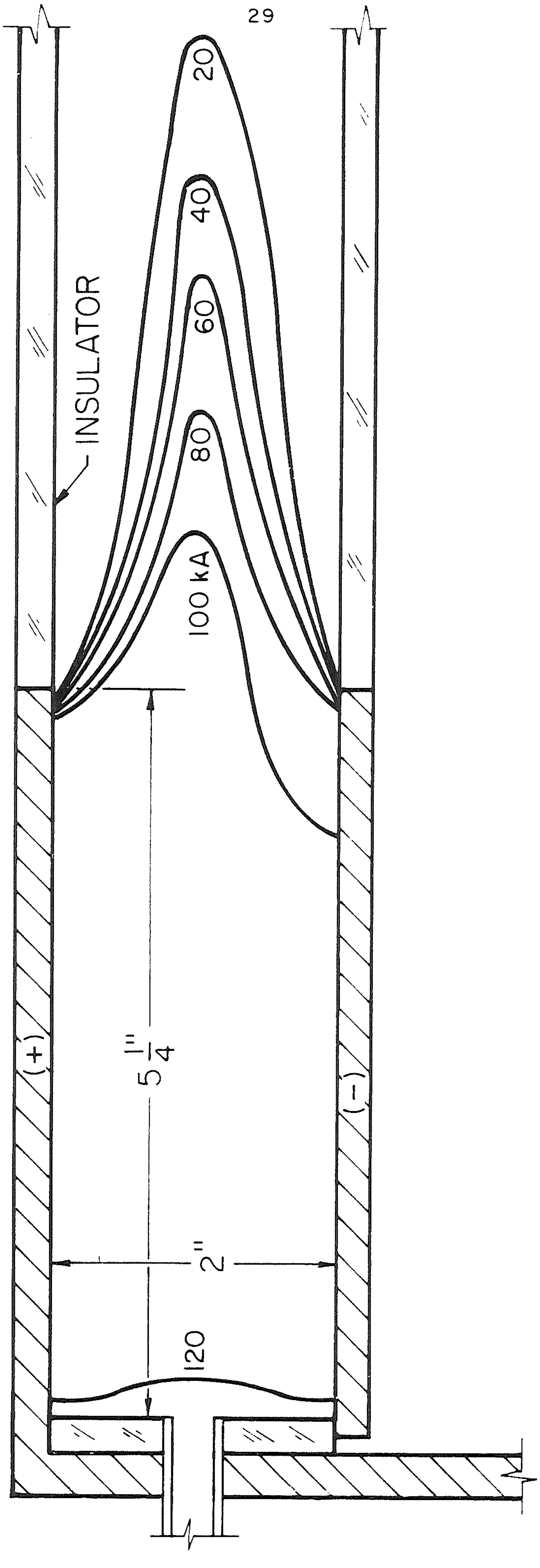

QUASI-STEADY ENCLOSED CURRENT CONTOURS

FIGURE 11

AP25 R 4680 70

accelerator operation,[97] and some portion remains upstream of the stabilized discharge region later to provide inlet mass flow for it. It is the outflow from the stabilized discharge which is the interest of this study.

C. Aerodynamic Observations of the Flow

Wedge-shaped airfoils inserted in the channel downstream of the arc region confirm that quasi-steady operation of the accelerator has been achieved, and provide an estimate of the flow Mach number. A typical photograph of bow shock waves formed on a wedge 1-in. wide, slightly inclined to the flow 8-in. downstream from the electrode insulator junction in the midplane of the channel is shown in Fig. 12. The photograph was taken on Polaroid Type 52 film with a conventional camera through a 5 μsec Kerr-cell shutter delayed 150 μsec after discharge initiation. The shock angles observed on a sequence of such photographs are found to be constant over a large fraction of the current pulse, indicating that quasi-steady flow indeed prevails. If the effective specific heat ratio of the plasma, γ, were known, one such photograph should suffice to determine the Mach number of the flow. Since γ is not known a priori, wedges of several different angles have been used in order to estimate both γ and M. Figure 13 shows indicated Mach number as a function of observed deflection angle for accelerator operation at 93 kA, 48 g/sec, for various assumed values of γ ranging from 1.3 to 1.7. Since the Mach number should be a constant for wedge angles up to the maximum deflection angle of the flow, the accepted Mach number is close to 2 with an effective γ of the plasma between 1.3 and 1.4.

Figure 14 shows the Mach numbers obtained in this manner for various currents in the range of 50 to 100 kA for two different input mass flows. Within experimental accuracy, the Mach number for 24 g/sec input mass flow remains approximately constant at a value of 1.9 ± 0.1 while for 96 g/sec its value is 2.1 ± 0.1.

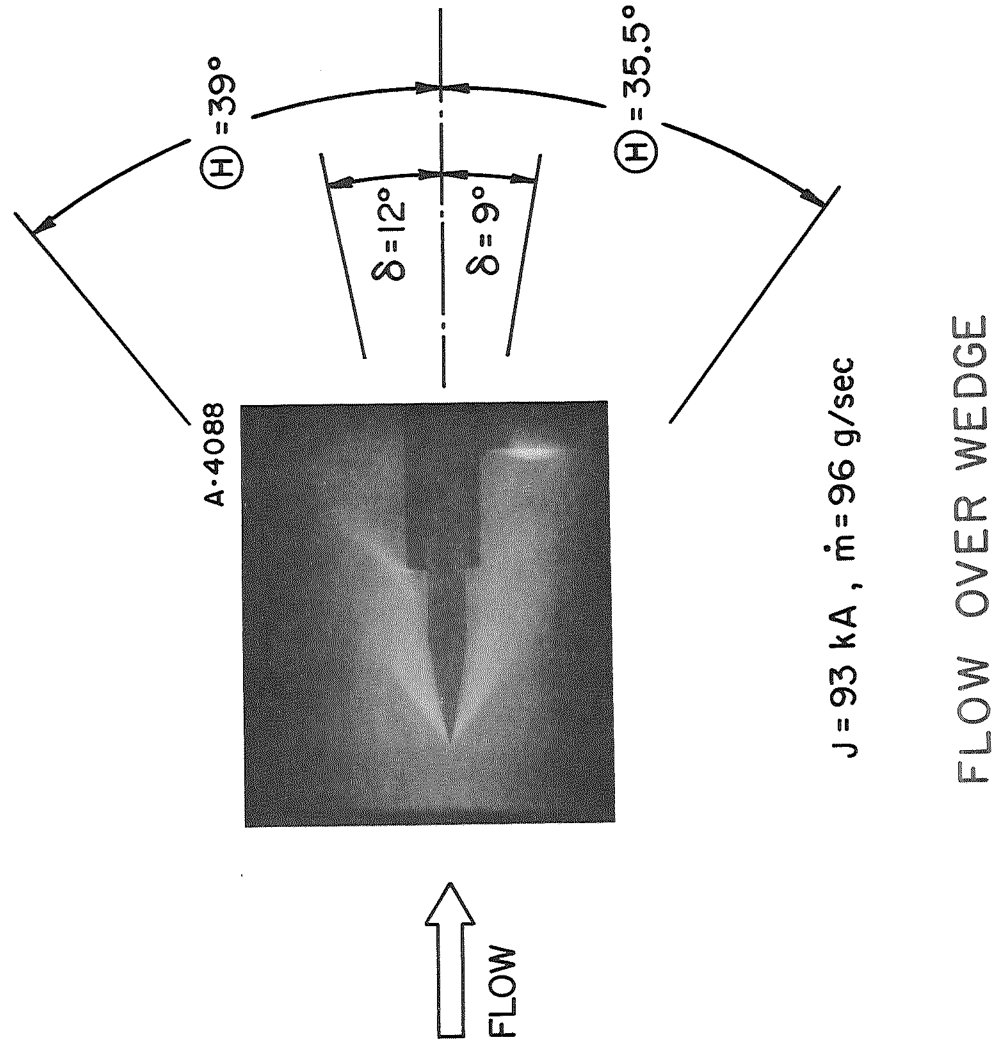

FIGURE 12

AP 25 P 357 70

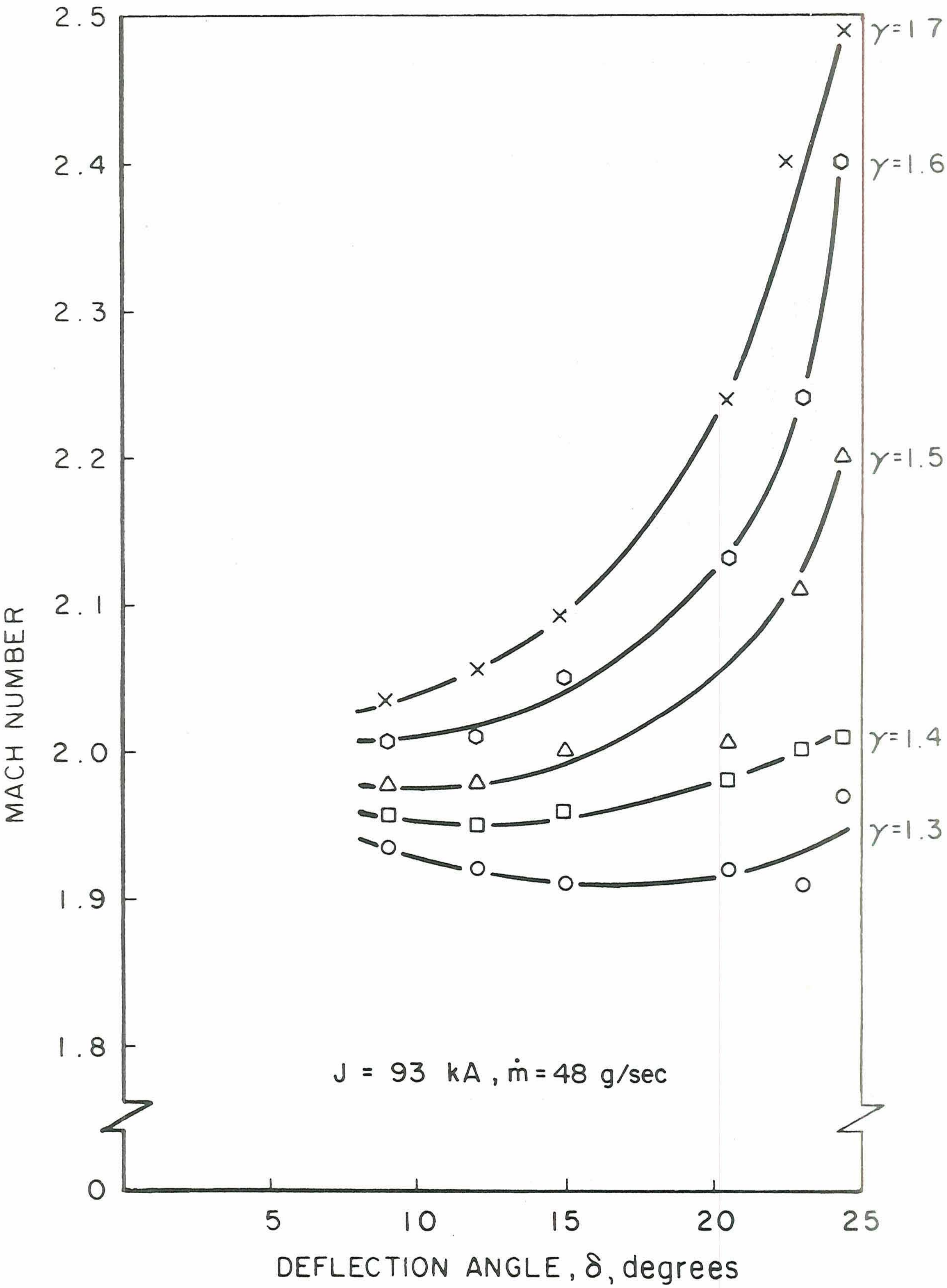

MACH NUMBER AS FUNCTION OF DEFLECTION ANGLE

FIGURE 13

AP 25 R 4625 70 A

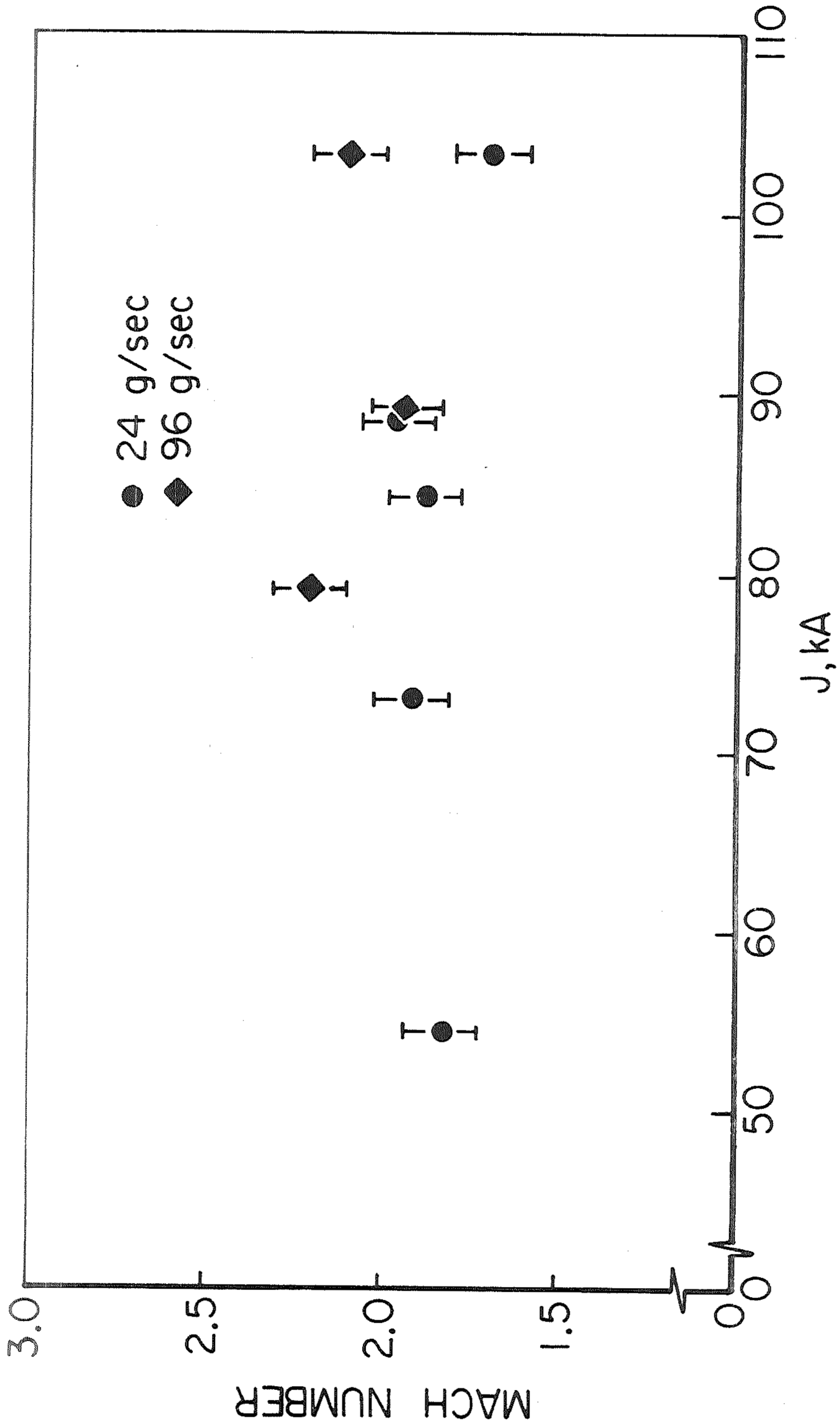

MACH NUMBER AS A FUNCTION OF CURRENT

FIGURE 14
AP 25 4675 70 A

D. Terminal Voltage

To obtain the quasi-steady current-voltage characteristics of the accelerator, it is necessary to ascertain that all inductive components of the terminal voltage associated with propagation of the discharge current distributions have subsided to negligible value. One voltage probe, V_M, is connected downstream of the current distribution, as shown in Fig. 10, so that the circuit composed of the probe and discharge links no magnetic flux. This probe thus records the sum of the resistive voltage drop and motional emf across the accelerator. Any inductive voltage associated with a time derivative of the total discharge current, or with a motion of the current distribution, is monitored with a voltage probe connected to a "D" loop. This consists of one turn of wire, insulated from the electrodes and fastened along the edge of the channel sidewall. The circuit, formed in a plane perpendicular to the plane of the electrodes, encloses the same magnetic flux as the accelerator.

A typical simultaneous record of current J, downstream voltage V_M, and inductive voltage V_D taken at the 89 kA-96 g/sec operating condition is shown in Fig. 15. The current remains constant over a large fraction of the pulse. The inductive voltage drops to less than 10 V some 60 μsec after pulse initiation, indicating that gross motions of the current distribution have subsided. At approximately the same time, the downstream voltage, V_M, achieves a plateau which lasts 140 μsec, indicating a quasi-steady regime of operation.

The measured plateau in the downstream voltage, V_M, as a function of discharge current, for three different input mass flows is presented in Fig. 16. Note that the voltage is nearly linear with current for a given input mass flow, and that the slope of the current-voltage characteristic increases with decreasing mass flow. To interpret these characteristics further, it is necessary to determine the velocity of the plasma in the accelerator.

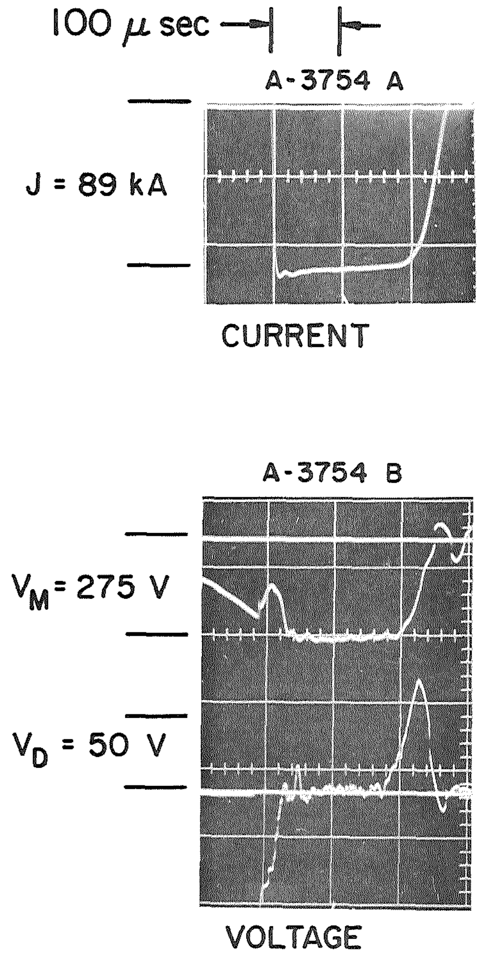

CURRENT AND VOLTAGE SIGNATURES
$J = 89$ kA, $\dot{m} = 96$ g/sec

FIGURE 15
AP25 P 358 70

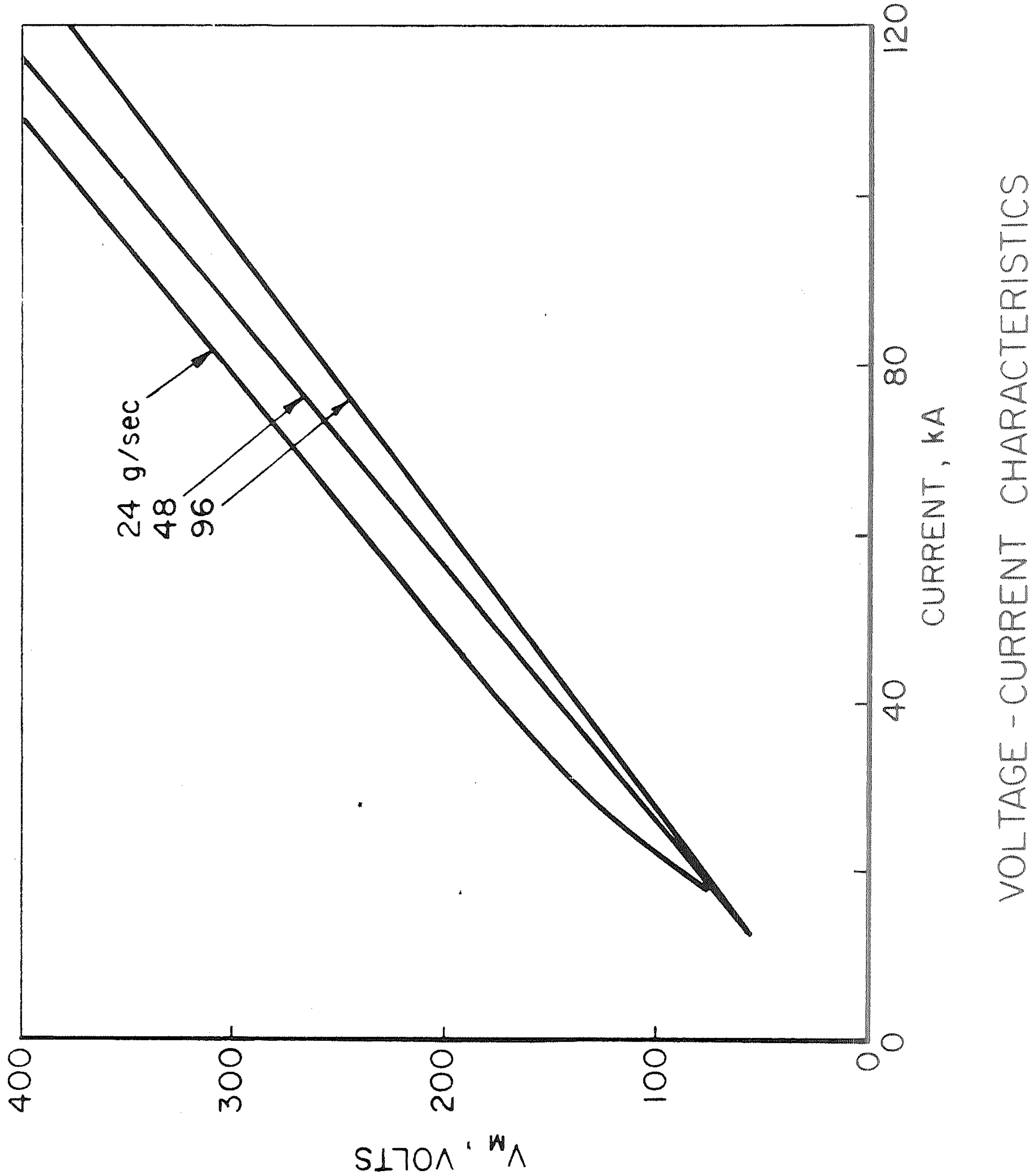

FIGURE 16
AP 25 R 4623 70 A

E. Velocity Measurements

Measurement of plasma velocity downstream of the acceleration zone is desirable for several purposes: (a) it participates directly in any momentum balance calculation; (b) it complements constructively the Mach number observations, (c) it is needed to compute the motional emf; and (d) it is the most interesting property from a propulsion standpoint. Of the various methods available for velocity measurement, a standard Doppler-shift technique has been employed because of its simplicity, and its relation to the temperature measurement discussed below.

The experimental arrangement compares optical spectra observed along two lines of sight through a common point in the plasma, one of which makes an angle of 51° with the flow direction, and the other of which makes an angle of $\pi - 51^{\circ}$. Each beam illuminates one-half of the entrance slit of a Steinheil GH glass prism spectrograph of linear dispersion from 5.4 to 40 Å/mm over the range 4300 Å to 6600 Å. The plasma region observed corresponds roughly to the location of the airfoil shown in Fig. 12, i.e., about 8 in. downstream of the electrode-insulator junction. The resulting spectra are photographed with open shutter, and therefore represent an integrated record of the discharge over the full length of the pulse. However, since it was found in the course of the photographic observation of the flow that the maximum radiance occurs during the quasi-steady portion of the pulse, it is presumed that the measured Doppler shifts correspond to actual velocities during quasi-steady operation. The velocities determined in this way are plotted as a function of current for the 24 g/sec and the 96 g/sec input mass flows in Figs. 17 and 18 respectively. Each point represents the average of the velocities obtained from the 4348.11 Å AII, 4401.02 Å AII, and 4426.01 Å AII lines. All of the averaged values are contained within the error bars. The velocities are seen to increase with current for a given input mass flow, and to decrease with

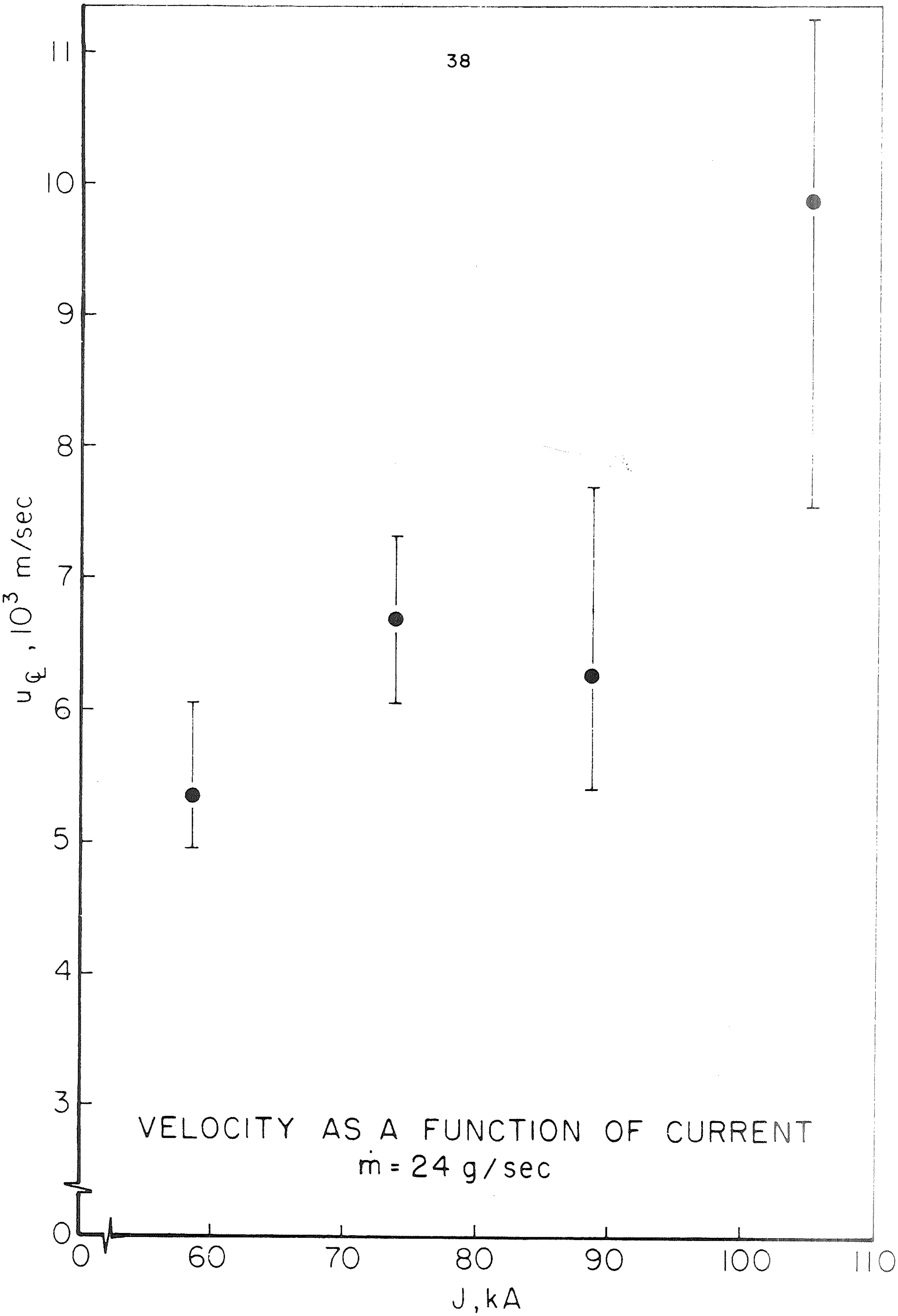

FIGURE 17

AP 25 R 4676 70

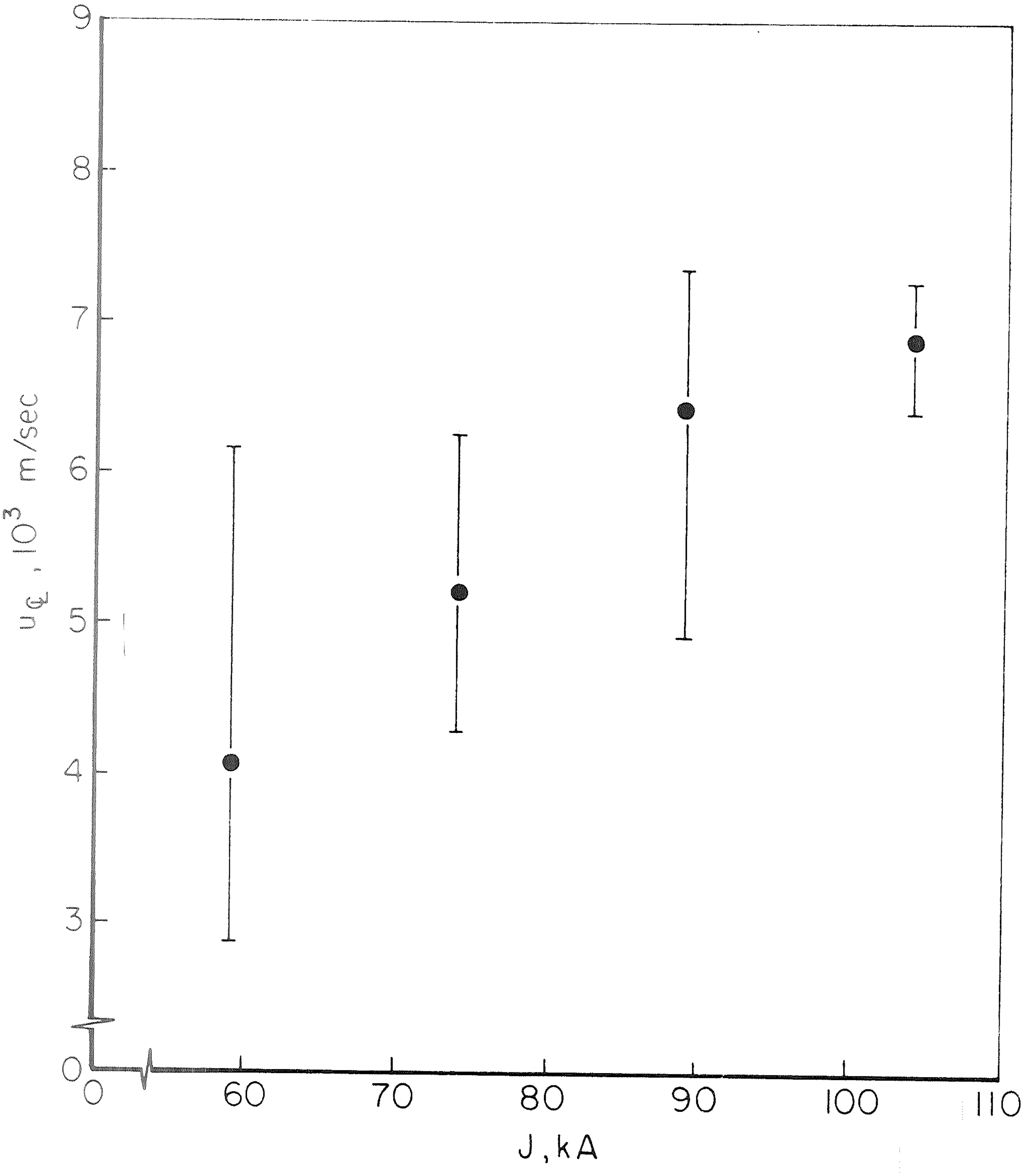

VELOCITY AS A FUNCTION OF CURRENT, $\dot{m}$ = 96 g/sec

FIGURE 18

AP 25 R 4677 70

increasing mass flow for a given current. The maximum velocity observed is 10^4 m/sec, for the 104 kA, 24 g/sec operating condition. The minimum velocity is 4×10^3 m/sec for the 59 kA, 96 g/sec condition.

F. Temperature Measurements

To compare the measured plasma velocity with the Mach number data, it is necessary to estimate the local sound speed in the plasma. If the plasma can be treated as an ideal gas, a measurement of the temperature, coupled with previously determined value of γ should suffice to calculate the sound speed. To this end, a Fabry-Perot interferometer was introduced in the optical path just in front of the object lens of the spectrograph. The interferometer spreads the intensity distribution of each spectral line into a system of concentric rings which are imaged on the entrance slit of the spectrograph. The temperature may then be calculated from the radius and half-width of the rings recorded on photographic film.[A-12] Temperatures obtained from the 4401.02 Å AII and the 4426.01 Å AII lines observed in the midplane are plotted as a function of current in Figs. 19 and 20 for the 24 and 96 g/sec input mass flows. The temperatures appear to increase with current at a fixed mass flow, and to decrease with increased mass flow at fixed current. The highest temperature observed is about 10^5 °K, for the 104 kA, 24 g/sec operating condition, while the lowest is 3×10^4 K, corresponding to the 74 kA, 96 g/sec operating condition.

G. Interpretation

Relation of the elements of data described above to the central interest of the study--the energy deposition ratio--can be attempted in several ways, but each of these must view the problem in a terminal or "black box" fashion. We have

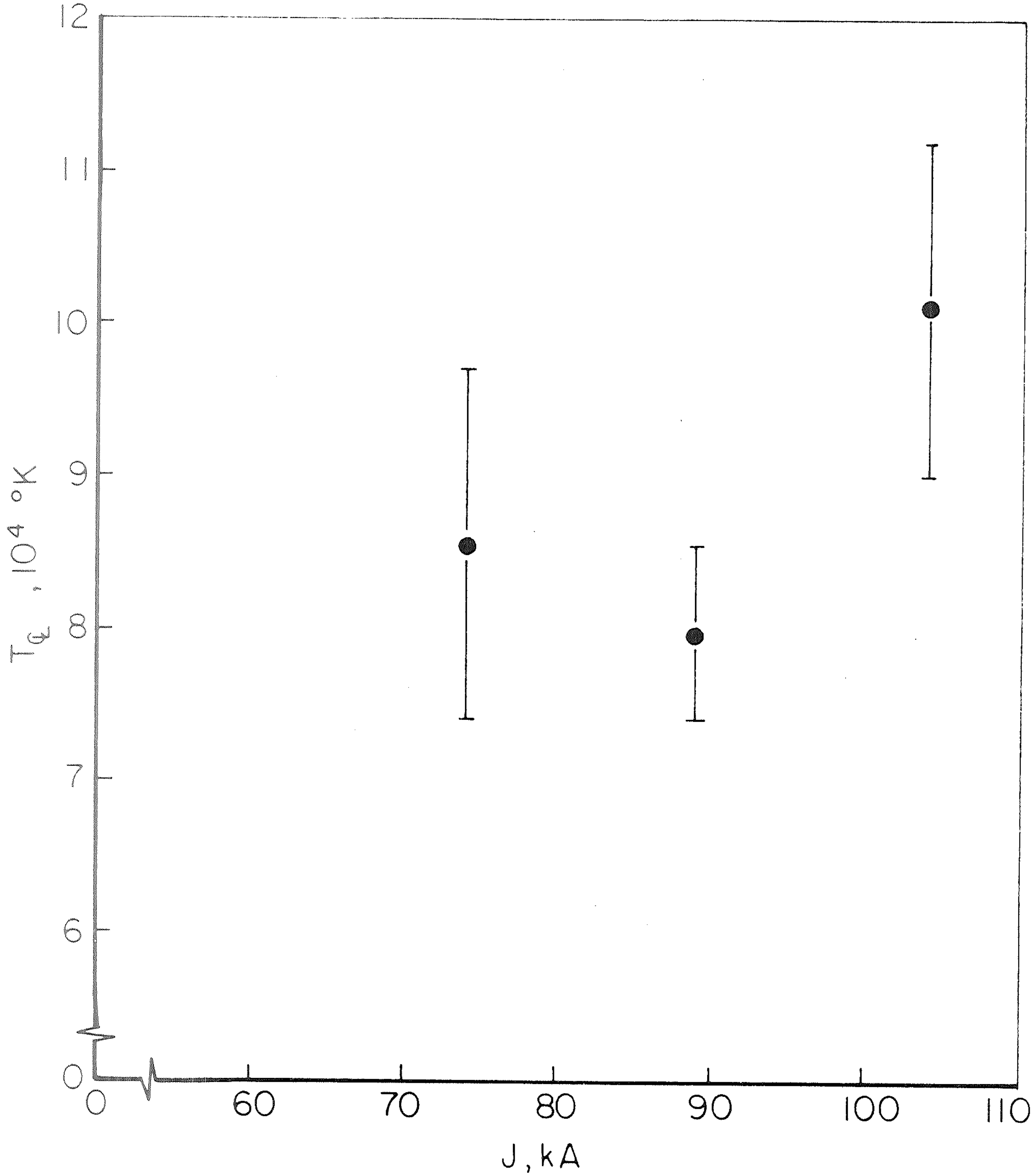

MIDPLANE TEMPERATURE AS A FUNCTION OF CURRENT
$\dot{m} = 24$ g/sec

FIGURE 19
AP 25 R 4678 70

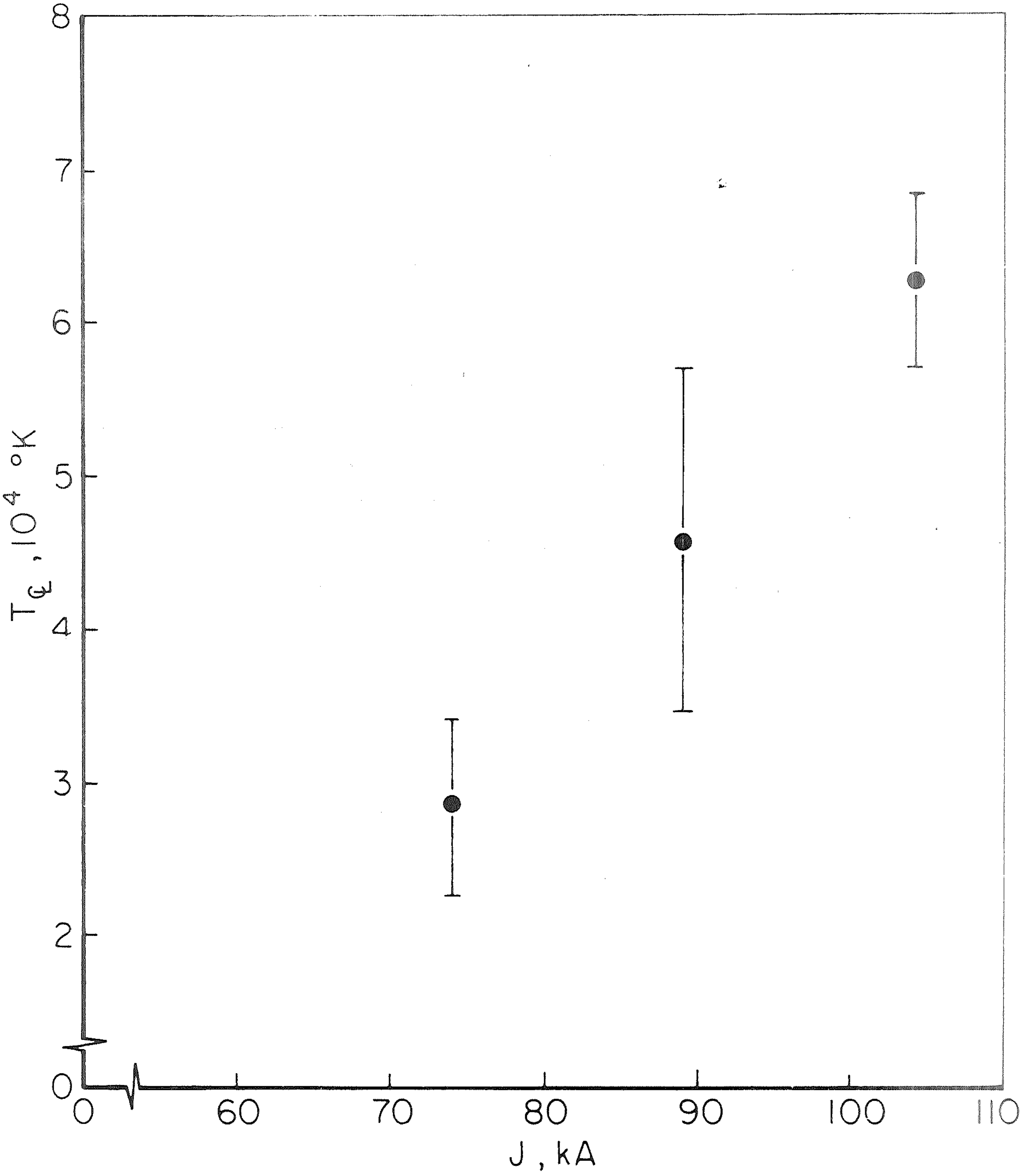

MIDPLANE TEMPERATURE AS A FUNCTION OF CURRENT
$\dot{m}$ = 96 g/sec

FIGURE 20
AP 25 R 4679 71

insufficient knowledge of the detailed structure of the field, current, mass flow, and thermodynamic patterns within the discharge region to attempt any analysis of this acceleration zone, and such formulation would doubtless become intolerably complex even if the interior data were available. Rather, the arguments shall be based solely on observed properties of the flow into and out of the acceleration zone, and on the terminal electrical parameters of the accelerator. Even on this basis, several complications are involved in translating the experimental data into the desired information, associated with the complex nonequilibrium state of the working fluid, and with the introduction of spurious mass into the flow through electrode and insulator erosion. To keep track of such effects, it is best to proceed rather deliberately via the conservation relations.

The one-dimensional momentum equation can be written in the jump form

$$F(u - u_1) + (p - p_1) = \frac{B_1{}^2}{2\mu} \qquad \text{(II-1)}$$

where $F = \rho u = \dot{m}/A$ is the mass flow per unit area, u and u_1 are the downstream and upstream velocities, p and p_1 the corresponding static pressures and B_1 is the upstream magnetic field and is related to the total arc current J by amperes law:[61]

$$B_1 = \frac{\mu_o J}{w} \qquad \text{(II-2)}$$

with w the width of the accelerator channel. Viscous forces have been omitted from the momentum equation on the basis of the observed negligible downstream deceleration and an elementary skin friction calculation. Henceforth we also shall neglect p_1, which has been measured to be about 10 Torr, and u_1 which is at best sonic at room temperature.

Downstream pressure, p, has not been measured, but is calculated from the measured temperature and known mass flow using an empirical equation of state. Our best experimental indications are that the downstream plasma is essentially fully (singly) ionized, and that the electron temperature is about 1.5 eV. We thus write:

$$p = nk(T_i + T_e) \tag{II-3}$$

where p is the total pressure, $n = n_i = n_e$ is the heavy particle of free electron density, alternatively, computed from the known mass flow and measured velocity, and $T_i > T_e$ are the measured ion and electron temperatures respectively.

Table II-1 assembles various properties of the downstream flows for several operating conditions, and also displays the results of other subsidiary calculations discussed below.

Table II-1. Momentum Balance

$\dot{m}$(gm/sec)...	24	24	24	96	96	96
J(10^3 A)....	104	89	74	104	89	74
u(10^3 m/sec)	9.8	7.3	6.8	6.9	6.4	5.2
T_i(10^4 °K)..	8.8	6.8	7.2	6.6	4.9	3.0
p(10^3 n/m^2).	7.0	7.6	8.5	32	30	24
M_p/M.......	1.9/1.9	1.5/1.9	1.4/1.9	1.5/2.1	1.5/2.1	1.5/2.1
Fu + p (10^3 n/m^2)..	38	31	31	120	120	100
$B^2/2\mu$ (10^3 n/m^2)..	300	220	150	300	220	150
$\dot{m}_p$(gm/sec)..	190	170	120	250	170	140

The column labeled M_p/M compares a Mach number, M_p, computed as $(\rho u^2/\gamma p)^{1/2}$, to the Mach number extracted from the wedge shock angles, and serves merely to indicate the level of consistency of the velocity, temperature, and Mach number data within the framework of the assumed equation of state. It is tempting to regard the ratio of downstream pressure, p, to the inertial term, Fu, as an index of the thermal dissipation of the accelerator, but because of the complex state of the flow this assessment must be deferred until the energy relation is considered. What must be dealt with here is the evident discrepancy between Fu + p and the driving magnetic body force $B^2/2\mu$. The clue to this problem probably lies in the increase in the size of the discrepancy as the ratio of current to mass flow increases, which is reminiscent of the tendency of conventional MPD arcs to ablate insulator and electrode material, or to re-ingest background gas when their external mass supply drops below a critical or "matched" value.[116] We believe the parallel-plate device is particularly vulnerable to such involvement of spurious mass because of the relatively large ratio of electrode surface area to channel cross section, the high downstream pressure in the confined channel, and the large reservoir of gas trapped in the electrode gap at the time of discharge initiation. The column labeled $\dot{m}_p$ is a calculation of the mass flow from all sources that would just balance the momentum equation. Note that this "effective mass" varies with the discharge current in much the same manner as the empirical relation for critical mass flow in an MPD arc, i.e., $\dot{m}_p \sim J^2$.[101,A-13]

Leaving this matter for the moment, we turn to the one-dimensional energy equation in the form

$$\left(h + \frac{u^2}{2}\right) - \left(h_1 + \frac{u_1^2}{2}\right) = \frac{1}{\dot{m}}\,(VJ - P_r - P_e) = \alpha\frac{VJ}{\dot{m}} \qquad \text{(II-4)}$$

where h is the plasma enthalpy, V the total voltage drop across the discharge, and P_r and P_e account for power losses to radiation and to the electrodes respectively. The inlet kinetic energy is again quite negligible, and the enthalpy change is evaluated on a two-fluid approximation:[103]

$$h - h_1 = \int_{T_1}^{T_e} C_p dt + \frac{5}{2} R \int_{T_e}^{T_i} dt \qquad \text{(II-5)}$$

where, as before, the electron temperature which is presumed to establish the ionization level is set at 1.5 eV. The first term may be read from a Mollier chart, the second is evaluated directly for each observed value of ion temperature. No direct measurements of radiation loss or heat transfer to the electrodes have been made in this accelerator. In a coaxial MPD accelerator of comparable size and range of operation it appears that the radiation loss is a few percent of the total input power, and that the anode and cathode falls are about 10 and 20 V, respectively.[106,115] Based on these analogies, we estimate that somewhere between 10% and 20% of the input power is lost to radiation and to the electrodes, and for the following estimates an empirical factor $\alpha = 0.85$ is used to denote the fraction of input power available to the flow.

Table II-2 displays the various components of the energy equation, along with the ratio $(u^2/2)/(h - h_1)$, which is our first true indication of the energy deposition ratio. Also included in the table is a calculation of the motional emf in the form

$$V_{uB} = uB_1 sQ \qquad \text{(II-6)}$$

where B_1 is the upstream magnetic field, u is the downstream velocity, s is the interelectrode gap, and Q is a nondimensional factor associated with the profile of u and B across the current distribution, which can be shown to be roughly one-quarter for any reasonable cases.[117] The comparison of $(V_{uB})/(\alpha V - V_{uB})$ with $(u^2/2)/(h - h_1)$ lends some credibility to both calculations.

Table II-2. Energy Balance

$\dot{m}$(gm/sec)	24	24	24	96	96	96
J(kA)	104	89	74	104	89	74
V(volts)	380	330	290	330	280	240
$h - h_1$ (m^2/sec^2)	89×10^6	81×10^6	83×10^6	75×10^6	68×10^6	61×10^6
$u^2/2$ (m^2/sec^2)	48×10^6	27×10^6	23×10^6	24×10^6	20×10^6	14×10^6
$(u^2/2)/(h-h_1)$	0.54	0.33	0.28	0.32	0.29	0.23
V_{uB}(volts) ...	107	70	54	75	60	40
$(V_{uB})/(\alpha V-V_{uB})$	0.51	0.33	0.27	0.37	0.33	0.25
$\alpha VJ/\dot{m}$ (m^2/sec^2)	1400×10^6	1000×10^6	760×10^6	304×10^6	220×10^6	160×10^6
$\dot{m}_e$ (gm/sec) ...	250	230	170	300	240	200
$\dot{m}_e/\dot{m}_p$	1.33	1.34	1.41	1.21	1.46	1.42

Again there appears a substantial discrepancy in the overall balance, in this case between the total input power to the flow, $\alpha VJ/\dot{m}$, and that accountable in the sum of kinetic energy,

$u^2/2$, and enthalpy, $h - h_1$. This again suggests that the accelerator is employing considerable spurious mass. The column labeled $\dot{m}_e$ denotes the total mass flow from all sources that would just balance the energy equation. Note again that these values scale roughly as J^2, and that their magnitude is comparable with the calculation of $\dot{m}_p$ from the momentum balance. Ideally, one would like to operate this accelerator in a regime where the injected mass flow was adequate to match the arc current on the indicated scale, but at present various experimental limitations preclude this. Indeed, the original experiments were just so designed, but on the basis of the matching criterion experienced for coaxial MPD arcs, $\dot{m} \geqslant 2 \times 10^{-2} J^2$ gm/sec-kA^2, rather than that indicated by the above experiments for this accelerator, $\dot{m} \geqslant 3.5 \times 10^{-2} J^2$ gm/sec-kA^2.

Returning to the energy deposition as indicated by either of the measured ratios $(u^2/2)/(h - h_1)$ or $(V_{uB})/(\alpha V - V_{uB})$, we conclude that the discharge itself imparts less energy to the flow by direct body-force acceleration than by resistive heating. In the absence of downstream expansion, this inevitably predicates rather low exhaust speeds and high downstream pressures and temperatures, as observed. Conversely, it seems reasonable to infer that the comparatively high exhaust speeds found in conventional MPD arcs of the same power must be derived in substantial part from electrothermal conversion from the high enthalpy arc plasma, via the downstream expansion permitted in that geometry.

III. SELECTION OF PROGRAMS IN PROGRESS

A. Spectroscopic Studies (Von Jaskowsky)

Previous spectroscopic studies of the electron density patterns throughout a quasi-steady MPD arc discharge at 17.5 kA x 1 msec x 5.9 gm/sec argon mass flow[103,107] have been extended to yield ion temperatures and flow velocities in the exhaust plume. Again the data have been recorded without attempt at time resolution, based on two a priori evidences of the quasi-steady nature of the optical phenomena:

1. The time-resolved signal from an indicator of the emitted radiation is found to be constant over 600 μsec of the 900 μsec current pulse (Fig. 21).

2. The patterns of color and the level of radiance recorded in Kerr-cell photographs of the arc discharge stay constant over almost the entire duration of the current pulse.

The method of temperature measurement takes advantage of the high spectral resolution of a Fabry-Perot interferometer to obtain the width of various lines of AII and CIII which are present in the spectrum. The experimental arrangement differs from that described previously[103] in the use of an interim image of the object space by an additional lens (Fig. 22). A typical spectrogram of the axial region 1 cm upstream of the anode is shown in Fig. 23. Ion temperatures thus determined by observation of a projected area of $\approx$ 0.65-cm height by 0.05-cm width on the discharge axis at four axial stations are noted on Fig. 24. Each temperature point is the average of determinations from two to eight spectral lines of widely different wavelengths. The magni-

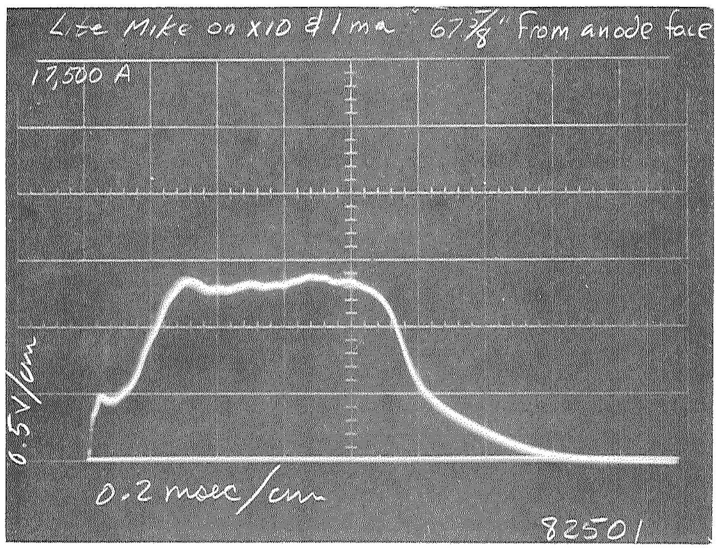

RADIANCE FROM DISCHARGE

FIGURE 21
AP 25 P-356 70

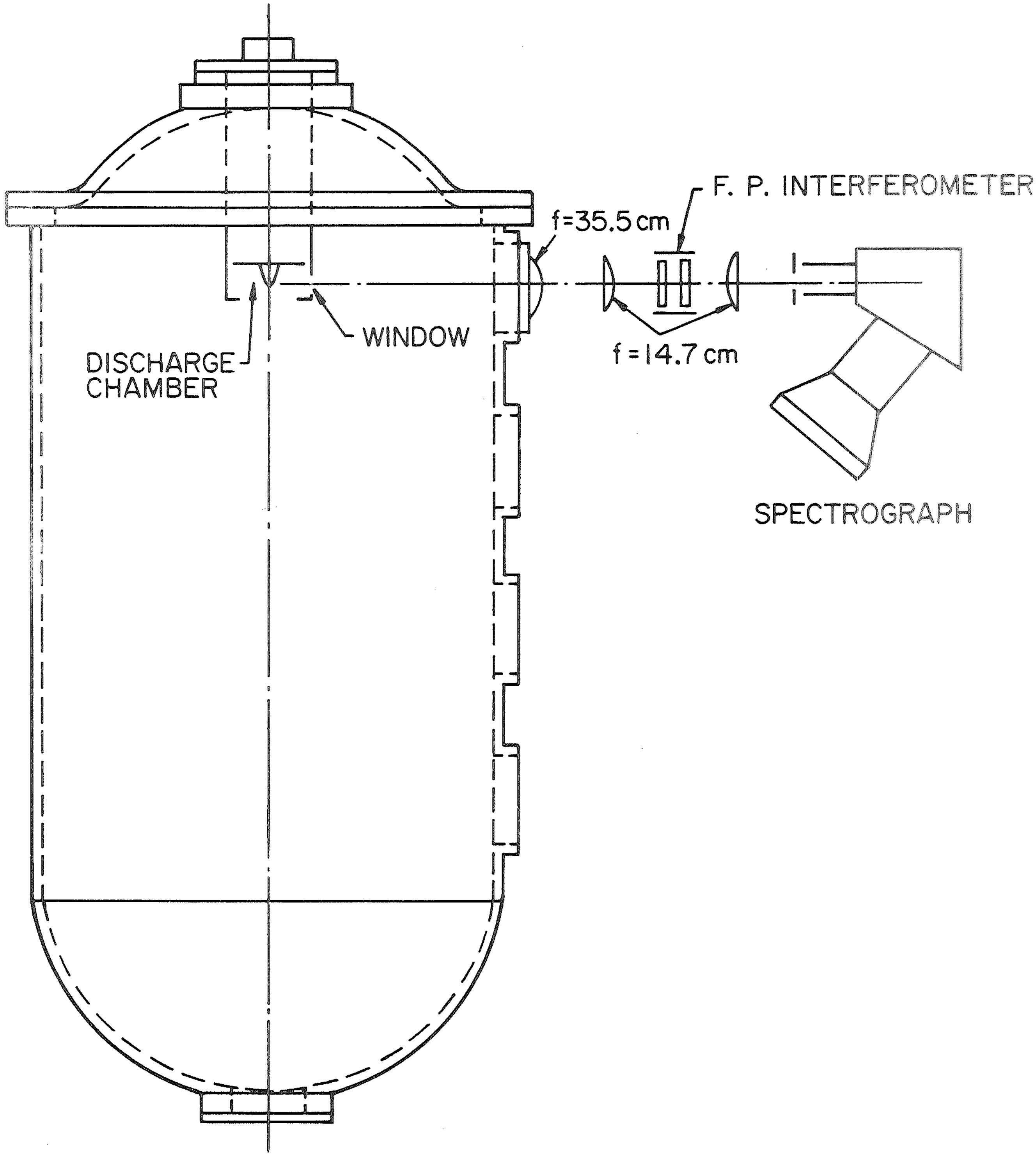

ARRANGEMENT FOR SPECTROSCOPIC STUDIES

FIGURE 22
AP 25 R 4695 71

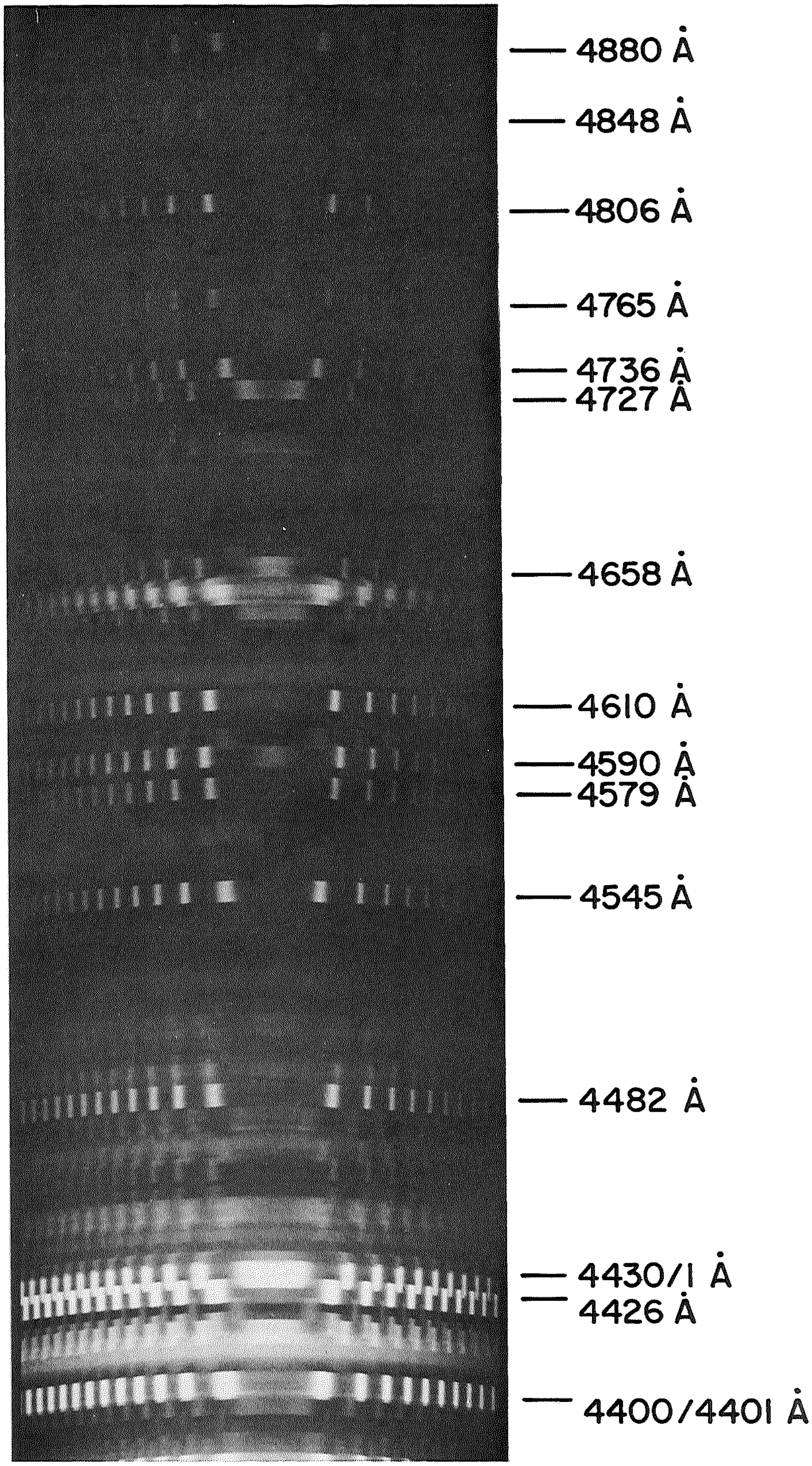

SPECTROGRAM 1 cm UPSTREAM OF ANODE

FIGURE 23
AP 25 P-364 71

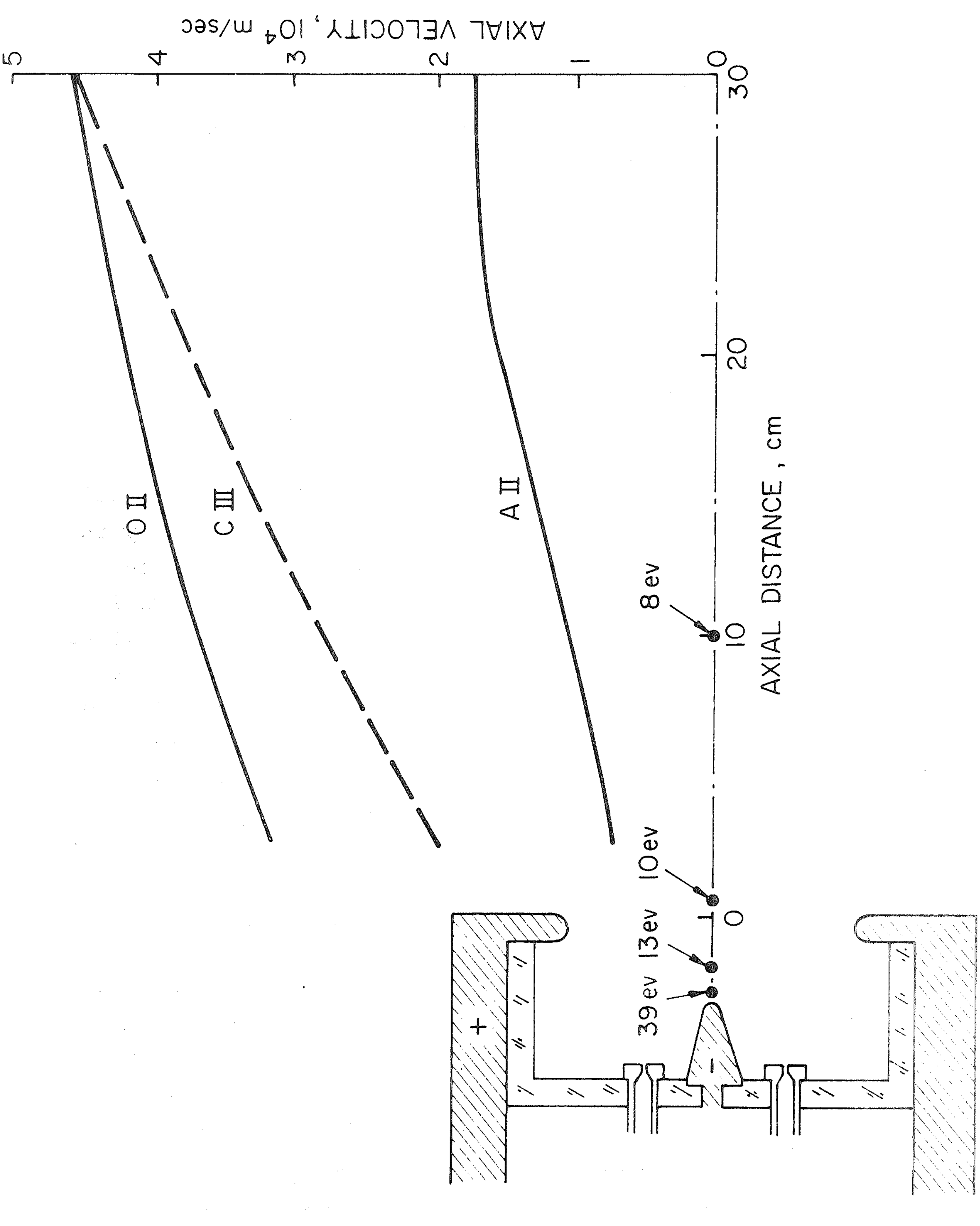

TEMPERATURES AND AXIAL VELOCITIES

FIGURE 24
AP 25 R 4696 71

tude of these temperatures is of interest, in the first instance, as an indication of the fraction of the input energy which is initially deposited in the random thermal energy of the flow, compared to its eventual organized streaming energy. Further, the axial profile of these temperatures offers some indication of the thermodynamic conversion in the exhaust process. In this case we note a relaxation of temperature from about 40 eV near the cathode tip, to less than 10 eV downstream of the anode orifice, where we know from velocity measurements that the streaming kinetic energy is of the order of 100 eV.

One form of velocity measurement employs direct observation of the Doppler shift of selected spectral lines. When the radiating object of a spectroscopic observation has a significant component of velocity along the line of sight, the observed frequencies will be shifted in proportion to the flow velocity and can thus be directly read from the spectrogram. The experimental arrangement used to exploit this effect is shown schematically in Fig. 25. The enlargement of a portion of a typical record obtained with a slit width of 1.25×10^{-3} cm (0.073 Å) is shown in Fig. 26. One upper half of the spectrogram contains the unshifted line; the lower half the Doppler-shifted line. Observed shifts range from 0.17 Å for AII lines to as much as 0.43 Å for OII, compared to line widths of about 0.2 Å. Since all emitters along the line of sight contribute to the line image, the line shape may be distorted by contributions from emitters moving at different velocities, at other than the desired object portion of the discharge. The reduction of such spectral records to yield axial velocity profiles with radius clearly requires knowledge of integrated radiance across the entire exhaust beam. The curved spectral lines produced by this particular prism spectrograph do not lend themselves to unfolding of this sort, and hence only approximate values of even the axial velocities can be deduced from the shifts. The results, shown in Fig. 24, display a sizeable discrepancy between the argon velocities and those of impurities like oxygen. While this is by no means yet understood, it may be speculated that flow of such particles is confined to a region

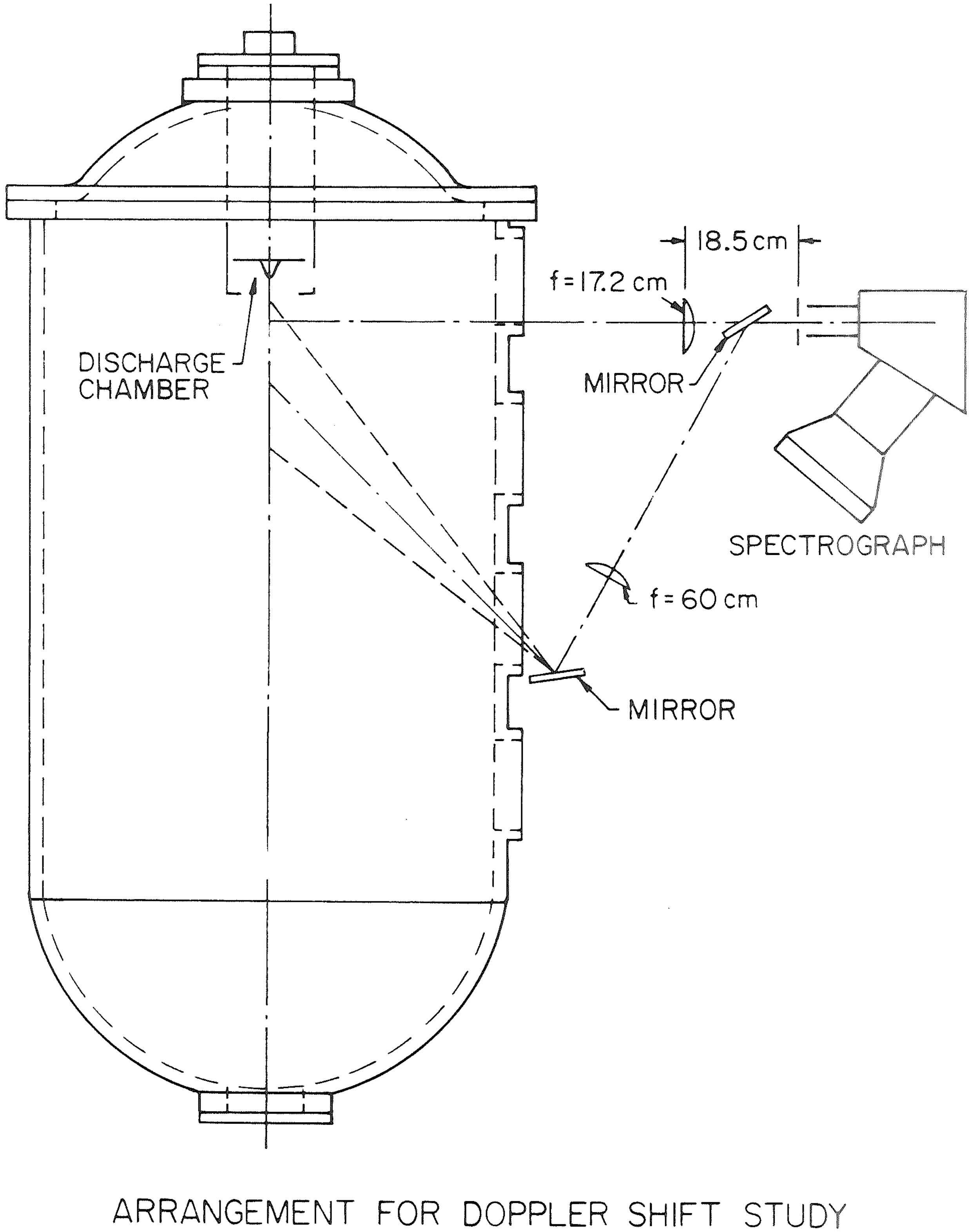

ARRANGEMENT FOR DOPPLER SHIFT STUDY

FIGURE 25
AP 25 R 4694 71

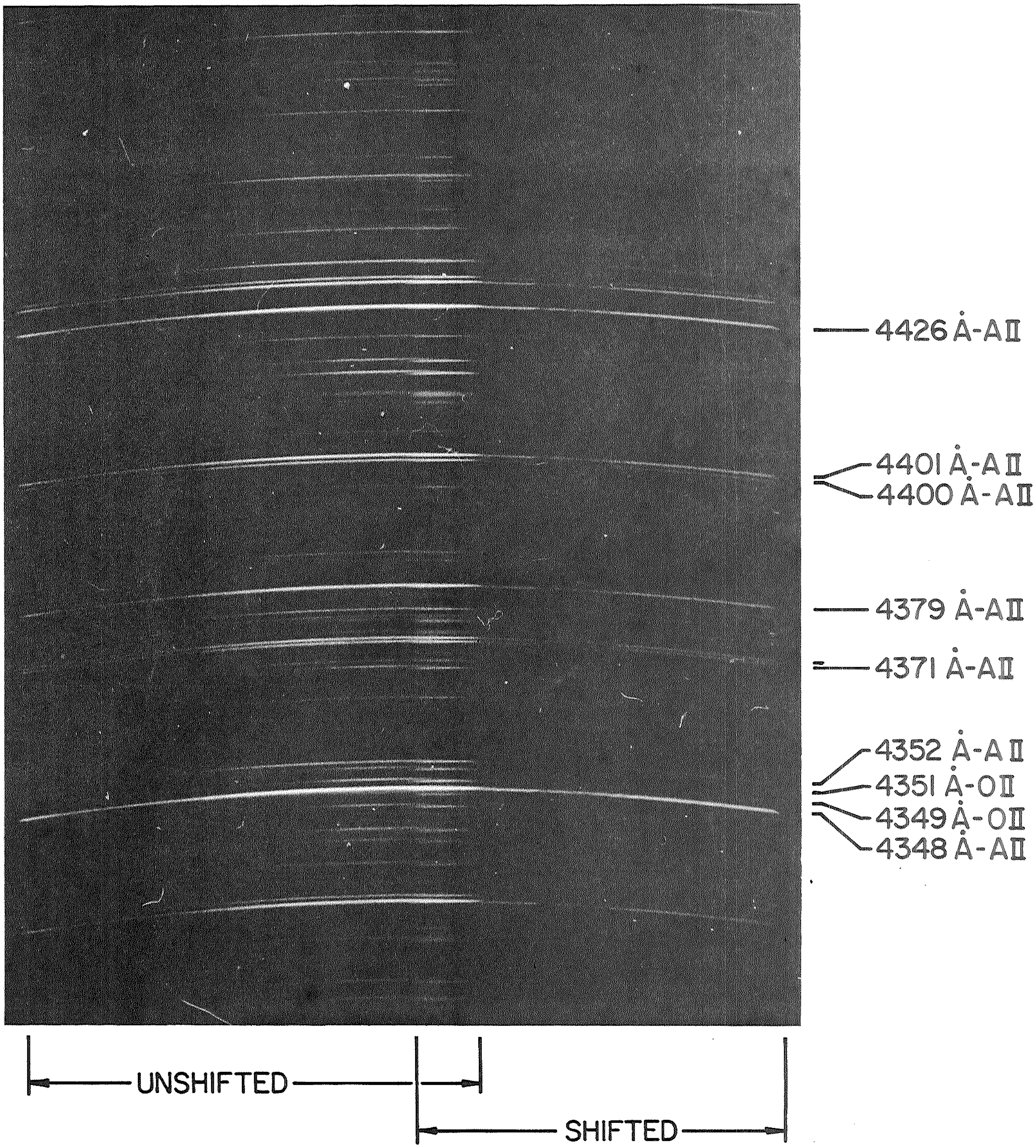

SPECTRUM WITH DOPPLER SHIFT

FIGURE 26
AP 25 P-363 71

around the axis. If so, their measured line shifts would be less susceptible to reduction by inclusion in the line of sight of slower velocity radiators from the outer portion of the plume. That is, the plume may have a high-velocity core, of whose speed the impurities are the best indicators.

B. Measurements for the Jump Model (Cory)

To explore the applicability of MHD jump relations[103] to the acceleration zone of our MPD arcs, it is desirable to obtain data on three properties heretofore not studied. In order of difficulty these are tht total radiation energy loss, the dynamic pressure profile in the jet, and the chamber pressure upstream of the arc. Knowledge of these, combined with previous data on other downstream flow properties and terminal parameters, should completely specify--indeed overspecify--the jump conditions. This redundancy is actually desirable to guard against cumulative effects of many small errors in the measurables, and to check the initial assumption of the model.

The radiation loss has now been estimated by recording the incident flux on an EG&G Model 560 Lite-Mike which has been absolutely calibrated (see Fig. 27a). Assuming spherical symmetry and neglecting the sensitivity decay of the lite-mike at wavelengths far from its optimum of 0.8 μ, the indicated radiation loss from the plasma is at the rate of 3×10^4 W or about 1% of the total applied power. Correction for the spectral sensitivity profile of the instrument will raise this estimate somewhat. At present, a low dispersion monochrometer is being used to determine the spectral distribution of energy in the visible range. This, together with the lite-mike wavelength via sensitivity calibration will allow the radiated energy in the visible to be calculated more precisely.

Preliminary values of the dynamic pressure in the jet have now been obtained with pressure probes of the type developed here by York.[72,82,102] Thermal, electrostatic, induced EMF, and

9104

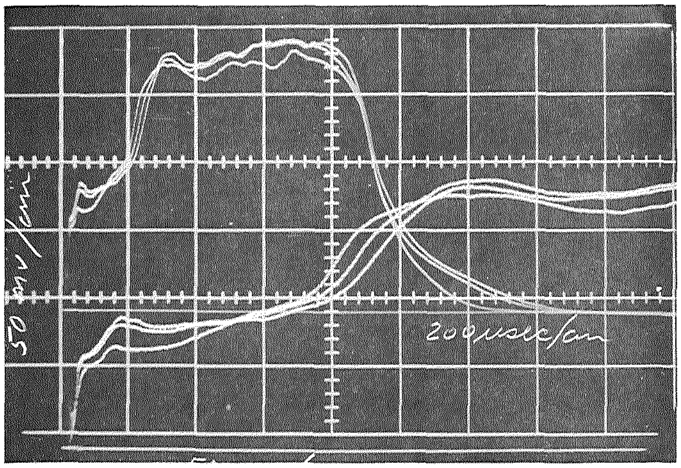

200 μsec/DIV

50 μsec/DIV

a) RADIATION FLUX HISTORY ON AXIS, 1.71 m FROM ANODE

91604

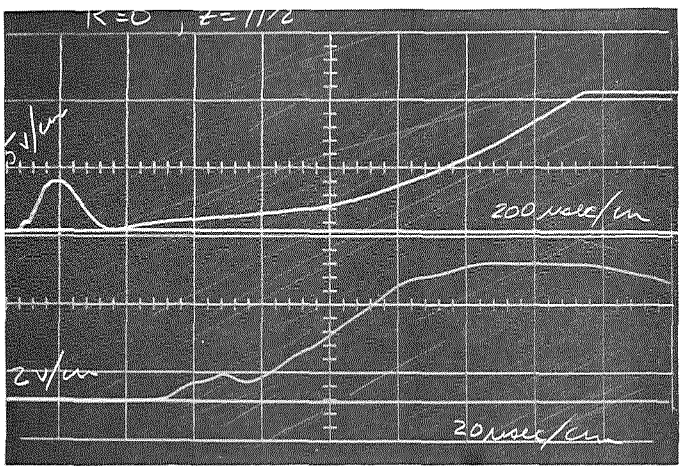

200 μsec/DIV

20 μsec/DIV

b) DYNAMIC PRESSURE (AND NOISE) SIGNALS

FIGURE 27

AP 25 P-362 71

acoustic noise have so far complicated efforts to obtain precise dynamic pressure histories for a 10^{-3} sec pulse, but some results have been obtained. The initial plateau on the lower trace of Fig. 27b indicates a dynamic pressure of ~ 3200 Nt/m^2, which compares well with the value of 4250 Nt/m^2 calculated from other data on downstream velocity and density. Moving the probe to different axial locations changes the time location of the plateau in agreement with the velocity probe indication of the arrival of the plasma, confirming that the pressure probe reacts to the plasma, not noise, in this portion of the flow. Unfortunately, subsequent behavior, as indicated on the upper trace of Fig. 27b is completely unreasonable, indicating that at these later times noise problems do arise, or the probe ceases to respond properly to the flow for other reasons.

A new type of pressure probe has been constructed to reduce the noise pick up at some expense of response time. This probe consists of a dielectric stub which transmits pressure, but not heat, electrical charge, or induced EMF to a thoroughly shielded PZT-5 piezoelectric crystal, and a backing rod whose function is to contain the propagating pressure wave for at least 10^{-3} sec to prevent reflected acoustic noise. The final design has not been fixed, as yet, but the present device (Fig. 28) uses 3/8-in. Plexiglas rod and provides a rise time of about 70 μsec, a 1.2 msec undistorted readout time, and 1 V/10 Torr sensitivity.

This probe has also proven serviceable for determination of the arc chamber pressure, upstream of the current zone. In this application it has a noise-equivalent background signal corresponding to less than 5 Torr. Since substantially higher chamber pressures are to be expected, we are optimistic that this device will faithfully reproduce their profiles throughout the entire pulse duration. In addition to its use in the jump model, chamber pressure data will shed considerable light on the long-standing question of the role of electrothermal effects in the overall acceleration process.

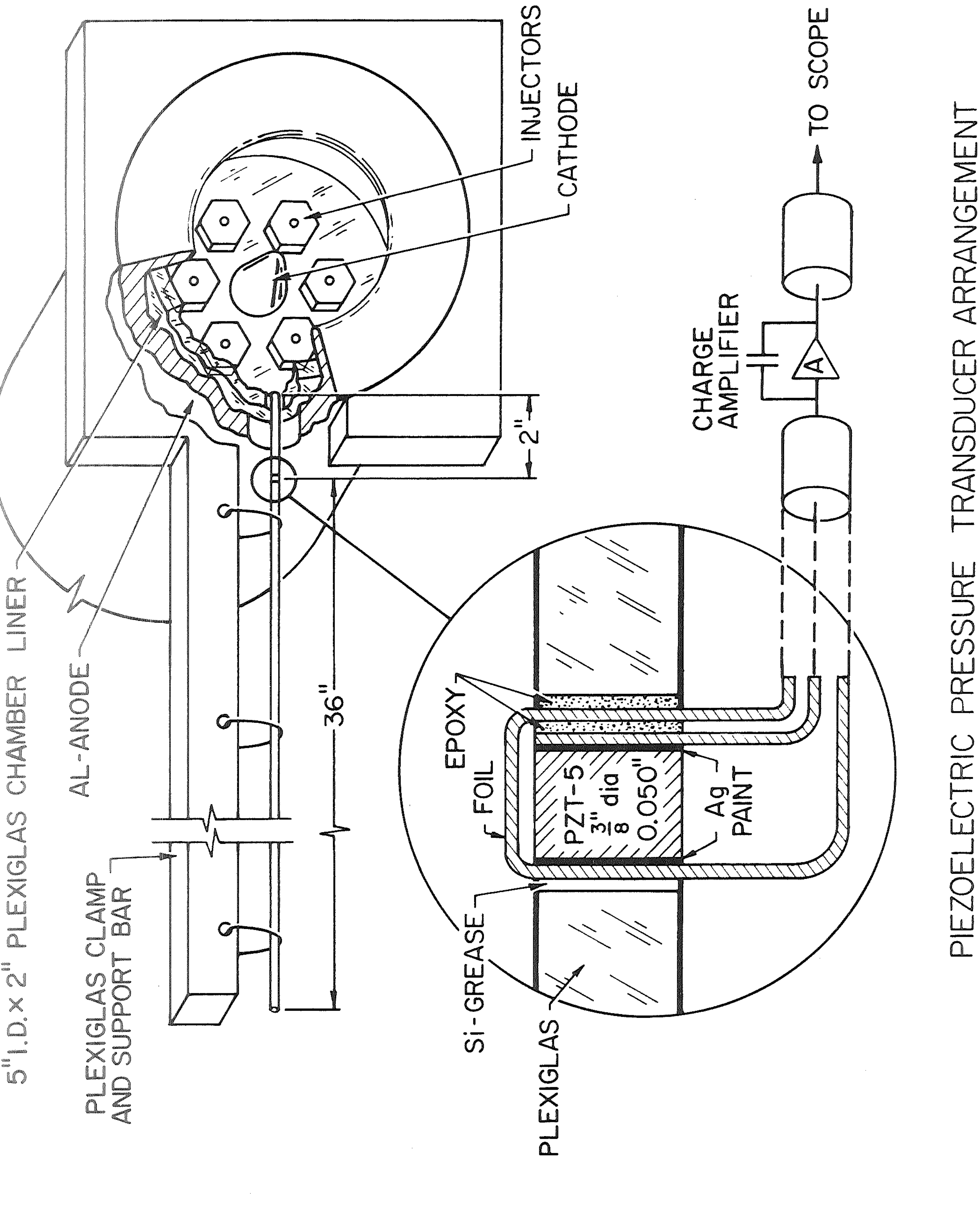

FIGURE 28
AP 25 R 4697 71

C. Anode-Size Effects in MPD Operation (Clark)

Recent terminal voltage measurements obtained at the Avco Laboratory on a quasi-steady arc configuration similar to that studied here indicate substantially lower arc voltages than those found here for comparable operating conditions. For example, Avco finds about 100 V for currents of 17 kA and mass flows of a few grams per second of argon, compared to our values of approximately 160 V, i.e., our arc displays a 50% greater effective impedance than the Avco version.

Although both configurations consist of a conical tungsten cathode and a flat plate anode, one of the few differences between these accelerators is the diameter of the anode orifice--2.8 in. for the Avco geometry compared to our 4-in. orifice. To determine whether this factor alone can cause the indicated voltage difference, a series of experiments have been performed wherein the anode orifice diameter is systematically decreased from 4 in. to 1 in. at a fixed current of 17 kA and a fixed mass flow rate of 5.9 g/sec argon. The results of this survey are shown in Fig. 29, where the terminal voltage is plotted for the five anode orifice diameters. The data indicate little change from the nominal 160 V until the anode orifice is decreased below approximately 2½ in. where the voltage drops rather abruptly to an apparent plateau of roughly 80 V.

For a fixed current, arc operation at a lower terminal voltage, as observed with the smaller anode orifices, would indicate a more efficient accelerator if the plasma outflow characteristics remain unchanged. To check this latter point, the centerline velocity has also been measured for each anode size, at a fixed axial position 11 in. downstream of the anode orifice. The data are deduced from the time-of-flight of characteristic plasma disturbances between biased boundary layer probes, a technique discussed previously.[96,98,116] The results, shown in Fig. 30, again show a marked change for diameters between 2 in. and 3 in., but this is now superimposed on a linearly increasing value throughout the entire range.

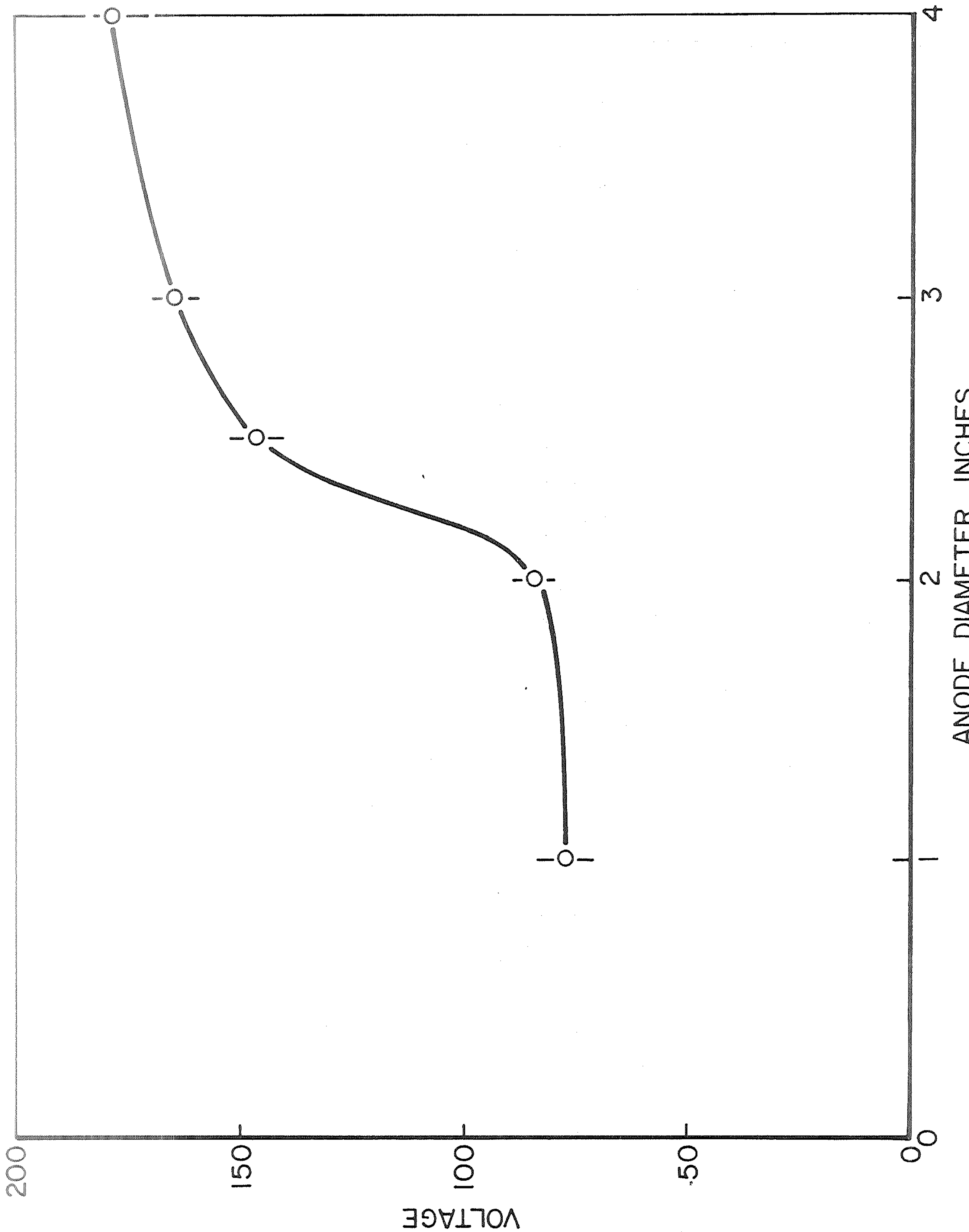

VOLTAGE VARIATION WITH ANODE DIAMETER

FIGURE 29
AP 25 R 4691 71

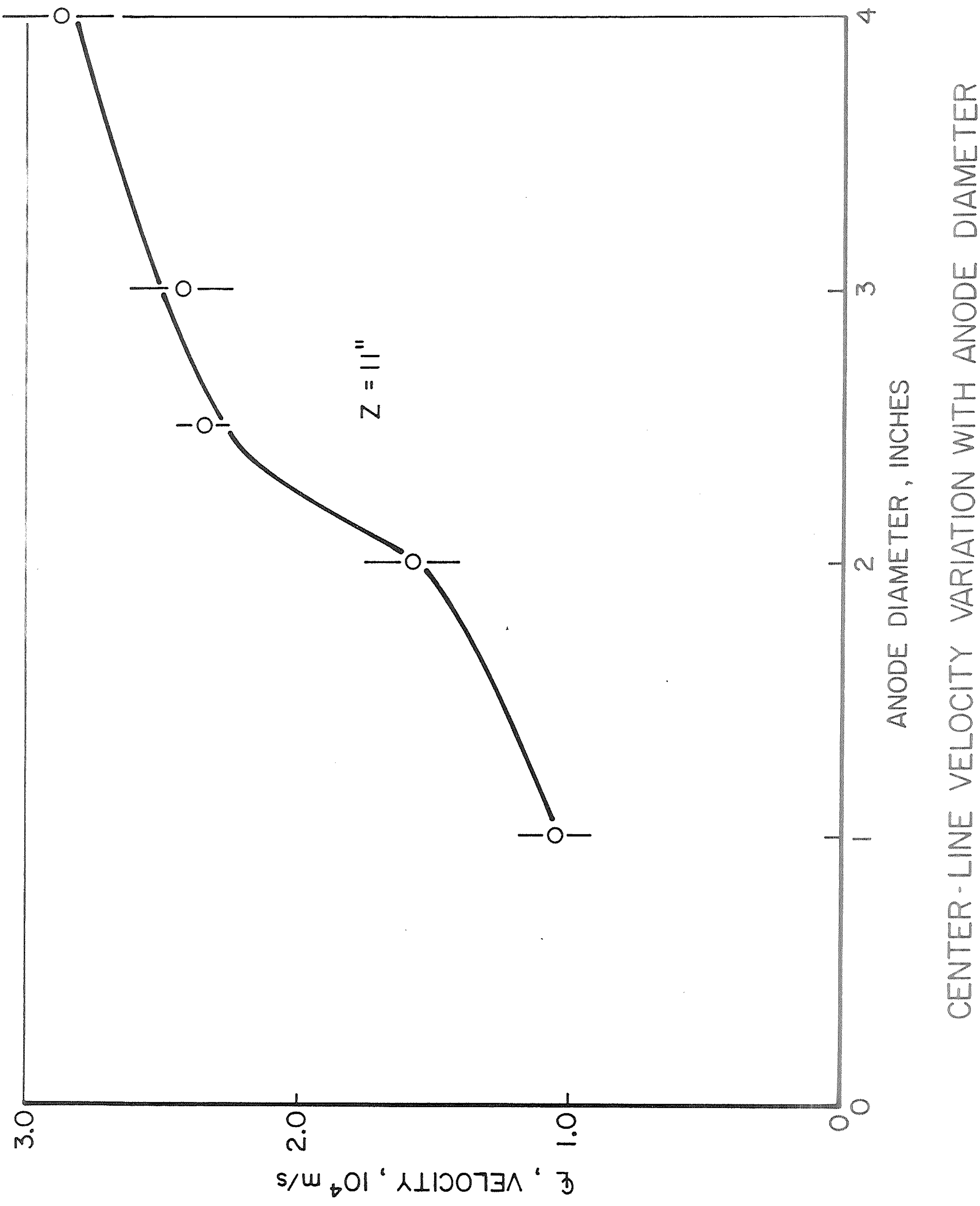

FIGURE 30
AP 25 R 4690 71

Since the overall efficiency η can be written as

$$\eta = 1/2\ \dot{m}v^2/VJ$$

where v = exhaust velocity and V = terminal voltage (a ratio of thrust power to input power), it follows that for fixed mass flow and current, as in the present case, the quantity v^2/V should be an index of the influence of the anode orifice on the efficiency of arc operation. As shown in Fig. 31, the data indicate a nearly linear increase in v^2/V as anode size increases. Thus, the preliminary indication is that it is the higher voltage (larger anode) arcs which are in fact the more efficient, a result that clearly requires further study. As a tentative hypothesis, one may speculate that there is a "critical anode size," for given range of arc operating parameters, below which intrusion of the anode lip into the important cathode envelope region of the discharge[109,111] interferes with optimum functioning of the acceleration processes.

D. Multiple-Gas Survey--Solenoid Valve Mass Injection System (Villani)

To expedite the ongoing survey of many types of propellant gas in quasi-steady MPD accelerator operation, the simple shock tube mass injection system used exclusively heretofore has been supplanted by a system based on more conventional valve control. This change has been undertaken for two reasons: (a) since the shock tube characteristics are strongly dependent on gas properties, this type of injection system would need be redesigned and recalibrated for each propellant to be used; and (b) mass flow shut-off is more easily controlled by a valve system than by a shock tube, thus restricting the total mass deposited in the vacuum tank, and expediting the pumping cycle of the operating procedure.

The new gas-handling system is sketched in Fig. 32. In order to provide rise times comparable to those achieved by the shock tube, the solenoid valves are driven by a voltage up to 10 times their rated values for times on the order of 10 milli-

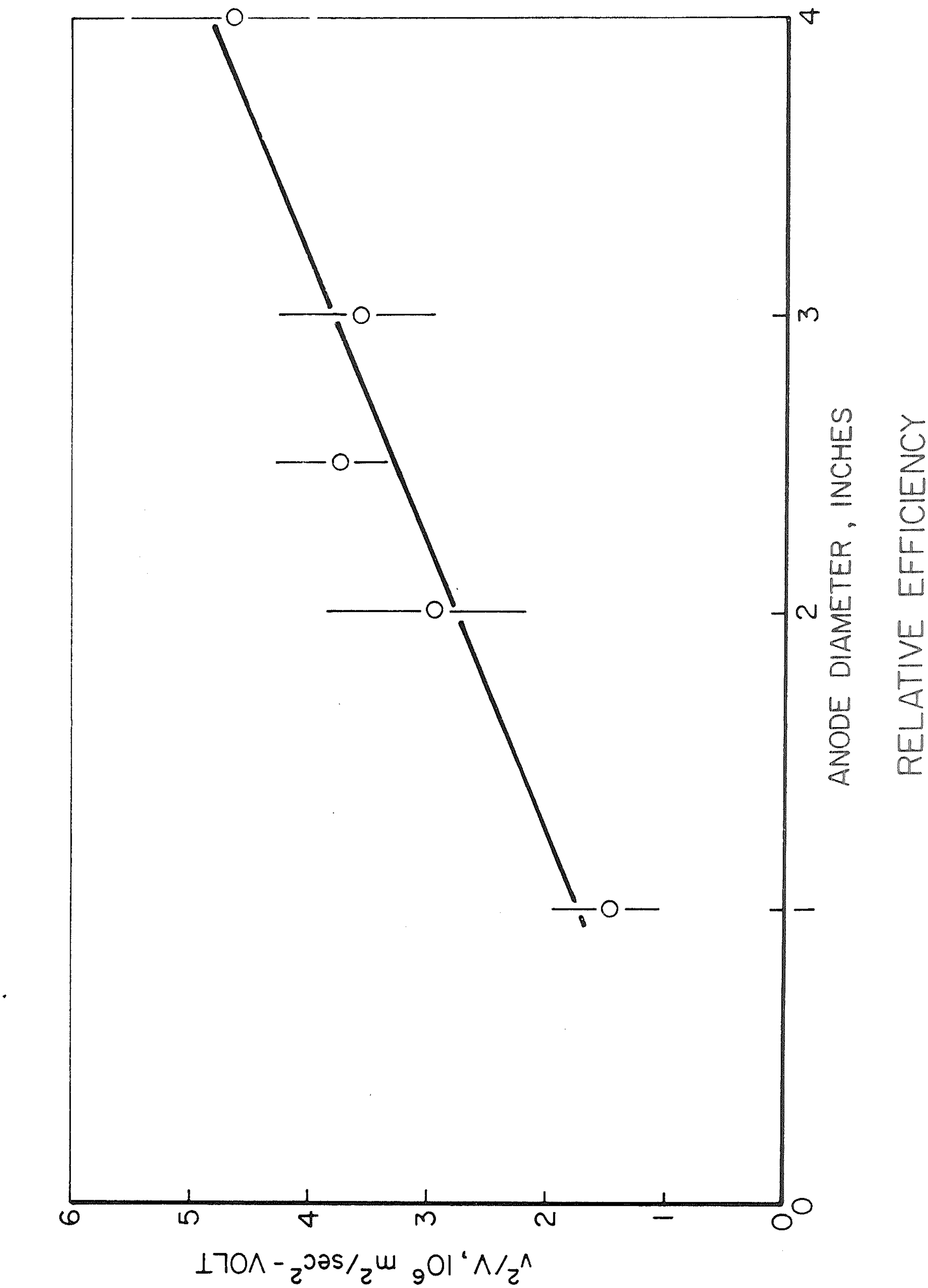

FIGURE 31
AP 25 R 4692 71

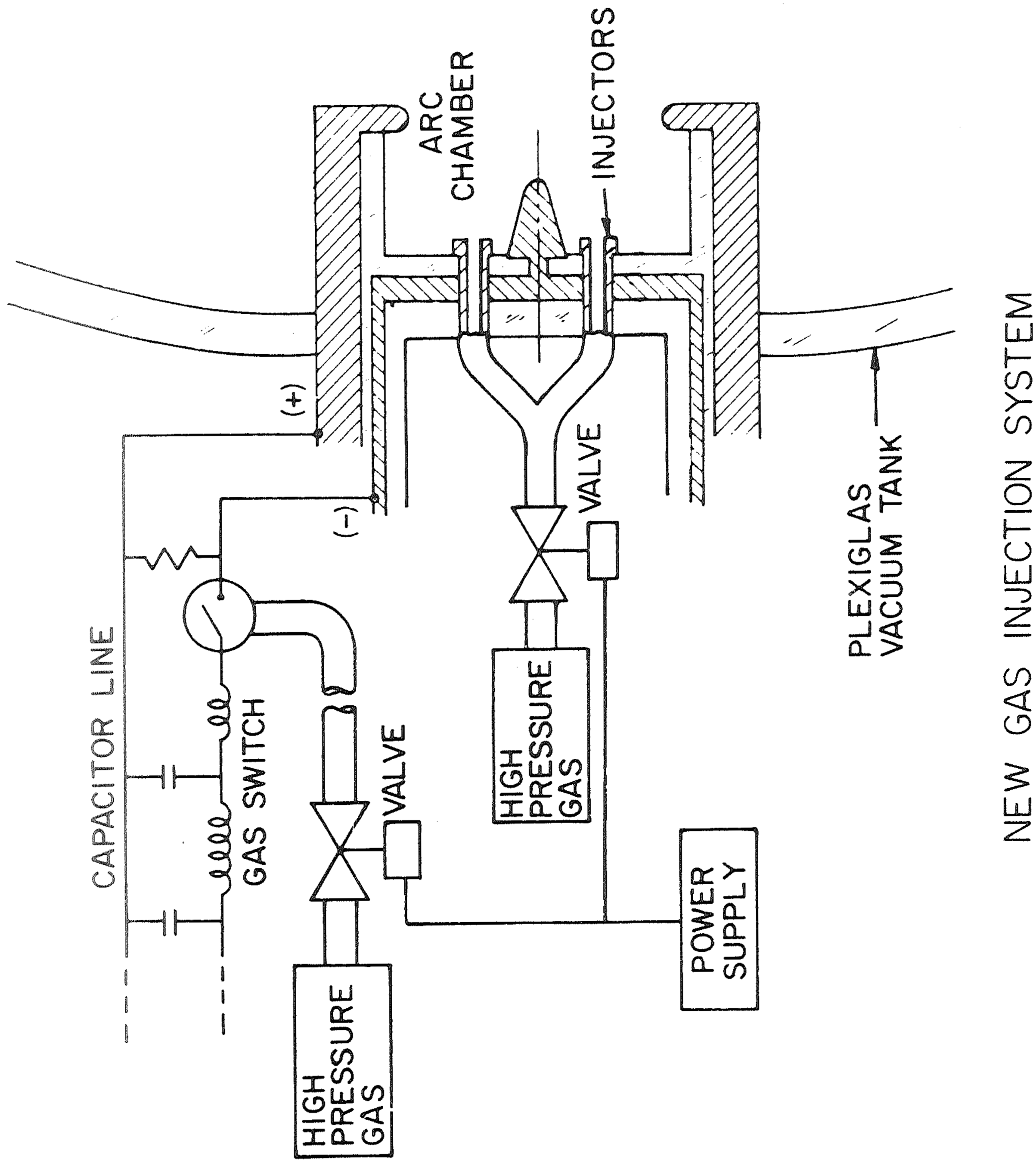

FIGURE 32
AP 25 R 4681 71

seconds, by the circuit shown in Fig. 33. To examine the gas pulse shape, the density in the anode exhaust plane was monitored by a Varian Millitorr (T.M.) fast ionization gauge. Ion gauge output and valve current for a typical $\dot{m}$ cold flow shot are shown in Fig. 34. The length of the gasdynamic delay tube leading from the second valve to the switch can be adjusted to allow the current pulse from the capacitor bank to be applied to the arc just after the mass flow has stabilized.

Installation and calibration of this system on the small diagnostic accelerator is essentially complete, and is now being used in the hollow cathode investigations described in Sec. III-E. Installation and calibration of a similar system in the large Plexiglas vacuum tank is also virtually complete, and initial multiple-gas data are being accumulated.

E. Hollow-Cathode, Quasi-Steady MPD Arc (Parmentier)

In recent years, hollow cathodes have been studied in many types of low current discharges, and employed to substantial engineering advantage in a few discharge devices, most notably the electron bombardment ion engine.[A-14,A-15] While such studies have also included external field, steady MPD arcs, no known attempt had been made to employ hollow cathodes in multi-megawatt discharges, such as those characteristic of our quasi-steady, self-field accelerators. While the physics of hollow cathode operation is still incompletely understood, certain phenomenological aspects of their operation at low powers suggest that substantial benefit may derive from their use in high-power MPD units as well.

This year we are fortunate to have in our group a visiting Belgian scholar, Mr. Noël Parmentier, who has a strong background in electrical engineering, and who has developed an interest in this problem. His report of the first four months of his work follows.

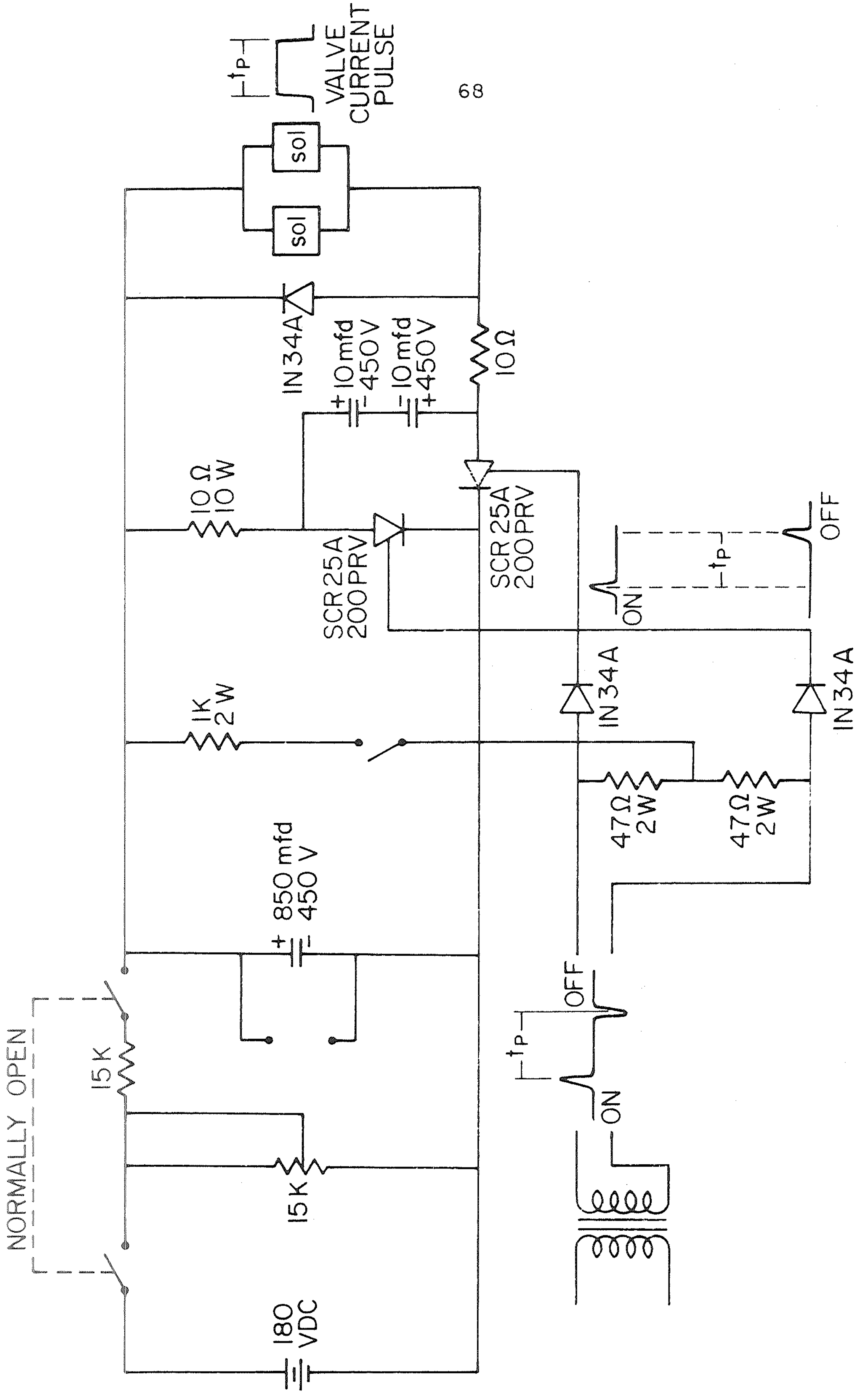

DOUBLE ACTION VALVE CIRCUIT

FIGURE 33

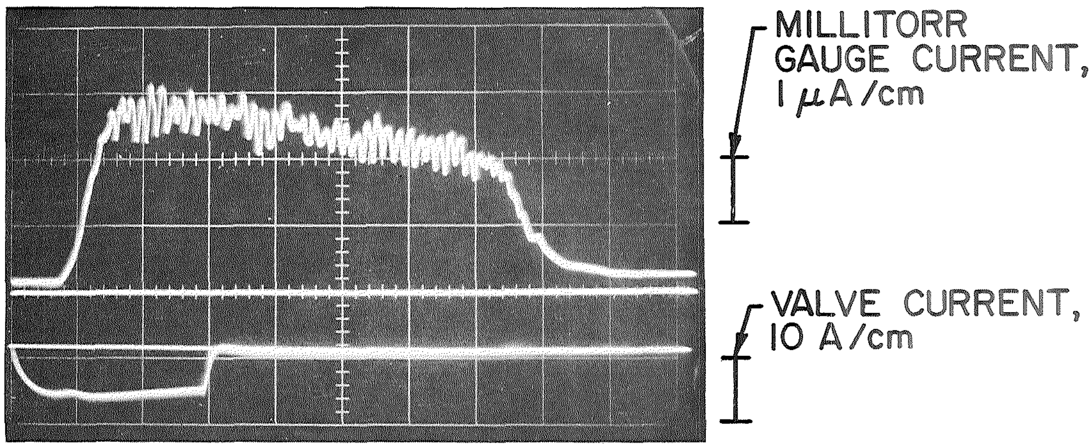

t: 2 msec/cm

TYPICAL ṁ DATA SHOT

FIGURE 34
AP 25 P-360 71

1. Design

The interest of this research is the behavior of a hollow cathode in a pulsed magnetoplasmadynamic arc discharge. There exists previous work in the domain of low currents, but the main interest of this research is the study of the high-current region, with particular interest in the effects on overall characteristics of the discharge, such as the voltage-current characteristics, and power efficiency.

Published material on hollow cathode operation indicate that the length, l, and inner diameter, d, of the hollow cathode are significant parameters in its operation. Rawlin and Pawlik[A-16] suggest that the ratio l/d must be at least 6/1 in order that the electrons emitted from the cathode have time to be accelerated through a high enough electric field that they can ionize the neutral atom inside the cavity. These ions in turn must collide with the cavity wall with sufficient energy to provide the electron emission. The longer the length of the cavity, and the smaller its diameter, the more chance ions have to collide with the wall before leaving through the orifice. Initially, the outer surface configuration was chosen cylindrical, of diameter equal to the maximum diameter of our usual conical cathode. Both cathodes are shown in Fig. 35.

2. Discharge Characteristic

The first series of experiments provided a comparison of the voltage-current characteristics for the two types of cathode in otherwise identical discharge arrangements. Argon propellant is injected into the discharge chamber through a solenoid valve and multi-tube manifold to six 3/8-in. injectors in a configuration similar to that shown in Fig. 32, and also into the hollow cathode orifice. The mass flow rate is regulated by the initial argon pressure, and the orifice to the gas-triggered switch is so chosen that the discharge in the main chamber takes place during the constant mass flow time.

Power is supplied as an essentially rectangular pulse by

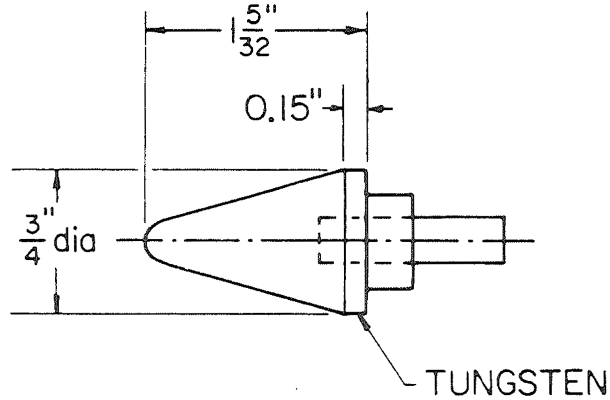

a) CONICAL CATHODE

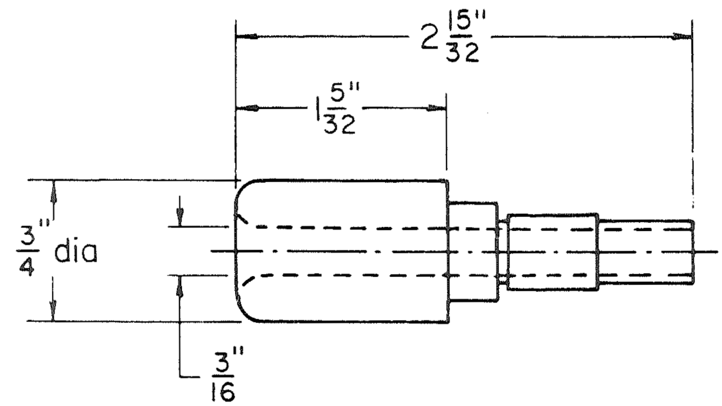

b) HOLLOW CATHODE

CATHODE CONFIGURATIONS

FIGURE 35

AP 25 R 4693 71

an electrolytic capacitor line.[103] Current, monitored by a Rogowski loop around the cathode lead, and terminal voltage, measured with a Tektronix P-6013A probe, are recorded on a Tektronix oscilloscope. A typical record of current and voltage is shown in Fig. 36.

Tests were conducted for various total mass flows, and combinations of mass flow through the outer injectors and cathode cavity. Figure 37 summarizes typical results for 6 gm/sec total mass flow, in comparison to solid cathode operation in the same regime. The main points to be noted are that for one mass flow combination, e.g., 1/7 of the total flow passing through the cathode, the hollow cathode arc displays substantially lower impedance than the solid cathode version. For other ratios, however, this comparison is reversed, thus indicating both a potential reduction of cathode losses by hollow cathode techniques, and a sensitivity of this benefit to mass flow distribution.

To pursue this point a bit further, Fig. 38 shows similar characteristics for total mass flows of 3 g/sec and 10.5 g/sec, respectively, and compares the 1/7 ratio characteristics for all three mass flows. Clearly indicated is a sensitivity to the absolute value of the flow through the cathode, as well as the ratio, suggesting that a full survey of all reasonable permutations will be necessary to identify the optimum operating conditions.

In an effort to assess what fraction of the emission current was in fact emerging from the interior of the cathode cavity, a series of 5 μsec Kerr-cell photographs of the luminosity patterns in this region of the discharge were taken. Typical samples are shown in Fig. 39. In no case was the desired intense interior jet observed, but rather a general shroud over most of the exterior surface, suggesting that complete hollow cathode function had not been achieved, even in those cases displaying lower terminal impedance.

In an empirical attempt to improve this, the exterior sur-

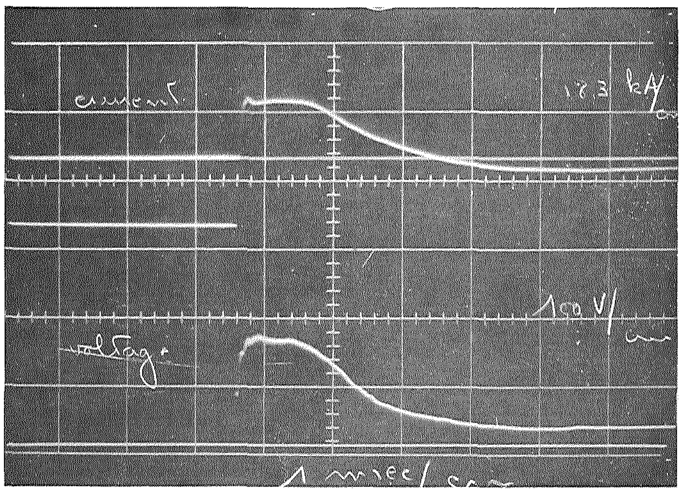

18.3 kA/DIV

100 V/DIV

TYPICAL CURRENT AND VOLTAGE RECORD

FIGURE 36
AP 25 P-365 71

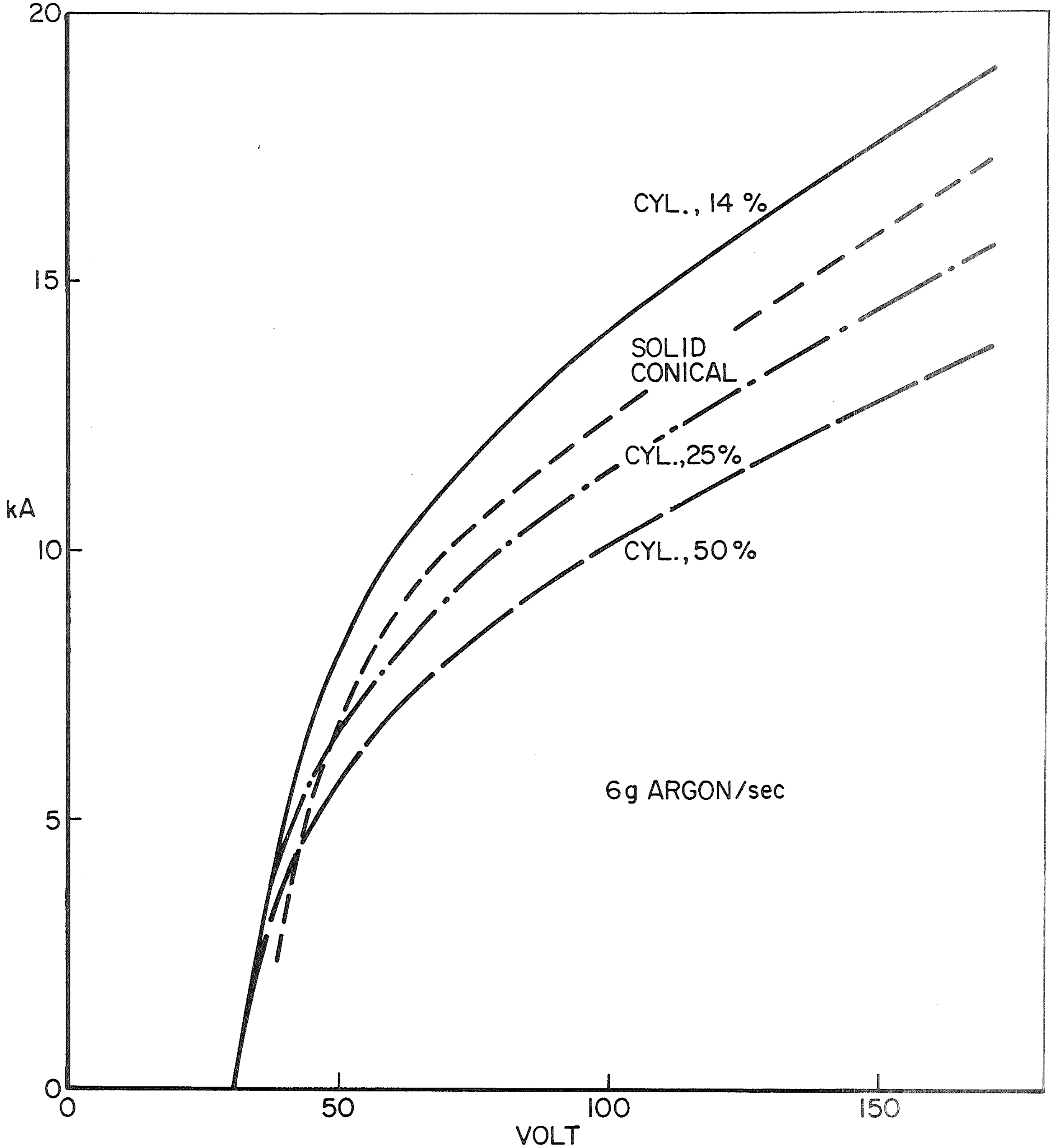

COMPARISON OF DISCHARGE CHARACTERISTICS

FIGURE 37
AP 25 R 4700 71

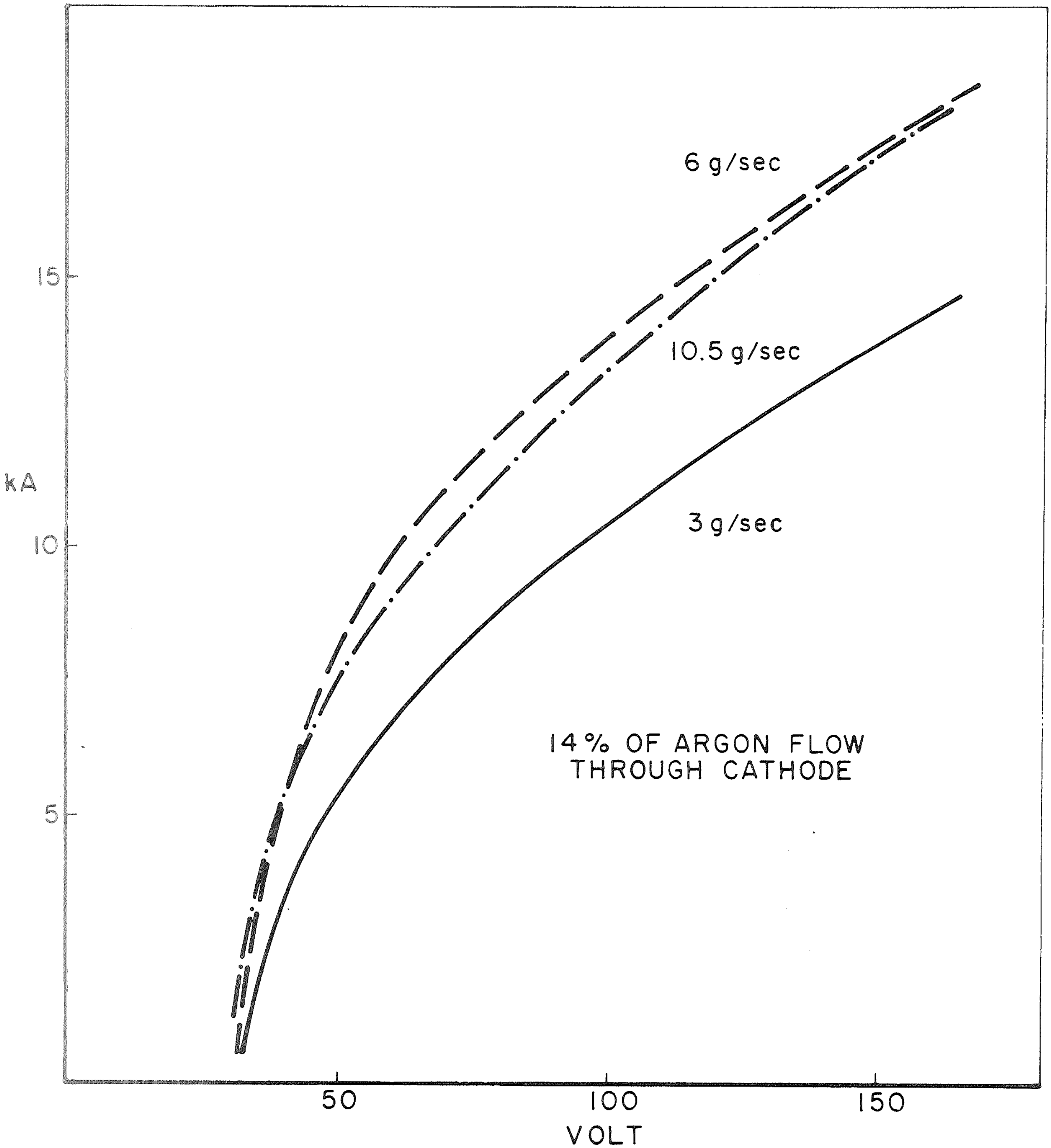

HOLLOW CYLINDRICAL CATHODE
DISCHARGE CHARACTERISTICS

FIGURE 38
AP 25 R 4702 71

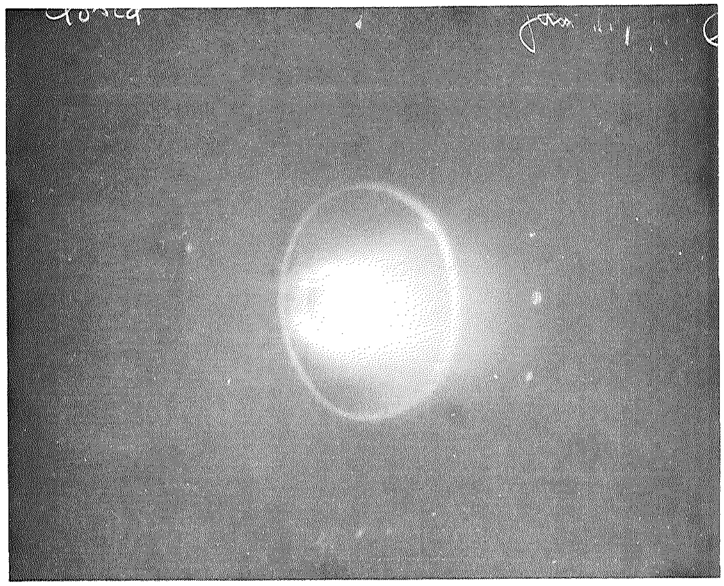

a) 90 V × 11.9 kA
6 g/sec ARGON
NO CATHODE FLOW

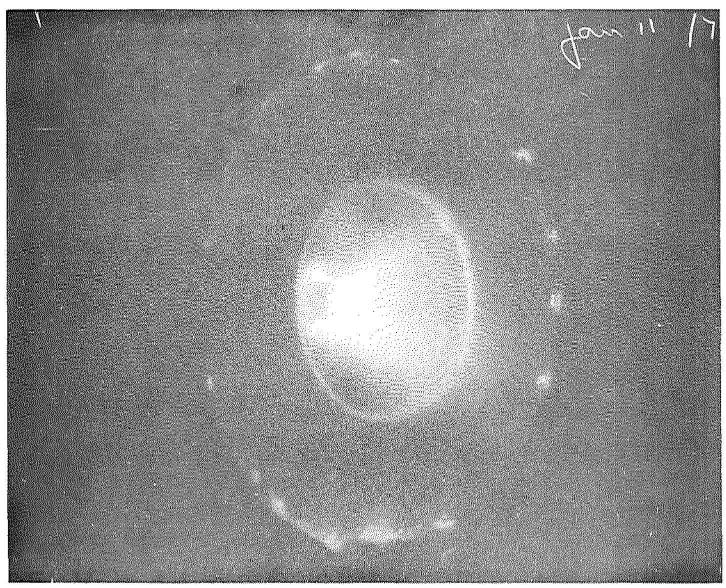

b) 95 V × 13.5 kA
6 g/sec ARGON
1 g/sec THROUGH CATHODE

DISCHARGE WITH CYLINDRICAL HOLLOW CATHODE

FIGURE 39
AP 25 P-367 71

face of the cathode was modified to a conical shape, replicating the old solid cathode, except for the cavity. The logic of this change was to remove the downstream outer corner of the cathode, where current could attach at relatively large radius where the prevailing magnetic pressure might be inadequate to force it into the cavity against the ambient gas pressure there, and encourage initial attachment at the orifice lip where upstream migration into the cavity might be more readily achieved. The success of this maneuver is indicated by the photographs in Fig. 40 which shows the quasi-steady discharge appearance for various current levels, some of which display the desired interior jet indicative of proper hollow cathode function.

As yet no detailed terminal data have been accumulated on this new cathode configuration, but the appearance of the discharge allows some optimism that this may indeed be an attractive configuration.

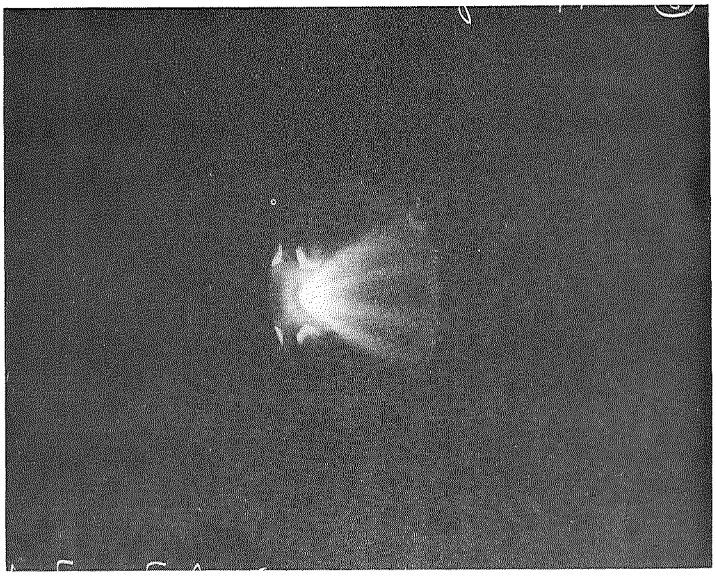

a) 90 V × 9.2 kA

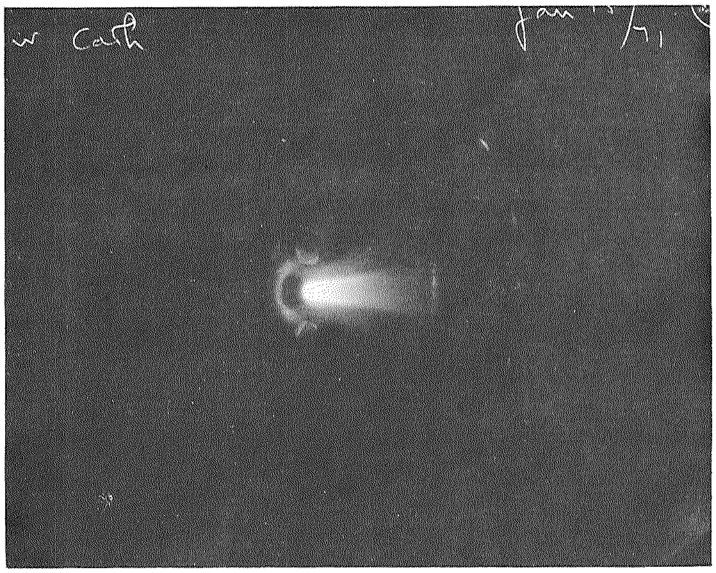

b) 170 V × 13.2 kA

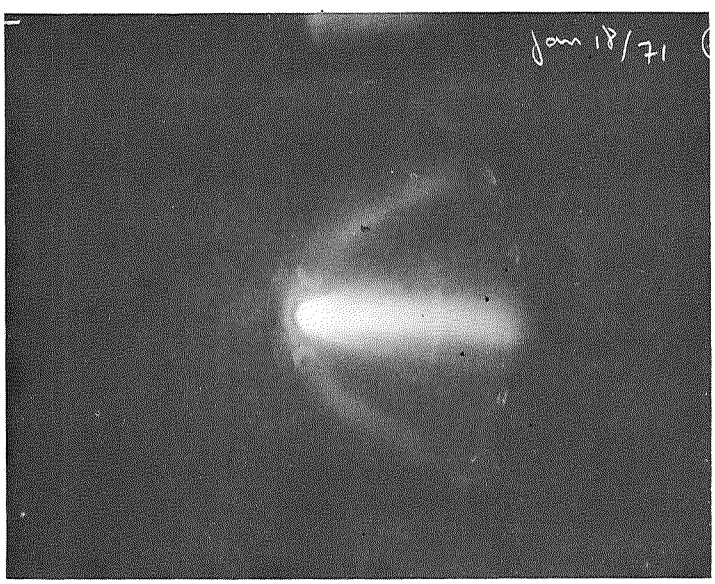

c) 190 V × 14.1 kA

DISCHARGE WITH CONICAL HOLLOW CATHODE
(6 g/sec ARGON ; 1 g/sec THROUGH CATHODE)
FIGURE 40
AP 25 P - 366 71

PROJECT REFERENCES

[1] Jahn, R. G. et al., "Proposed Studies of the Formation and Stability of an Electromagnetic Boundary in a Pinch," Proposal for NASA Research Grant NsG-306-63, Mar. 5, 1962, Princeton Univ., Princeton, N. J.

[2] Jahn, R. G. et al., "Pulsed Electromagnetic Gas Acceleration," NASA NsG-306-63 progress report for the period 1 July 1962 to 31 December 1962, Aeron. Eng. Rept. No. 634, Jan. 1963, Princeton Univ., Princeton, N. J.

[3] Jahn, R. G. and W. F. Von Jaskowsky, "The Plasma Pinch as a Gas Accelerator," A.I.A.A. Preprint 63013, A.I.A.A. Electric Propulsion Conference, Colorado Springs, Colo., 11-13 Mar. 1963.

[4] Jahn, R. G. et al., "Pulsed Electromagnetic Gas Acceleration," NASA NsG-306-63 progress report for the period 1 January 1963 to 30 June 1963, Aeron. Eng. Rept. No. 634a, June 1963, Princeton Univ., Princeton, N. J.

[5] Jahn, R. G. and W. Von Jaskowsky, "Structure of a Large-radius Pinch Discharge," A.I.A.A. Journal, Vol. 1, No. 8, Aug. 1963, pp. 1809-1814.

[6] Jahn, R. G., W. F. Von Jaskowsky, and A. L. Casini, "A Gas-triggered Inverse Pinch Switch," NASA NsG-306-63, Aeron. Eng. Tech. Note No. 660, Aug. 1963, Princeton Univ., Princeton, N. J.

[7] Jahn, R. G., W. F. Von Jaskowsky, and A. L. Casini, "Gas-triggered Inverse Pinch Switch," The Review of Scientific Instruments, Vol. 34, No. 12, Dec. 1963, pp. 1439-1440.

[8] Jahn, R. G. and W. F. Von Jaskowsky, "Pulsed Electromagnetic Gas Acceleration," (Paper delivered at the 4th NASA Intercenter Conference on Plasma Physics, Washington, D. C., 2-4 Dec. 1963), p. 8.

[9] Jahn, R. G. et al., "Pulsed Electromagnetic Gas Acceleration," NASA NsG-306-63 progress report for the period 1 July 1963 to 31 December 1963, Aeron. Eng. Rept. No. 634b, Dec. 1963, Princeton Univ., Princeton, N. J.

[10] Jahn, R. G. and W. F. Von Jaskowsky, "Current Distributions in Large-radius Pinch Discharges," A.I.A.A. Preprint 64-25, A.I.A.A. Aerospace Sciences Meeting, New York, N. Y., 20-22 Jan. 1964.

PROJECT REFERENCES

[11] Jahn, R. G. and W. F. Von Jaskowsky, "Current Distributions in Large-radius Pinch Discharges," A.I.A.A. Bulletin, Vol. 1, No. 1, Jan. 1964, p. 12.

[12] Jahn, R. G. et al., "Pulsed Electromagnetic Gas Acceleration," NASA NsG-306-63 renewal proposal for 15-months extension, Jan. 15, 1964, Princeton Univ., Princeton, N. J.

[13] Jahn, R. G. et al., "Pulsed Electromagnetic Gas Acceleration," NASA NsG-306-63 progress report for the period 1 January 1964 to 30 June 1964, Aeron. Eng. Rept. No. 634c, July 1964, Princeton Univ., Princeton, N. J.

[14] Jahn, R. G., W. F. Von Jaskowsky, and A. L. Casini, "Gas-triggered Pinch Discharge Switch," NASA NsG-306-63, Aerospace and Mechanical Sciences Tech. Note No. 101, July 1964, Princeton Univ., Princeton, N. J.

[15] Corr, J. M., "Double Probe Studies in an 8" Pinch Discharge," M.S.E. thesis, Sept. 1964, Princeton Univ., Princeton, N. J.

[16] Jahn, R. G. and W. F. Von Jaskowsky, "Exhaust of a Pinched Plasma From an Axial Orifice," A.I.A.A. Bulletin, Vol. 1, No. 10, Oct. 1964, p. 570.

[17] Jahn, R. G. and W. F. Von Jaskowsky, "Current Distributions in Large-radius Pinch Discharges," A.I.A.A. Journal, Vol. 2, No. 10, Oct. 1964, pp. 1749-1753.

[18] Jahn, R. G., W. F. Von Jaskowsky, and A. L. Casini, "Gas-triggered Pinch Discharge Switch," The Review of Scientific Instruments, Vol. 36, No. 1, Jan. 1965, pp. 101-102.

[19] Jahn, R. G. and W. F. Von Jaskowsky, "Exhaust of a Pinched Plasma From an Axial Orifice," A.I.A.A. Paper 65-92, A.I.A.A. 2nd Aerospace Sciences Meeting, New York, N. Y., 25-27 Jan. 1965.

[20] Jahn, R. G. et al., "Pulsed Electromagnetic Gas Acceleration," NASA NsG-306-63 progress report for the period 1 July 1964 to 31 December 1964, Aerospace and Mechanical Sciences Rept. No. 634d, Jan. 1965, Princeton Univ., Princeton, N. J.

[21] Wright, E. S., "The Design and Development of Rogowski Coil Probes for Measurement of Current Density Distribution in a Plasma Pinch," M.S.E. thesis, May 1965, Princeton Univ., Princeton, N. J.

PROJECT REFERENCES

[22] Jahn, R. G. et al., "Pulsed Electromagnetic Gas Acceleration," NASA NsG-306-63 renewal proposal for 12-months extension, June 7, 1965, Princeton Univ., Princeton, N. J.

[23] Jahn, R. G. and N. A. Black, "On the Dynamic Efficiency of Pulsed Plasma Accelerators," A.I.A.A. Journal, Vol. 3, No. 6, June 1965, pp. 1209-1210.

[24] Black, N. A., "Linear Pinch Driven by a High-current Pulse-forming Network," A.I.A.A. Bulletin, Vol. 2, No. 6, June 1965, p. 309.

[25] Wright, E. S. and R. G. Jahn, "The Design and Development of Rogowski Coil Probes for Measurement of Current Density Distribution in a Plasma Pinch," NASA NsG-306-63, Aerospace and Mechanical Sciences Rept. No. 740, June 1965, Princeton Univ., Princeton, N. J.

[26] Rowell, G. A., "Cylindrical Shock Model of the Plasma Pinch," M.S.E. thesis, July 1965, Princeton Univ., Princeton, N. J.

[27] Black, N. A., "Linear Pinch Driven by a High-current Pulse-forming Network," A.I.A.A. Paper 65-336, A.I.A.A. 2nd Annual Meeting, San Francisco, Calif., 26-29 July 1965.

[28] Jahn, R. G. et al., "Pulsed Electromagnetic Gas Acceleration," NASA NsG-306-63 progress report for the period 1 January 1965 to 30 June 1965, Aerospace and Mechanical Sciences Rept. No. 634e, July 1965, Princeton Univ., Princeton, N. J.

[29] Jahn, R. G. and A. C. Ducati, "Design and Development of a Thermo-Ionic Electric Thrustor," 5QS 085-968 Interim Report, NASA Contract NASw-968, Aug. 1965, Giannini Scientific Corp., Santa Ana, Calif.

[30] Jahn, R. G. W. F. Von Jaskowsky, and R. L. Burton, "Ejection of a Pinched Plasma From an Axial Orifice," A.I.A.A. Journal, Vol. 3, No. 10, Oct. 1965, pp. 1862-1866.

[31] Jahn, R. G. and E. S. Wright, "Miniature Rogowski Coil Probes for Direct Measurement of Current Density Distribution in Transient Plasmas," The Review of Scientific Instruments, Vol. 36, No. 12, Dec. 1965, pp. 1891-1892.

PROJECT REFERENCES

[32] Jahn, R. G. et al., "Pulsed Electromagnetic Gas Acceleration," NASA NsG-306-63 progress report for the period 1 July 1965 to 31 December 1965, Aerospace and Mechanical Sciences Rept. No. 634f, Jan. 1966, Princeton Univ., Princeton, N. J.

[33] Burton, R. L. and R. G. Jahn, "Electric and Magnetic Field Distributions in a Propagating Current Sheet," A.I.A.A. Bulletin, Vol. 3, No. 1, Jan. 1966, p. 35.

[34] Rowell, G. A. and R. G. Jahn, "Cylindrical Shock Model of the Plasma Pinch," NASA NsG-306-63, Aerospace and Mechanical Sciences Rept. No. 742, Feb. 1966, Princeton Univ., Princeton, N. J.

[35] Burton, R. L. and R. G. Jahn, "Electric and Magnetic Field Distributions in a Propagating Current Sheet," A.I.A.A. Paper 66-200, A.I.A.A. 5th Electric Propulsion Conference, San Diego, Calif., 7-9 Mar. 1966.

[36] Black, N. A., "Pulse-forming Networks for Propulsion Research," Proceedings of the 7th Symposium on Engineering Aspects of Magnetohydrodynamics, Princeton Univ., Princeton, N. J., Mar. 30-April 1, 1966, pp. 10-11.

[37] Jahn, R. G., "Electromagnetic Propulsion," Astronautics and Aeronautics, Vol. 4, No. 4, April 1966, p. 69.

[38] Black, N. A., "Dynamics of a Pinch Discharge Driven by a High-current Pulse-forming Network," Ph.D. thesis, May 1966, Princeton Univ., Princeton, N. J.

[39] Black, N. A. and R. G. Jahn, "Dynamics of a Pinch Discharge Driven by a High-current Pulse-forming Network," NASA NsG-306-63, Aerospace and Mechanical Sciences Rept. No. 778, May 1966, Princeton Univ., Princeton, N. J.

[40] Jahn, R. G., "Pulsed Plasma Propulsion," Proceedings of the 5th NASA Intercenter and Contractors Conference on Plasma Physics, Washington, D. C., 24-26 May 1966, pt. V, pp. 75-81.

[41] Jahn, R. G. et al., "Pulsed Electromagnetic Gas Acceleration," NASA NsG-306-63 renewal proposal for 24-months extension, May 25, 1966, Princeton Univ., Princeton, N. J.

[42] Ducati, A. C., R. G. Jahn, E. Muehlberger, and R. P. Treat, "Design and Development of a Thermo-Ionic Electric Thrustor," FR-056-968 Final Report, NASA CR-54703, May 1966, Giannini Scientific Corp., Santa Ana, Calif.

PROJECT REFERENCES

[43] Jahn, R. G. and K. E. Clark, "A Large Dielectric Vacuum Facility," A.I.A.A. Journal, Vol. 4, No. 6, June 1966, p. 1135.

[44] John, R. R., S. Bennett, and R. G. Jahn, "Current Status of a Plasma Propulsion," A.I.A.A. Bulletin, Vol. 3, No. 6, June 1966, p. 264.

[45] John, R. R., S. Bennett, and R. G. Jahn, "Current Status of a Plasma Propulsion," A.I.A.A. Paper 66-565, A.I.A.A. 2nd Propulsion Joint Specialist Conference, Colorado Springs, Colo., 13-17 June 1966.

[46] Jahn, R. G. et al., "Pulsed Electromagnetic Gas Acceleration," NASA NsG-306-63 progress report for the period 1 January 1966 to 30 June 1966, Aerospace and Mechanical Sciences Rept. No. 634g, July 1966, Princeton Univ., Princeton, N. J.

[47] Burton, R. L., "Structure of the Current Sheet in a Pinch Discharge," Ph.D. thesis, Sept. 1966, Princeton Univ., Princeton, N. J.

[48] Burton, R. L. and R. G. Jahn, "Structure of the Current Sheet in a Pinch Discharge," NASA NsG-306-63, Aerospace and Mechanical Sciences Rept. No. 783, Sept. 1966, Princeton Univ., Princeton, N. J.

[49] Jahn, R. G. et al., "Pulsed Electromagnetic Gas Acceleration," NASA NsG-306-63 progress report for the period 1 July 1966 to 31 December 1966, Aerospace and Mechanical Sciences Rept. No. 634h, Jan. 1967, Princeton Univ., Princeton, N. J.

[50] Burton, R. L. and R. G. Jahn, "Structure of the Current Sheet in a Pinch Discharge," Bulletin of the American Physical Society, Vol. 12, Ser. II, Paper L1, May 1967, p. 848.

[51] Jahn, R. G., "Plasma Propulsion for Deep Space Flight," Bulletin of the American Physical Society, Vol. 12, Ser. II, Paper BC-1, May 1967, p. 646.

[52] Ellis, W. R., Jr., "An Investigation of Current Sheet Structure in a Cylindrical Z-Pinch," Ph.D. thesis, July 1967, Princeton Univ., Princeton, N. J.

[53] Ellis, W. R., Jr. and R. G. Jahn, "An Investigation of Current Sheet Structure in a Cylindrical Z-Pinch," NASA NsG-306-63, Aerospace and Mechanical Sciences Rept. No. 805, July 1967, Princeton Univ., Princeton, N. J.

PROJECT REFERENCES

[54] Jahn, R. G. et al., "Pulsed Electromagnetic Gas Acceleration," NASA NsG-306-63 progress report for the period 1 January 1967 to 30 June 1967, Aerospace and Mechanical Sciences Rept. No. 634i, July 1967, Princeton Univ., Princeton, N. J.

[55] Clark, K. E. and R. G. Jahn, "The Magnetoplasmadynamic Arc," Astronautica Acta, Vol. 13, No. 4, 1967, pp. 315-325.

[56] Jahn, R. G., "The MPD Arc," NASA Contract NASw-1513, Aug. 1967, Giannini Scientific Corp., Santa Ana, Calif.

[57] Eckbreth, A. C., K. E. Clark, and R. G. Jahn, "Current Pattern Stabilization in Pulsed Plasma Accelerators," A.I.A.A. Bulletin, Vol. 4, No. 9, Sept. 1967, p. 433.

[58] Clark, K. E., A. C. Eckbreth, and R. G. Jahn, "Current Pattern Stabilization in Pulsed Plasma Accelerators," A.I.A.A. Paper 67-656, A.I.A.A. Electric Propulsion and Plasmadynamics Conference, Colorado Springs, Colo., 11-13 Sept. 1967.

[59] Jahn, R. G. et al., "Pulsed Electromagnetic Gas Acceleration," NASA NsG-306-63 progress report for the period 1 July 1967 to 31 December 1967, Aerospace and Mechanical Sciences Rept. No. 634j, Jan. 1968, Princeton Univ., Princeton, N. J.

[60] Ducati, A. C., R. G. Jahn, E. Muehlberger, and R. P. Treat, "Exploratory Electromagnetic Thruster Research," TR 117-1513 Annual Report, NASA CR 62047, Feb. 1968, Giannini Scientific Corp., Santa Ana, Calif.

[61] Jahn, R. G., PHYSICS OF ELECTRIC PROPULSION (McGraw-Hill Book Company, New York, 1968).

[62] Burton, R. L. and R. G. Jahn, "Acceleration of Plasma by a Propagating Current Sheet," The Physics of Fluids, Vol. 11, No. 6, June 1968, pp. 1231-1237.

[63] Jahn, R. G. et al., "Pulsed Electromagnetic Gas Acceleration," NASA NGR 31-001-005 step-funding renewal proposal for the period 1 October 1968 to 30 September 1971, June 1, 1968, Princeton Univ., Princeton, N. J.

[64] Jahn, R. G. et al., "Pulsed Electromagnetic Gas Acceleration," NASA NsG-306/31-001-005 progress report for the period 1 January 1968 to 30 June 1968, Aerospace and Mechanical Sciences Rept. No. 634k, July 1968, Princeton Univ., Princeton, N. J.

PROJECT REFERENCES

[65] Wilbur, P. J., "Energy Transfer from a Pulse Network to a Propagating Current Sheet," Ph.D. thesis, Sept. 1968, Princeton Univ., Princeton, N. J.

[66] Wilbur, P. J. and R. G. Jahn, "Energy Transfer from a Pulse Network to a Propagating Current Sheet," NASA NGR 31-001-005, Aerospace and Mechanical Sciences Rept. No. 846, Sept. 1968, Princeton Univ., Princeton, N. J.

[67] Ducati, A. C., R. G. Jahn, E. Muehlberger, and R. P. Treat, "Exploratory Electromagnetic Thruster Research, Phase II," 2SS108-1513 Interim Report, NASA Contract NASw-1513, Oct. 1968, Giannini Scientific Corp., Santa Ana, Calif.

[68] Eckbreth, A. C., K. E. Clark, and R. G. Jahn, "Current Pattern Stabilization in Pulsed Plasma Accelerators," A.I.A.A. Journal, Vol. 6, No. 11, Nov. 1968, pp. 2125-2132.

[69] Eckbreth, A. C., "Current Pattern and Gas Flow Stabilization in Pulsed Plasma Accelerators," Ph.D. thesis, Dec. 1968, Princeton Univ., Princeton, N. J.

[70] Eckbreth, A. C. and R. G. Jahn, "Current Pattern and Gas Flow Stabilization in Pulsed Plasma Accelerators," NASA NGL 31-001-005, Aerospace and Mechanical Sciences Rept. No. 857, Dec. 1968, Princeton Univ., Princeton, N. J.

[71] York, T. M., "Pressure Distribution in the Structure of a Propagating Current Sheet," Ph.D. thesis, Dec. 1968, Princeton Univ., Princeton, N. J.

[72] York, T. M. and R. G. Jahn, "Pressure Distribution in the Structure of a Propagating Current Sheet," NASA NGL 31-001-005, Aerospace and Mechanical Sciences Rept. No. 853, Dec. 1968, Princeton Univ., Princeton, N. J.

[73] Eckbreth, A. C. and R. G. Jahn, "Current Pattern and Gas Flow Stabilization in Pulsed Plasma Accelerators," A.I.A.A. Bulletin, Vol. 5, No. 12, Dec. 1968, p. 730.

[74] Wilbur, P. J. and R. G. Jahn, "Energy Transfer From a Pulse Network to a Propagating Current Sheet," A.I.A.A. Bulletin, Vol. 5, No. 12, Dec. 1968, p. 730.

[75] Ellis, W. R. and R. G. Jahn, "Ion Density and Current Distributions in a Propagating Current Sheet, Determined by Microwave Reflection Technique," Rept. No. CLM-P-187, Dec. 1968, Culham Laboratory, Abingdon, Berkshire, Great Britain.

PROJECT REFERENCES

[76] Jahn, R. G. et al., "Pulsed Electromagnetic Gas Acceleration," NASA NGL 31-001-005 progress report for the period 1 July 1968 to 31 December 1968, Aerospace and Mechanical Sciences Rept. No. 634l, Jan. 1969, Princeton Univ., Princeton, N. J.

[77] Eckbreth, A. C. and R. G. Jahn, "Current Pattern and Gas Flow Stabilization in Pulsed Plasma Accelerators," A.I.A.A. Paper 69-112, A.I.A.A. 7th Aerospace Sciences Meeting, New York, N. Y., 20-22 Jan. 1969.

[78] Wilbur, P. J. and R. G. Jahn, "Energy Transfer From a Pulse Network to a Propagating Current Sheet," A.I.A.A. Paper 69-113, A.I.A.A. 7th Aerospace Sciences Meeting, New York, N. Y., 20-22 Jan. 1969.

[79] Ellis, W. R. and R. G. Jahn, "Ion Density and Current Distributions in a Propagating Current Sheet, Determined by Microwave Reflection Technique," Journal of Plasma Physics, Vol. 3, Pt. 2, 1969, pp. 189-213.

[80] York, T. M. and R. G. Jahn, "Pressure Distribution in the Structure of a Propagating Current Sheet," A.I.A.A. Bulletin, Vol. 6, No. 2, Feb. 1969, p. 75.

[81] Clark, K. E. and R. G. Jahn, "Quasi-steady Plasma Acceleration," A.I.A.A. Bulletin, Vol. 6, No. 2, Feb. 1969, p. 75.

[82] York, T. M. and R. G. Jahn, "Pressure Distribution in the Structure of a Propagating Current Sheet," A.I.A.A. Paper 69-264, A.I.A.A. 7th Electric Propulsion Conference, Williamsburg, Va., 3-5 Mar. 1969.

[83] Clark, K. E. and R. G. Jahn, "Quasi-steady Plasma Acceleration," A.I.A.A. Paper 69-267, A.I.A.A. 7th Electric Propulsion Conference, Williamsburg, Va., 3-5 Mar. 1969.

[84] Jahn, R. G. and W. R. Mickelsen, "Electric Propulsion Notebook," A.I.A.A. Professional Study Series, Williamsburg, Va., 1-2 Mar. 1969.

[85] Boyle, M. J., "Plasma Velocity Measurements with Electric Probes," B.S.E. thesis, April 1969, Princeton Univ., Princeton, N. J.

PROJECT REFERENCES

[86] Clark, K. E., "Quasi-steady Plasma Acceleration," Ph.D. thesis, May 1969, Princeton Univ., Princeton, N. J.

[87] Clark, K. E. and R. G. Jahn, "Quasi-steady Plasma Acceleration," NASA NGL 31-001-005, Aerospace and Mechanical Sciences Rept. No. 859, May 1969, Princeton Univ., Princeton, N. J.

[88] Boyle, M. J., "Plasma Velocity Measurements with Electric Probes," Paper No. 4 (Paper presented at the Northeastern Regional Student Conference, Princeton Univ., Princeton, N. J., 9-10 May 1969).

[89] Mickelsen, W. R. and R. G. Jahn, "Status of Electric Propulsion," A.I.A.A. Bulletin, Vol. 6, No. 6, June 1969, p. 257.

[90] Mickelsen, W. R. and R. G. Jahn, "Status of Electric Propulsion," A.I.A.A. Paper 69-497, A.I.A.A. 5th Propulsion Joint Specialist Conference, U. S. Air Force Academy, Colo., 9-13 June 1969.

[91] Ducati, A. C. and R. G. Jahn, "Electron Beam from a Magnetoplasmadynamic Arc," The Physics of Fluids, Vol. 12, No. 6, June 1969, pp. 1177-1181.

[92] Jahn, R. G. et al., "Pulsed Electromagnetic Gas Acceleration," NASA NGL 31-001-005 progress report for the period 1 January 1969 to 30 June 1969, Aerospace and Mechanical Sciences Rept. No. 634m, July 1969, Princeton Univ., Princeton, N. J.

[93] Jahn, R. G., K. E. Clark, R. C. Oberth, and P. J. Turchi, "Acceleration Patterns in Quasi-steady MPD Arcs," A.I.A.A. Bulletin, Vol. 6, No. 12, Dec. 1969, p. 701.

[94] Ducati, A. C. and R. G. Jahn, "Repetitively Pulsed, Quasi-steady Vacuum MPD Arc," A.I.A.A. Bulletin, Vol. 6, No. 12, Dec. 1969, p. 701.

[95] Jahn, R. G., W. F. Von Jaskowsky, and K. E. Clark, "Pulsed Electromagnetic Gas Acceleration: Acceleration Processes in Quasi-steady Arcs," (Paper delivered at the 6th NASA Intercenter and Contractors Conference on Plasma Physics, NASA Langley Research Center, Hampton, Va., 8-10 Dec. 1969), pp. 8-15.

[96] Jahn, R. G. et al., "Pulsed Electromagnetic Gas Acceleration," NASA NGL 31-001-005 progress report for the period 1 July 1969 to 31 December 1969, Aerospace and Mechanical Sciences Rept. No. 634n, Jan. 1970, Princeton Univ., Princeton, N. J.

[97] Eckbreth, A. C. and R. G. Jahn, "Current Pattern and Gas Flow Stabilization in Pulsed Plasma Accelerators," A.I.A.A. Journal, Vol. 8, No. 1, Jan. 1970, pp. 138-143.

PROJECT REFERENCES

98 Jahn, R. G., K. E. Clark, R. C. Oberth, and P. J. Turchi, "Acceleration Patterns in Quasi-steady MPD Arcs," A.I.A.A. Paper 70-165, A.I.A.A. 8th Aerospace Sciences Meeting, New York, N. Y., 19-21 Jan. 1970.

99 Ducati, A. C. and R. G. Jahn, "Repetitively Pulsed, Quasi-steady Vacuum MPD Arc," A.I.A.A. Paper 70-167, A.I.A.A. 8th Aerospace Sciences Meeting, New York, N. Y., 19-21 Jan. 1970.

100 Wilbur, P. J. and R. G. Jahn, "Energy Transfer from a Pulse Network to a Propagating Current Sheet," A.I.A.A. Journal, Vol. 8, No. 1, Jan. 1970, pp. 144-149.

101 Clark, K. E. and R. G. Jahn, "Quasi-steady Plasma Acceleration," A.I.A.A. Journal, Vol. 8, No. 2, Feb. 1970, pp. 216-220.

102 York, T. M. and R. G. Jahn, "Pressure Distribution in the Structure of a Propagating Current Sheet," The Physics of Fluids, Vol. 13, No. 5, May 1970, pp. 1303-1309.

103 Jahn, R. G. et al., "Pulsed Electromagnetic Gas Acceleration," NASA NGL 31-001-005 progress report for the period 1 January 1970 to 30 June 1970, Aerospace and Mechanical Sciences Rept. No. 634o, July 1970, Princeton Univ., Princeton, N. J.

104 Turchi, P. J. and R. G. Jahn, "The Cathode Region of a Quasi-steady MPD Arcjet," A.I.A.A. Bulletin, Vol. 7, No. 9, Sept. 1970, p. 449.

105 Clark, K. E., M. S. Di Capua, R. G. Jahn, and W. F. Von Jaskowsky, "Quasi-steady Magnetoplasmadynamic Arc Characteristics," A.I.A.A. Bulletin, Vol. 7, No. 9, Sept. 1970, p. 449.

106 Turchi, P. J. and R. G. Jahn, "The Cathode Region of a Quasi-steady MPD Arcjet," A.I.A.A. Paper 70-1094, A.I.A.A. 8th Electric Propulsion Conference, Stanford, Calif., 31 Aug.-2 Sept. 1970.

107 K. E. Clark, M. S. Di Capua, R. G. Jahn, and W. F. Von Jaskowsky, "Quasi-steady Magnetoplasmadynamic Arc Characteristics," A.I.A.A. Paper 70-1095, A.I.A.A. 8th Electric Propulsion Conference, Stanford, Calif., 31 Aug.-2 Sept. 1970.

108 Turchi, P. J., "The Cathode Region of a Quasi-steady Magnetoplasmadynamic Arcjet," Ph.D. thesis, Sept. 1970, Princeton Univ., Princeton, N. J.

109 Turchi, P. J. and R. G. Jahn, "The Cathode Region of a Quasi-steady Magnetoplasmadynamic Arcjet," NASA NGL 31-001-005, Aerospace and Mechanical Sciences Rept. No. 940, Oct. 1970, Princeton Univ., Princeton, N. J.

PROJECT REFERENCES

110 Oberth, R. C., "Anode Phenomena in High-Current Discharges," Ph.D. thesis, Dec. 1970, Princeton Univ., Princeton, N. J.

111 Oberth, R. C. and R. G. Jahn, "Anode Phenomena in High-Current Discharges," NASA NGL 31-001-005, Aerospace and Mechanical Sciences Rept. No. 961, Dec. 1970, Princeton Univ., Princeton, N. J.

112 Di Capua, M. S. and R. G. Jahn, "Voltage-Current Characteristics of Parallel-Plate Plasma Accelerators," A.I.A.A. Bulletin, Vol. 8, No. 1, Jan. 1971, p. 40.

113 Oberth, R. C. and R. G. Jahn, "Anode Phenomena in High-Current Accelerators," A.I.A.A. Bulletin, Vol. 8, No. 1, Jan. 1971, p. 40.

114 Di Capua, M. S. and R. G. Jahn, "Energy Deposition in Parallel-Plate Plasma Accelerators," A.I.A.A. Paper 71-197, A.I.A.A. 9th Aerospace Sciences Meeting, New York, N. Y., 25-27 Jan. 1971.

115 Oberth, R. C. and R. G. Jahn, "Anode Phenomena in High-Current Accelerators," A.I.A.A. Paper 71-198, A.I.A.A. 9th Aerospace Sciences Meeting, New York, N. Y., 25-27 Jan. 1971.

116 Jahn, R. G., K. E. Clark, R. C. Oberth, and P. J. Turchi, "Acceleration Patterns in Quasi-steady MPD Arcs," A.I.A.A. Journal, Vol. 9, No. 1, Jan. 1971, pp. 167-172.

117 Di Capua, M. S., Ph.D. dissertation, Princeton Univ., Princeton, N. J., 1971, forthcoming.

GENERAL REFERENCES

A-1 Shih, K. T., E. Pfender, W. E. Ibele, and E. R. G. Eckert, "Experimental Studies of the Electrode Heat Transfer in a MPD Arc Configuration," AIAA Paper 67-673 (1967).

A-2 Shih, K. T. and E. Pfender, "Electrode Energy Transfer Mechanics in a MPD Arc," AIAA Journal, Vol. 8, No. 2, Feb. 1970, pp. 211-215.

A-3 Pfender, E., G. D. Raithby, and E. R. G. Eckert, "An Anode Comparison Study in a Wall Stabilized Argon Arc," ARL Rept. 65-232, Nov. 1965.

A-4 Lovberg, R. H., "Magnetic Probes," Plasma Diagnostic Techniques, Huddlestone, R. H. and Leonard, S. L. (Eds.) Academic Press, New York, 1965.

A-5 Chen, F. F., "Electric Probes," Plasma Diagnostic Techniques, Huddlestone, R. H. and Leonard, S. L. (Eds.), Academic Press, New York, 1965.

A-6 Bez, W. and K. H. Höcker, "Theorie des Anodenfalls I," Zeitschrift fur Naturforschung, Vol. 10a, 1955, pp. 714-717.

A-7 Höcker, K. H. and W. Bez, "Theorie des Anodenfalls II," Zeitschrift fur Naturforschung, Vol. 11a, 1956, pp. 118-123.

A-8 Eckert, E. R. G., "Survey on Heat Transfer at High Speeds," WADC Tech. Rept. 54-70, April 1954.

A-9 Kalikhman, L. E., Elements of Magnetogasdynamics, W. B. Saunders Co., Phila., Pa., 1967, pp. 9-16.

A-10 Cobine, J. D., Gaseous Conductors, Dover Publications, Inc., New York, 1958, p. 82.

A-11 Spitzer, Jr., L., Physics of Fully Ionized Gases, Interscience Publishers, New York, 1962, Chap. 5.

A-12 Meissner, K. H., "Interference Spectroscopy, Part I," J. Opt. Soc. Am. 31, 6, 405 (1941).

A-13 Hoell, Jr., J. M., J. Burlock, and O. Jarrett, Jr., "Velocity and Thrust Measurements in a Quasi-Steady Magnetoplasmadynamic Thruster," AIAA Paper 70-1080 (1970).

A-14 Csiky, G. A., "Measurement of Some Properties of a Discharge from a Hollow Cathode," NASA TN D-4966 (Feb. 1969).

GENERAL REFERENCES

[A-15] Byers, D. C. and A. Snyder, "Parametric Investigation of Mercury Hollow Cathode Neutralizer," AIAA Paper 70-1090, AIAA 8th Electric Propulsion Conference, Stanford, Calif., 31 Aug.-2 Sept. 1970.

[A-16] Rawlin, V. K. and E. V. Pawlik, "A Mercury Plasma-Bridge Neutralizer," J. Spacecraft, Vol. 5, No. 7, (1968), pp. 841-820.

Appendix A: Semiannual Statement of Expenditures

PULSED ELECTROMAGNETIC GAS ACCELERATION
NASA NGL 31-001-005

1 July 1970 — 31 December 1970

Direct Costs

I.	Salaries and Wages		
	A. Professional	$19,682	
	B. Students	5,437	
	C. Technicians	10,051	
	D. Supporting Staff	6,944	
			$42,114
II.	Employee Benefits (19% of IA, IB, and ID)		6,970
III.	Equipment		0
IV.	Expendable Materials and Services		4,729
V.	Travel		1,840
VI.	Tuition		1,050
	Total Direct Costs		$56,703

Indirect Costs

VII.	Overhead (68% of I)	28,639
	TOTAL	$85,342